State of Wyoming
Department of Transportation

U.S. Department of Transportation
Federal Highway Administration

FINAL REPORT

Report No. FHWA-WY-16/07F

INVESTIGATION OF SILICA FUME
CONCRETE BRIDGE DECK OVERLAY FAILURES

by
Kim Basham, PhD. PE, FACI
KB Engineering, LLC
1716 Capitol Avenue
Cheyenne, WY 82001
kbashamatKBEngLLC.com

February 23, 2016

1. Report No. FHWA-WY–16/07F	2. Government Accession No.	3. Recipients Catalog No.
4. Title and Subtitle INVESTIGATION OF SILICA FUME CONCRETE BRIDGE DECK OVERLAY FAILURES		5. Report Date February 23, 2016
		6. Performing Organization Code:
7. Author(s) Kim Basham, PhD, PE, FACI		8. Performing Organization Report No.
9. Performing Organization Name and Address KB Engineering, LLC 1716 Capitol Ave. Cheyenne, WY 82001 Tel (307) 635-7240		10. Work Unit No.
		11. Contract or Grant No. RS04-211
12. Sponsoring Organization Name and Address Wyoming Department of Transportation Research Center 5300 Bishop Blvd. Cheyenne, Wyoming 82009-3340 Tel (307) 777-4182		13. Type of Report and Period Covered Final Report 04/22/11 - 2/23/16
		14. Sponsoring Agency Code FHWA & WYDOT
15. Supplementary Notes		

16. Abstract

Many of these microsilica-modified concrete or silica fume concrete (SFC) bridge deck overlays across the State of Wyoming are suffering from premature distress that includes random cracking, loss of bond and delaminations. To determine the most likely cause of the premature overlay failures and to develop a mitigation scheme, this author with the assistance of Dr. David Rothstein, PhD, PG, FACI with DRP Consulting, Inc. (DRP) and Mr. Larry Mott, PE with GES Tech Group, Inc. (GES) undertook a multi-task research study.

Tasks consisted of measuring bond strengths of existing and new SFC overlays representing different surface preparation techniques and measuring both plastic and hardened properties including drying shrinkages for typical SFC overlay mixtures. DRP performed petrographic examinations of bond lines and failure zones of core samples. GES modeled the overlay and substrate and performed non-linear finite element analyses focusing on the cracking potential of the overlay and the bond-line stresses created by varying the strength and drying shrinkage of the overlay.

Results show bond strengths for most of the existing and new SFC overlays was insufficient. In general, bond strength failures occurred superficially in the concrete substrate and the petrographic examinations revealed cracks and microcracks located within the top ¼ inch of the substrate, most likely caused by an external applied stress after initial bonding. The finite element analyses showed significant tensile stresses in the overlay material, shrinkage cracks and high bond-line stresses occurred when the drying shrinkage of the SFC overlay exceeding about 0.03 percent. Results indicate the magnitude of the drying shrinkage of the existing SFC overlays was too large.

Using the 0.03 percent as the upper limit for the field shrinkage, maximum 28-day allowable shrinkages as determined by a standard laboratory procedure were computed using a concrete shrinkage model for different overlay thickness and relative humidities. By limiting the 28-day laboratory shrinkages, SFC overlay shrinkages should not exceed 0.03 percent; thereby, limiting the cracking potential of the overlay and maintaining acceptable bond line stresses.

17. Key Words Wyoming, David Rothstein, Larry Mott, bridge deck, concrete, overlay, microsilica, silica fume, cracks, delamination, surface preparation, finite element, petrographic, pull-off test, bond strength		18. Distribution Statement No restrictions. Document is available through National Tech Info Service (NTIS), National Transportation Library (NTL) & WY State Library	
19. Security Classif. (of this report) Unclassified	20. Security Classif. (of this page) Unclassified	21. No. of Pages 387	22. Price -0-

Form DOT F 1700.7 (8-72)   **Reproduction of completed page authorized**

SI* (MODERN METRIC) CONVERSION FACTORS

APPROXIMATE CONVERSIONS TO SI UNITS

Symbol	When You Know	Multiply By	To Find	Symbol
LENGTH				
in	inches	25.4	millimeters	mm
ft	feet	0.305	meters	m
yd	yards	0.914	meters	m
mi	miles	1.61	kilometers	km
AREA				
in^2	square inches	645.2	square millimeters	mm^2
ft^2	square feet	0.093	square meters	m^2
yd^2	square yard	0.836	square meters	m^2
ac	acres	0.405	hectares	ha
mi^2	square miles	2.59	square kilometers	km^2
VOLUME				
fl oz	fluid ounces	29.57	millimeters	mL
gal	gallons	3.785	liters	L
ft^3	cubic feet	0.028	cubic meters	m^3
yd^3	cubic yards	0.765	cubic meters	m^3
Note: volumes greater than 1000 L shall be shown in m^3				
MASS				
oz	ounces	28.35	grams	g
lb	pounds	0.454	kilograms	kg
T	short tons (2000 lb)	0.907	Megagrams (or "metric ton")	Mg (or "t")
TEMPERATURE (exact degrees)				
ºF	Fahrenheit	5 (F-32)/9 or (F-32)/1.8	Celsius	ºC
ILLUMINATION				
fc	foot-candles	10.76	lux	lx
fl	Foot-Lamberts	3.426	Candela/m^2	cd/m^2
FORCE and PRESSURE or STRESS				
lbf	poundforce	4.45	newtons	N
lbf/in^2	poundforce per square inch	6.89	kilopascals	kPa

APPROXIMATE CONVERSIONS FROM SI UNITS

Symbol	When You Know	Multiply By	To Find	Symbol
LENGTH				
mm	millimeters	0.039	inches	in
m	meters	3.28	feet	ft
m	meters	1.09	yards	yd
km	kilometers	0.621	miles	mi
AREA				
mm^2	square millimeters	0.0016	square inches	in^2
m^2	square meters	10.764	square feet	ft^2
m^2	square meters	1.195	square yard	yd^2
ha	hectares	2.47	acres	ac
km^2	square kilometers	0.386	square miles	mi^2
VOLUME				
mL	millimeters	0.034	fluid ounces	fl oz
L	liters	0.264	gallons	gal
m^3	cubic meters	35.314	cubic feet	ft^3
m^3	cubic meters	1.307	cubic yards	yd^3
MASS				
g	grams	0.035	ounces	oz
kg	kilograms	2.202	pounds	lb
Mg (or "t")	Megagrams (or "metric ton")	1.103	short tons (2000 lb)	T
TEMPERATURE (exact degrees)				
ºC	Celsius	1.8C + 32	Fahrenheit	ºF
ILLUMINATION				
lx	lux	0.0929	foot-candles	fc
cd/m^2	Candela/m^2	0.2919	Foot-Lamberts	fl
FORCE and PRESSURE or STRESS				
N	newtons	0.225	poundforce	lbf
kPa	kilopascals	0.145	poundforce per square inch	lbf/in^2

*SI is the symbol for the International System of Units. Approximate rounding should be made to comply with Section 4 of ASTM E380. (Revised March 2003)

EXCUTIVE SUMMARY

The Wyoming Department of Transportation uses microsilica-modified bonded concrete overlays with thicknesses varying from ¾ to 1¼ inches to resurface or rehabilitate deteriorated reinforced concrete bridge decks. Many of these microsilica-modified concrete bridge deck overlays across the State of Wyoming are suffering from premature distress that includes random cracking, loss of bond and delaminations. Commonly referred to as silica-fume concrete overlays or SFC overlays, they provide new wear surfaces but also provide protection of the concrete substrate and steel reinforcing by minimizing the penetration of water and chloride ions associated with deicing chemicals.

Premature SFC overlay failures shorten the service life of bridge decks, increase maintenance and repair costs, and potentially create safety concerns for motorists. In addition, cracks allow the penetration of chloride ions into the overlays increasing the potential for steel reinforcing corrosion and additional deterioration of the concrete bridge deck, concrete superstructure and substructure. The annual cost of repairing premature cracking and debonding of the overlays and related damage is significant.

To determine the most likely cause of the premature overlay failures and to develop a mitigation scheme, this author with the assistance of Dr. David Rothstein, PhD, PG, FACI with DRP Consulting, Inc. (DRP) and Mr. Larry Mott, PE with GES Tech Group, Inc. (GES) undertook a multi-task research study. Tasks consisted of measuring bond strengths of existing and new SFC overlays representing different surface preparation techniques and measuring both plastic and hardened properties including drying shrinkages for typical SFC overlay mixtures used in Wyoming. DRP performed petrographic examinations of bond lines and failure zones of drilled core samples. GES modeled the overlay and substrate and performed non-linear finite element analyses focusing on the cracking potential of the overlay and the bond-line stresses created by varying the strength and drying shrinkage of the overlay.

Results show the bond strength of most of the existing and new SFC overlays was insufficient to ensure an adequate bond and a long service life of overlays. In general, bond strength failures occurred superficially in the concrete substrate. The petrographic examinations revealed cracks and microcracks located within the top ¼ inch of the substrate, most likely caused by an externally applied stress after initial bonding. The finite element analyses showed significant tensile stresses in the overlay material, shrinkage cracks and high bond-line stresses occurred when the drying shrinkage of the SFC overlay exceeding about 0.03 percent. Results indicate the magnitude of the drying shrinkage of the existing SFC overlays was too large.

Using the 0.03 percent as the upper limit for the field shrinkage, maximum 28-day allowable shrinkages as determined by a standard laboratory procedure were computed using a concrete shrinkage model for different overlay thickness and relative humidities. By limiting the 28-day laboratory shrinkages, SFC overlay shrinkages should not exceed 0.03 percent; thereby, limiting the cracking potential of the overlay and maintaining acceptable bond line stresses.

TABLE OF CONTENTS

LIST OF FIGURES

LIST OF TABLES

1.0   INTRODUCTION

The Wyoming Department of Transportation (WYDOT) uses microsilica-modified bonded concrete overlays with thicknesses varying from ¾ to 1¼ inches to resurface or rehabilitate deteriorated reinforced concrete bridge decks. Many of these microsilica-modified concrete bridge deck overlays across the State of Wyoming are suffering from premature distress that includes random cracking, loss of bond and delaminations as illustrated in Figure 1 below. Loss of bond (debonding) is loss of adhesion between the overlay concrete and the underlying concrete or substrate.
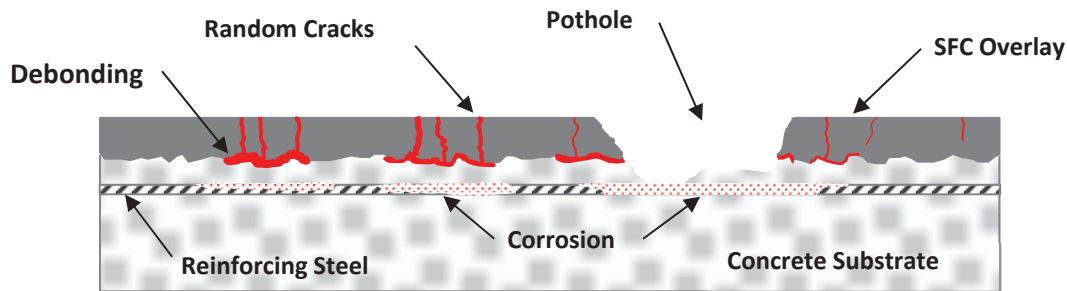
Figure 1.1.   Illustration of SFC overlay distress – cracks, debonding, steel reinforcement corrosion and potholes.

Overlays consist of low water/cement ratio microsilica-modified portland cement concrete that is commonly referred to as silica fume concrete (SFC). In addition to reestablishing new wearing surfaces, bonded SFC overlays provide concrete and reinforcement protection by minimizing penetration of chloride ions associated with deicing chemicals. Water and chloride ions that penetrate into concrete promote corrosion of the reinforcing steel.

Random cracks, debonding and delaminations of SFC overlays provide additional pathways for water and chloride ions to enter the concrete decks. Subsequently, the potential increases for reinforcing steel corrosion, formation of potholes and general deterioration of bridge decks. Premature SFC overlay distress and failures shorten the life cycle of bridge decks, increase maintenance and repair costs, and create potential safety concerns for motorists.

Due to the extreme winter conditions and the application of deicing chemicals, premature SFC overlay failures are costly to repair and if not repaired in a timely manner, allow chloride ions to penetrate further into the concrete increasing the potential for steel reinforcing corrosion and additional deterioration of the bridge deck. The annual cost of repairing premature distress and failures of SFC bridge overlays in Wyoming is significant. In addition to the repair costs, premature overlay distress and failures increase the potential for accelerated corrosion of the steel reinforcement; shortening the service life of the entire structure.

Figure 1.2 below summarizes these concerns and defines the problem statement for this research project.

> Premature distress and failures of SFC bridge deck overlays shorten the life cycle of bridge decks, increase maintenance and repair costs, and potentially may shorten the life cycle of the entire structure and create safety concerns for motorists.

Figure 1.2. Problem statement for this research project.

1.1 RESEARCH OBJECTIVES

The first step to extending the service life of the SFC bridge deck overlays in Wyoming was to identify and characterize the failure mechanisms that were responsible for the premature overlay failures. By understanding the failure mechanisms, WYDOT engineers can modify and/or enhance the material design and construction techniques to mitigate the failure mechanisms and extend the service life of the SFC overlays.

Summarized below in Figure 1.3 were the primary objectives for this research project.

> Identify the failure mechanisms and root causes of the premature SFC overlay distress and failures. Make design, material and construction recommendations to minimize premature SFC bridge deck overlay distress and failures. Provide WYDOT engineers with critical information needed to improve SFC overlay designs, SFC mixtures and construction techniques.

Figure 1.3. Primary research objectives.

Results from this research project will provide WYDOT engineers critical information to make informed decisions regarding the design, material requirements and construction techniques needed to minimize premature SFC overlay distress and failures.

1.2. LITERATURE SERACH

From an extensive literature search, this author found many condition survey publications that addressed applicability and service life of concrete overlays. However, the majority of the publications reviewed primarily investigated and addressed the various factors that influence the bond strength of concrete overlays. The factors included: surface preparation, substrate microcracking (bruising), surface cleanliness and laitance, surface roughness, substrate moisture content, bonding agents, overlay compaction, bond strength versus time, traffic vibrations, and

curing. Many comprehensive publications are available that address and summarize the industry's understanding of concrete overlays. [See references 1 – 6.]

Investigators reported using direct tension (pull-off), shear-bond and split-tensile tests to investigate the various factors that affect the bond strength of concrete overlays to concrete substrates. Most of the publications present findings and conclusions of focused and limited research efforts. Except for the condition overlay survey publications, this author did not find forensic or research type publications that specifically addressed the failure mechanisms responsible for random cracking and debonding of bridge deck concrete overlays.

In many of the publications reviewed, researchers sometimes mentioned that shrinkage stresses and perhaps curling of the overlay concrete are likely factors that contribute to overlay cracking, debonding and delaminations. However, the literature search did not produce any publications that investigated, measured and quantified shrinkage, cracking and debonding of concrete overlays. More importantly, the amount of information addressing overlay failures and design recommendations to minimize overlay cracking and debonding was extremely limited.

The lack of research and publications dealing with concrete overlay failures and design recommendations, especially addressing overlay shrinkage, cracking and debonding helped determine the scope of work for this research project.

1.3   SCOPE OF WORK

1. Investigate and establish typical bond strengths for existing and new SFC overlays by the direct tension or the pull-off method for different surface preparation methods in accordance with ASTM C1583/C1583M - Standard Test Method for Tensile Strength of Concrete Surfaces and the Bond Strength or Tensile Strength of Concrete Repair and Overlay Materials by Direct Tension (Pull-off Method). [7]

    Chapter 2 presents a total of 178 pull-off strengths and compares the results to acceptable industry standards for both existing and new SFC overlays.   In addition, different surface preparations including rotomilling, hydroblasting with and without a portland cement primer (bonding slurry) are presented and compared.

2. Investigate various material properties including the drying shrinkage characteristics of 12 typical silica fume concrete mixtures used by WYDOT to construct bridge deck overlays. In addition to measuring plastic concrete properties including slump, total air content, and unit weight, WYDOT technicians measured hardened concrete properties including compressive strength, resistance to chloride penetration, concrete drying

shrinkage (bar length change), and concrete restrained ring shrinkage. Technicians determined SFC overlay shrinkage characteristics in accordance with the following laboratory tests:

a. ASTM C157/C157M – Standard Test Method for Length Change of Hardened Hydraulic-Cement Mortar and Concrete [8]

b. ASTM C1581/C1581M - Standard Test Method for Determining Age at Cracking and Induced Tensile Stress Characteristics of Mortar and Concrete under Restrained Shrinkage [9]

In addition to the plastic and hardened properties of the SFC overlay mixtures used during the 2011 and 2012 construction season, Chapter 3 shows the mix proportions including water to cementitious ratios and gradations for the fine and coarse aggregates.

3. Petrographically examine and compare substrate micro-damage (bruising) associated with different surface preparation techniques including roto-milling and hydroblasting with and without a portland cement primer. Microscopically examine the bond lines and failure surfaces to characterize the failure zones between the SFC overlays and bond interfaces of drilled core samples. Dr. David Rothstein, PhD, PG, FACI with DRP Consulting Inc. (DRP) performed the petrographic examinations and used several microscopic techniques including a scanning electron microscope to complete the task.

Chapter 4 presents a summary of DRP's findings and conclusions. Appendix A presents DRP's lengthy report including appendices with detail descriptions and photographs of the petrographic findings.

4. Use a sophisticated non-linear finite element computer model specially developed for modelling concrete, investigate the cracking and bond line stresses associated with the restrained drying shrinkage of the SFC overlay. Mr. Larry Mott, PE with GES Tech Group, Inc. (GES) performed the finite element analysis by varying the SFC overlay drying shrinkages from 0.02 to 0.09 percent and investigated both the cracking potentials of the overlay and resulting bond line stresses or the stresses at the interface between the SFC overlay and concrete substrate. GES also investigated the effects of varying the compressive strength and stiffness of the SFC overlay material.

With numerous figures, Chapter 5 presents GES's findings and conclusions. Most importantly, Chapter 5 presents the maximum allowable field SFC shrinkage required to reduce the cracking potential of the overlay and to limit the bond line stresses associated with the restrained drying shrinkage of the SFC overlay to an acceptable level.

5. Identify the failure mechanisms and root causes of the premature SFC overlay distress and failures using tasks 1 through 5 above. Establish a maximum laboratory SFC shrinkage value that can be incorporated into the SFC overlay material acceptance criteria or concrete specifications. More specifically, use an established concrete shrinkage model to convert the maximum allowable SFC field shrinkage as determined by the finite element analysis into a usable laboratory shrinkage value.

Chapter 6 summarizes the results and conclusions from tasks 1 through 5 and presents the recommended laboratory SFC shrinkage values for different overlay thicknesses and relative humidity conditions that can be used as a SFC acceptance criterion or a specified concrete requirement. In addition, Chapter 6 presents future research recommendations associated with mitigating the premature SFC overlay failures and extending the service life of SFC bridge deck overlays.

2.0   IN-SITU BOND STRENGTH TESTING

To determine the bond strength of the old and new silica fume overlays to the concrete substrate and to evaluate various surface preparation techniques, investigators performed numerous tensile pull-off tests in accordance with ASTM C1583/C1583M-04. Specifically, technicians performed pull-off tests on the existing or old silica fume overlays and new silica fume overlays placed on substrates prepared with three different surface preparation techniques. Surface preparation techniques consisted of 1) rotomilling with a portland cement mortar slurry or primer, 2) rotomilling followed by hydroblasting with and without a mortar primer and 3) hydroblasting without a mortar primer.

Table 2.1 below summarizes the groupings of the tensile pull-off tests performed.

Table 2.1. Groupings of Tensile Pull-off Tests

Bridge Deck	Old Overlay	New Overlay	Surface Preparation Technique	Surface Primer	
				None	Mortar Slurry
Pine Bluffs East I-80 (BAH)	X	X	Rotomilling		X
Pine Bluffs West I-80 (BAI)	X	X	Rotomilling & Hydroblasting	X	X (5 ft)
Round Top East I-80 (AYR)	X	X	Hydroblasting	X	
Round Top West I-80 (AYS)	X	X	Hydroblasting	X	
Arlington, East I-80 (Bridges: 272-06, 272-50 and 272-76)		X	Hydroblasting	X	
Centennial, HWY 130, MP 22.04		X	Hydroblasting	X	

2.1   PULL-OFF STRENGTH TESTING

Test specimens were formed by drilling a 2¼ -inch diameter core bit into and perpendicular to the surface of the overlay to depths extending a minimum of 0.5-inches into the concrete substrate. The technicians used care to leave the 2-inch diameter core intact and attached to the substrate. Next, aluminum disks were epoxied to the top surface of the intact cores as shown below in Figure 2.1.

After the epoxy cured, the technician placed the pull-off testing device (Proceq-Dyna Z16 Pull-off Tester) over each disk and applied a direct tensile force to the disk until failure occurred as shown in Figures 2.2 and 2.3. Tables 2.2 – 2.7 in Section 2.3 summarize the pull-off strengths.

Figure 2.1. Photo - Two-inch diameter, aluminum disk epoxied to the intact drilled core with pull-ball attached. Specimen number was AYS-2N2.

Figure 2.2. Photo - A Proceq-Dyna Z16 Pull-off Tester was used for all pull-off testing.

Figure 2.3. Photo - Rotating the crank applied the tensile or pull-off load to the aluminum disk. The digital gauge recorded the maximum load applied.

As shown below in Figure 2.4, failure can occur at several different locations: a) concrete substrate, b) concrete/overlay interface, c) overlay and d) epoxy/overlay interface.

| a) Failure in substrate | b) Bond failure at concrete/overlay interface | c) Failure in overlay material | d) Bond failure at epoxy/overlay interface |

Failure Lines
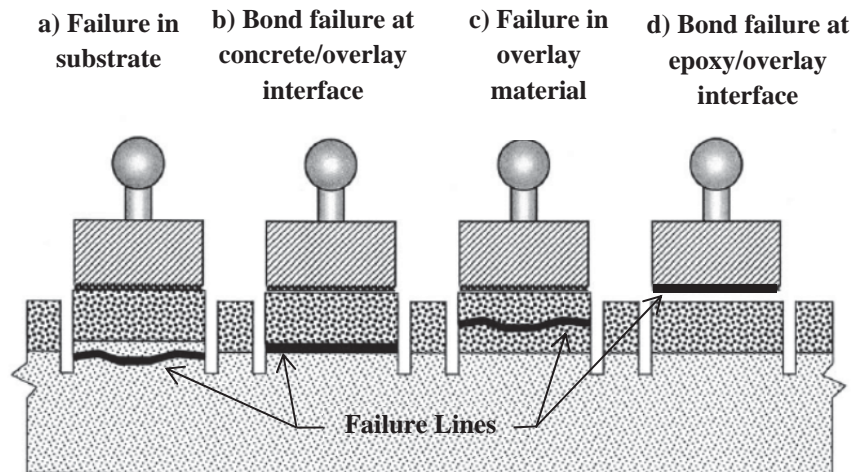
Figure 2.4. Schematic of tensile pull-off failure modes from ASTM C1583/C1583M.

For each pull-off test, the technician inspected the failure surface, estimated the percentage of each failure mode and recorded the percentages. See Figures 2.5 and 2.6 below and Tables 2.2 – 2.7 in Section 2.3.

Figure 2.5. Photo - Side view of pull-off test for AYS-3N2A as shown in Table 2.5 in Section 2. Measured pull-off strength was 181 psi.
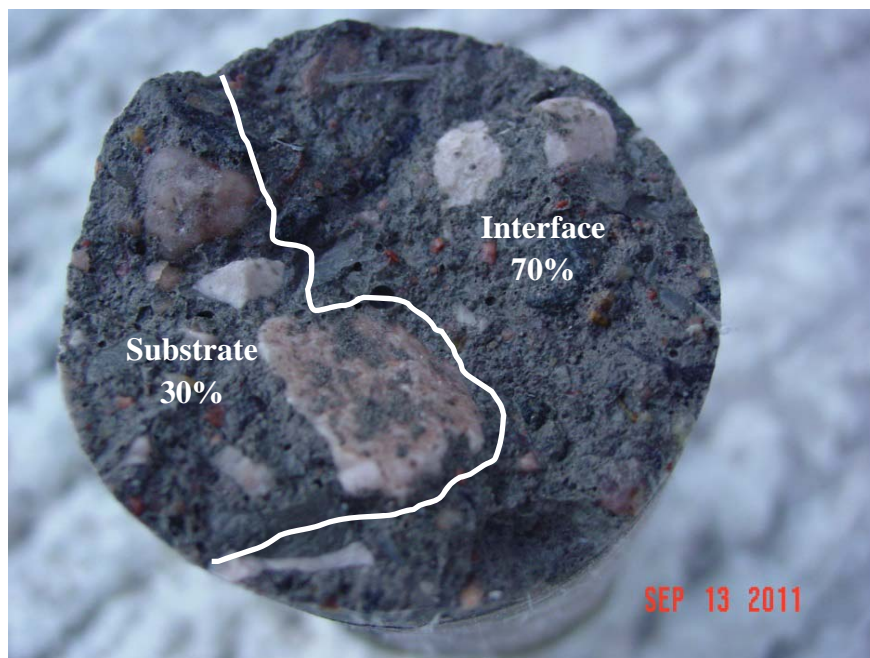
Figure 2.6. Photo - For pull-off test AYS-3N2A as shown in Table 2.5 in Section 3 below, 30-percent of the failure occurred in the concrete substrate and 70-percent was at the bond of the concrete/overlay interface.

2.2 BOND STRENGTH EVALUATION

Bond strengths of 250 psi or greater can be achieved with the available surface preparation techniques and concrete materials for moderate to good quality concrete substrates. [5] Strengths less than 250 psi that fail consistently within the concrete substrate may indicate inadequate surface preparation or poor quality concrete substrate. Strengths less than 175 psi where failure occurs at the bond interface or superficially within the concrete substrate may indicate damaged, contaminated, poorly prepared and/or an inadequate bond surface or a weakened bond surface caused by high shear stresses.

Shear stresses develop along the bond interface as the concrete substrate resists the drying shrinkage of the overlay material. The amount of drying shrinkage of the overlay material has a significant impact on the magnitude of the shear stresses. High shear stresses can reduce bonds by weakening the concrete substrate along the bond interface.

Bond strengths of 200 psi are considered sufficient for bonded concrete overlays with thicknesses of three inches or more. [2] For three-inch or thicker overlays, the bond line stresses associated with drying shrinkage of the overlay material typically fall below 200 psi and are negligible. There is no industry standard for the minimum bond strength to ensure adequate bonding for concrete overlays less than three inches thick.

2.3 PULL-OFF STRENGTH RESULTS

Tables 2.2 – 2.7 below show the pull-off strengths for the bridge decks tested. Table 2.8 shows the "Summary for Old and New Overlays" and Table 2.9 shows the "Average Pull-off Strength and Failure Mode" for all pull-off tests. Figures 2.7 – 2.9 show bar charts for the overall average pull-off strengths, average pull-off strengths, and average pull-off strength versus overlay surface preparation.

In addition to presenting the pull-off strengths, Tables 2.2 – 2.7 present the estimated percentage of each failure mode as shown above in Figure 2.4. For pull-off test AYS-3N2A (New Silica Fume Overlay) as shown in Table 2.5, 30-percent of the failure occurred in the concrete substrate and 70-percent was at the bond of the concrete/overlay interface as shown above in Figures 2.5 and 2.6.

Also shown in Tables 2.2 – 2.7 and referenced in Figures 2.7 – 2.9 are the test dates and the age of the overlays when the pull-off testing occurred.

Table 2.2. Pull-Off Strengths for Pine Bluffs East I-80 (BAH) [7]

Test No.	Strength (psi)	Failure Mode (percentage)			
		Substrate	Interface	Overlay	Epoxy
7/9/11	**Old Silica Fume Overlay**				
BAH-1A	44	80	20		
BAH-1B	25	95	5		
BAH-1C	51	95	5		
Average	40				
BAH-2A	164		100		
BAH-2B	298			100	
BAH-2C	91	90	10		
Average	184				
BAH-3A	30		100		
BAH-3B	NA				
BAH-3C	NA				
Average	30				
AVERAGE	**85**	**52**	**34**	**14**	
STD DEV	**86**				
New Silica Fume Overlay (Passing Lane, Placed 7/20/11)					
7/29/11	**Rotomilled with Primer (9 days old)**				
BAH-1NA	160	100			
BAH-1NB	67	100			
BAH-1NC	65	100			
BAH-1ND	139	100			
Average	108				
BAH-2NA	103	100			
BAH-2NB	129	100			
BAH-2NC	80	100			
Average	104				
BAH-3NA	160	100			
BAH-3NB	116	100			
BAH-3NC	NA	100			
BAH-3ND	48	100			
Average	108				
AVERAGE	**107**	**100**			
STD DEV	**41**				
New Silica Fume Overlay (Driving Lane, Placed 8/26/11)					
9/11/11	**Rotomilled with Primer (16 days old)**				
BAH-1N2A	72	30	70		
BAH-1N2B	234				100
BAH-1N2C	NA				
Average	153				

Table 2.2. Pull-Off Strengths for Pine Bluffs East I-80 (BAH)

Test No.	Strength (psi)	Failure Mode (percentage)			
		Substrate	**Interface**	**Overlay**	**Epoxy**
BAH-2N2A	302		100		
BAH-2N2B	327			100	
BAH-2N2C	281			100	
Average	303				
BAH-3N2A	323	100			
BAH-3N2B	304	100			
BAH-3N2C	260	100			
Average	296				
AVERAGE	**234**	**41**	**21**	**25**	**13**
STD DEV	**118**				
New Silica Fume Overlay (Driving Lane, Placed 8/26/11)					
9/7/12	**Rotomilled with Primer (378 days old)**				
BAH-A1	112		100		
BAH-A2	99	100			
BAH-A3	72	60	40		
BAH-A4	17	100			
BAH-A5	236			100	
Average	107				
BAH-B1	190			100	
BAH-B2	133	20	80		
BAH-B3	110			100	
BAH-B4	194	100			
BAH-B5	175			100	
Average	160				
BAH-C1	135	80		20	
BAH-C2	167	90	10		
BAH-C3	141		100		
BAH-C4	112		100		
BAH-C5	158		100		
Average	143				
AVERAGE	**137**	**37**	**42**	**21**	
STD DEV	**54**				

Table 2.3. Pull-Off Strengths for Pine Bluffs West I-80 (BAI)

Test No.	Strength (psi)	Failure Mode (percentage)			
		Substrate	**Interface**	**Overlay**	**Epoxy**
7/9/11	**Old Silica Fume Overlay**				
BAI-1A	61	80	20		
BAI-1B	25	100			
BAI-1C	57	100			
Average	48				
BAI-2A	10	100			
BAI-2B	13	100			
BAI-2C	8	90	10		
Average	10				
BAI-3A	87	100			
BAI-3B	15	100			
BAI-3C	NA	100			
Average	51				
AVERAGE	**36**	**97**	**3**		
STD DEV	**23**				
New Silica Fume Overlay (Passing Lane, Placed 7/19/11)					
7/29/11	**Rotomilled and Hydromilled without Primer (10 days old)**				
BAI-1NA	NA		100		
BAI-1NB	150		100		
BAI-1NC	101	100			
BAI-1ND	116			100	
Average	122				
BAI-2NA	127	100			
BAI-2NB	70	100			
BAI-2NC	160	100			
BAI-2ND	106	100			
Average	116				
AVERAGE	**119**	**63**	**25**	**12**	
STD DEV	**31**				
7/29/11	**Rotomilled and Hydromilled with Primer (10 days old)**				
BAI-3NA	169	100			
BAI-3NB	265	40	60		
BAI-3NC	241	40	60		
Average	225				
AVERAGE	**225**	**60**	**40**		
STD DEV	**50**				
New Silica Fume Overlay (Driving Lane, Placed 9/1/11)					
9/11/11	**Rotomilled and Hydromilled without Primer (10 days old)**				
BAI-1N2A	179	100			
BAI-1N2B	167	100			
BAI-1N2C	99	100			
Average	148				

Table 2.3. Pull-Off Strengths for Pine Bluffs West I-80 (BAI)

Test No.	Strength (psi)	Failure Mode (percentage)			
		Substrate	Interface	Overlay	Epoxy
BAI-2N2A	137	30	70		
BAI-2N2B	169		100		
BAI-2N2C	116	100			
Average	141				
AVERAGE	**146**	**43**	**57**		
STD DEV	**32**				
9/11/11	**Rotomilled and Hydromilled with Primer (10 days old)**				
BAI-3N2A	177			100	
BAI-3N2B	165	100			
BAI-3N2C	241			100	
Average	194				
AVERAGE	**194**	**33**		**67**	
STD	**41**				
New Silica Fume Overlay (Driving Lane, Placed 9/1/11)					
9/7/12	**Rotomilled and Hydromilled without Primer (372 days old)**				
BAI-A1	126	100			
BAI-A2	131	100			
BAI-A3	162	100			
BAI-A4	192	100			
BAI-A5	86	100			
Average	139				
BAI-B1	287	100			
BAI-B2	310	100			
BAI-B3	154	90	10		
BAI-B4	350	80	20		
BAI-B5	300	100			
Average	280				
BAI-C1	207	90	10		
BAI-C2	287	90	10		
BAI-C3	323	100			
BAI-C4	329	80	20		
BAI-C5	262		100		
Average	282				
AVERAGE	**234**	**89**	**11**		
STD DEV	**87**				

14

Table 2.4. Pull-Off Strengths for Round Top East I-80 (AYR)

Test No.	Strength (psi)	Failure Mode (percentage)			
		Substrate	Interface	Overlay	Epoxy
7/9/11	**Old Silica Fume Overlay**				
AYR-1A	124	100			
AYR-1B	137	100			
AYR-1C	65	100			
Average	109				
AYR-2A	89	80	20		
AYR-2B	49	70	30		
AYR-2C	120	70	30		
Average	86				
AYR-3A	135	90	10		
AYR-3B	49	100			
AYR-3C	114	50	50		
Average	99				
AVERAGE	**98**	**84**	**16**		
STD	**11**				
New Silica Fume Overlay (Passing Lane, Placed 7/22/11)					
7/29/11	**Hydromilled without Primer (7 days old)**				
AYR-1NA	NA				
AYR-1NB	NA				
AYR-1NC	NA				
Average	NA				
AYR-2NA	106		100		
AYR-2NB	186	100			
AYR-2NC	156	100			
Average	149				
AYR-3NA	72	100			
AYR-3NB	NA				
AYR-3NC	112	100			
Average	92				
AVERAGE	**126**	**80**	**20**		
STD DEV	**48**				

Table 2.4. Pull-Off Strengths for Round Top East I-80 (AYR)

Test No.	Strength (psi)	Failure Mode (percentage)			
		Substrate	Interface	Overlay	Epoxy
New Silica Fume Overlay (Driving Lane, Placed 9/1/11)					
9/11/11	**Hydromilled without Primer (10 days old)**				
AYR-1N2A	287			100	
AYR-1N2B	283			100	
AYR-1N2C	285			100	
Average	285				
AYR-2N2A	228			100	
AYR-2N2B	124	100			
AYR-2N2C	90		100		
Average	147				
AYR-3N2A	257				100
AYR-3N2B	312			100	
AYR-3N2C	236	90	10		
Average	268				
AVERAGE	**234**	**21**	**12**	**56**	**11**
STD	**77**				

Table 2.5. Pull-Off Strengths for Round Top West I-80 (AYS)

Test No.	Strength (psi)	Failure Mode (percentage)			
		Substrate	Interface	Overlay	Epoxy
7/10/11	**Old Silica Fume Overlay**				
AYS-1A	74		100		
AYS-1B	53		100		
AYS-1C	198		100		
Average	108				
AYS-2A	321				100
AYS-2B	40		100		
AYS-2C	169	60	40		
Average	177				
AYS-3A	331				100
AYS-3B	194	90	10		
AYS-3C	49	100			
Average	191				
AVERAGE	**159**	**28**	**50**		**22**
STD	**44**				
New Silica Fume Overlay (Passing Lane, Placed 7/20/11)					
7/29/11	**Hydromilled without Primer (9 days old)**				
AYS-1NA	129	10	90		
AYS-1NB	124	30	70		
AYS-1NC	80	10	90		
Average	111				
AYS-2NA	164	100			
AYS-2NB	169		100		
AYS-2NC	238		100		
Average	190				
AYS-3NA	91	100			
AYS-3NB	184		100		
AYS-3NC	260	100			
Average	178				
AVERAGE	**160**	**39**	**61**		
STD	**61**				

Table 2.5. Pull-Off Strengths for Round Top West I-80 (AYS)

Test No.	Strength (psi)	Failure Mode (percentage)			
		Substrate	Interface	Overlay	Epoxy
New Silica Fume Overlay (Driving Lane, Placed 9/8/11)					
9/13/11	**Hydromilled without Primer (5 days old)**				
AYS-1N2A	234	100			
AYS-1N2B	348	100			
AYS-1N2C	243	100			
Average	275				
AYS-2N2A	205	100			
AYS-2N2B	192			100	
AYS-2N2C	217			30	70
Average	205				
AYS-3N2A	181	30	70		
AYS-3N2B	114		100		
AYS-3N2C	156		100		
Average	150				
AVERAGE	**210**	**48**	**30**	**14**	**8**
STD	**65**				

Table 2.6. Pull-Off Strengths for Arlington, East I-80, Passing Lane (Three Closely Spaced Bridges: 272-06, 272-50 and 272-76)

Test No.	Strength (psi)	Failure Mode (percentage)			
		Substrate	Interface	Overlay	Epoxy
8/15/12	**272-06 - New Overlay, Placed 8/2/12 (13 days old)**				
06-1A	154	100			
06-1B	103	40	60		
O6-1C	232	80	20		
Average	163	73	27		
06-2A	148	90	10		
06-2B	194	100			
06-2C	186				100
Average	176	64	3		33
06-3A	316	100			
06-3B	241	60	40		
06-3C	NA	100			
Average	279	87	13		
AVERAGE	**197**	**75**	**14**		**11**
STD DEV	**66**				
8/15/12	**272-50 - New Overlay*, Placed 8/7/12 (8 days old)**				
50-1A	257	100			
50-1B	268	100			
50-1C	131	100			
Average	108	100			
AVERAGE	**219**	**100**			
STD DEV	**76**				
8/15/12	**272-76 - New Overlay, Placed 7/30/12 (16 days old)**				
76-1A	262	100			
76-1B	146	100			
76-1C	247	100			
Average	218	100			
76-2A	308		100		
76-2B	156		100		
76-2C	350		100		
Average	271		100		
76-3A	150		100		
76-3B	152	70	30		
76-3C	144	70	30		
Average	149	47	53		
AVERAGE	**213**	**49**	**51**		
STD DEV	**80**				
AVERAGE	**207**	**76**	**22**		4
STD DEV	**71**				

* Only test location available, other two locations were vandalized.

Table 2.7. Pull-Off Strengths for Centennial, HWY 130, MP 22.04, West Bound Lane, Placed 5/24/12

Test No.	Strength (psi)	Failure Mode (percentage)			
		Substrate	Interface	Overlay	Epoxy
9/6/12	**New Overlay (105 days old)**				
2204-1A	500		70	30	
2204-1B	460	100			
2204-1C	481	100			
2204-1D	333	100			
2204-1E	506	90	10		
Average	456	78	16	6	
2204-2A	401		100		
2204-2B	407	40	60		
2204-2C	405	100			
2204-2D	291			100	
2204-2E	118	50	50		
Average	324	38	42	20	
2204-2A	356	100			
2204-2B	496	100			
2204-2C	587	100			
2204-2D	318	100			
2204-2E	407	100			
Average	433	100			
AVERAGE	**404**	**72**	**19**	**9**	
STD DEV	**113**				

Table 2.8. Pull-Off Strengths, Summary for Old and New Overlays

	Strength (psi)			
	Old Overlay 7/9/11	**New Overlay 7/29/11**	**New Overlay 9/11/11**	**New Overlay 8/15/12 & 9/6/12**
Pine Bluffs East I-80 (BAH) - Rotomilled with Primer				
Average	85	107	234	137
Std. Dev.	86	41	118	54
Pine Bluffs West I-80 (AYS) - Rotomilled/Hydromilled without Primer				
Average	36	119	146	234
Std. Dev.	23	31	32	87
Pine Bluffs West I-80 (AYS) - Rotomilled/Hydromilled with Primer				
Average	36	225	194	
Std. Dev.	23	50	41	
Round Top East I-80 (AYR) - Hydromilled				
Average	98	126	234	
Std. Dev.	11	48	77	
Round Top West I-80 (AYS) - Hydromilled				
Average	159	160	210	
Std. Dev.	44	61	65	
Arlington, East I-80 (Three Decks) Hydromilled				
Average				207
Std. Dev.				71
Centennial WY HWY 130 (MP 22.04) - Hydromilled				
Average				404
Std. Dev.				113
AVERAGE	**95**	**147**	**204**	**186***

* Only for Pine Bluffs and Round Top Decks (excludes Arlington and Centennial)

Table 2.9. Average Pull-off Strength and Failure Mode

	Strength (psi)	Failure Mode (percentage)			
		Substrate	**Interface**	**Overlay**	**Epoxy**
Pine Bluffs East I-80 (BAH)					
Old Overlay	85	52	34	14	
New Overlay – Rotomilled with Primer					
7/29/11 (PL 9)	107	100			
9/11/11 (DL 16)	234	41	21	25	13
9/7/12 (DL 378)	137	37	42	21	
Pine Bluffs West I-80 (BAI)					
Old Overlay	36	97	3		
New Overlay – Rotomilled & Hydromilled without Primer					
7/29/11 (PL 10)	119	63	25	12	
9/11/11 (DL 10)	146	43	57		
9/7/12 (DL 372)	234	89	11		
New Overlay – Rotomilled & Hydromilled with Primer					
7/29/11 (PL 10)	225	60	40		
9/11/11 (DL 10)	194	33		67	
Round Top East I-80 (AYR)					
Old Overlay	98	84	16		
New Overlay – Hydromilled					
7/29/11 (PL 7)	126	80	20		
9/11/11 (DL 10)	234	21	12	56	11
Round West I-80 (AYS)					
Old Overlay	159	28	50		22
New Overlay – Hydromilled					
7/29/11 (PL 9)	160	39	61		
9/11/11 (DL 5)	210	48	30	14	8
Arlington East I-80 (3 Bridges)					
New Overlay – Hydromilled					
8/15/12 (PL 13)	197	75	14		11
8/15/12 (PL 8)	219	100			
8/15/12 (PL 16)	213	49	51		
Centennial WY HWY 130 (MP 22.04)					
New Overlay – Hydromilled					
9/6/12 (WB 105)	404	72	19	9	
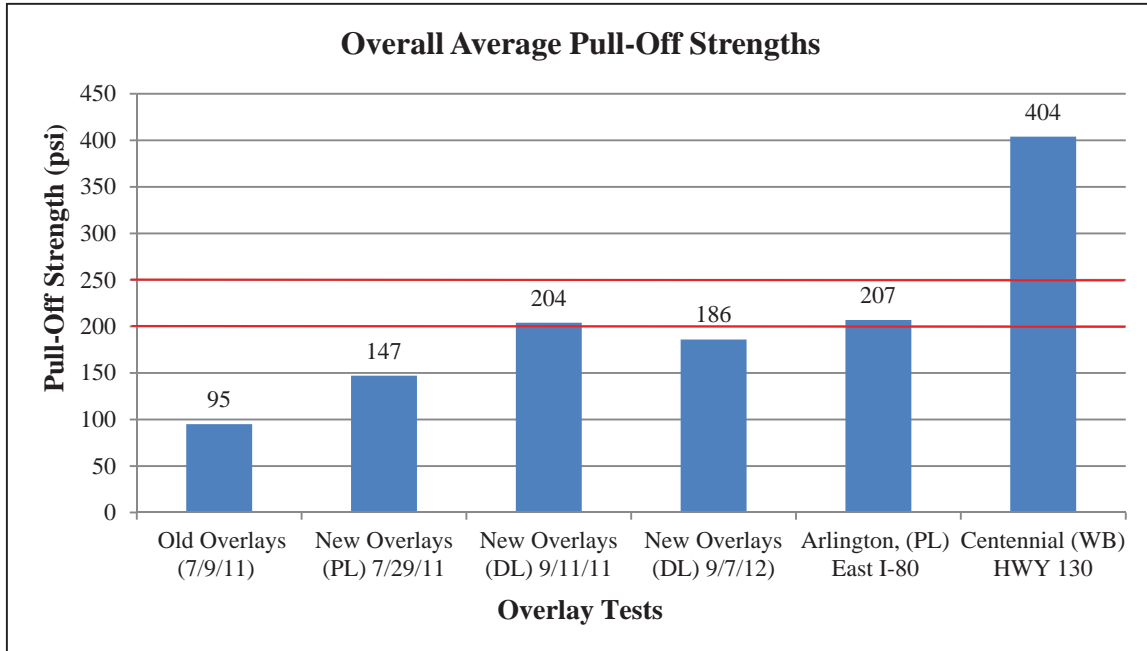
Figure 2.7. Bar chart of overall average pull-off strengths.
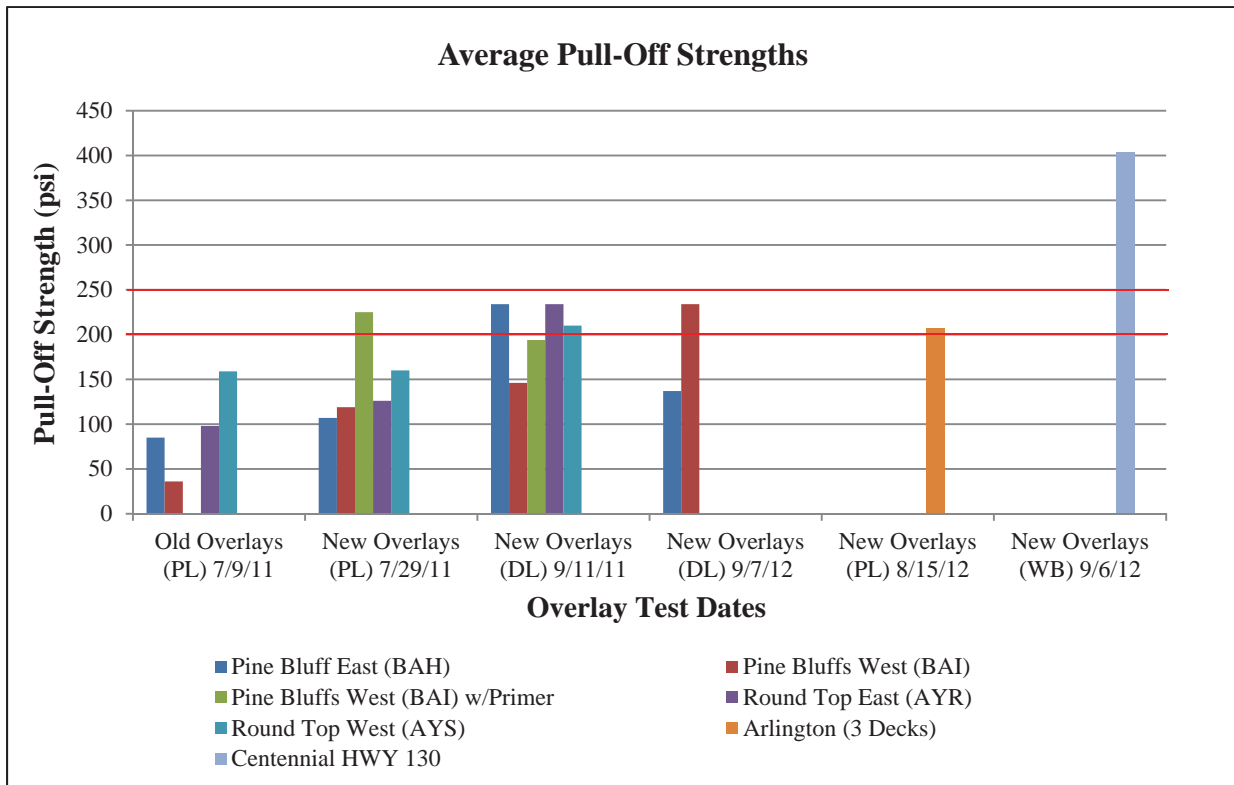
Figure 2.8. Bar chart for average pull-off strengths for each bridge deck.
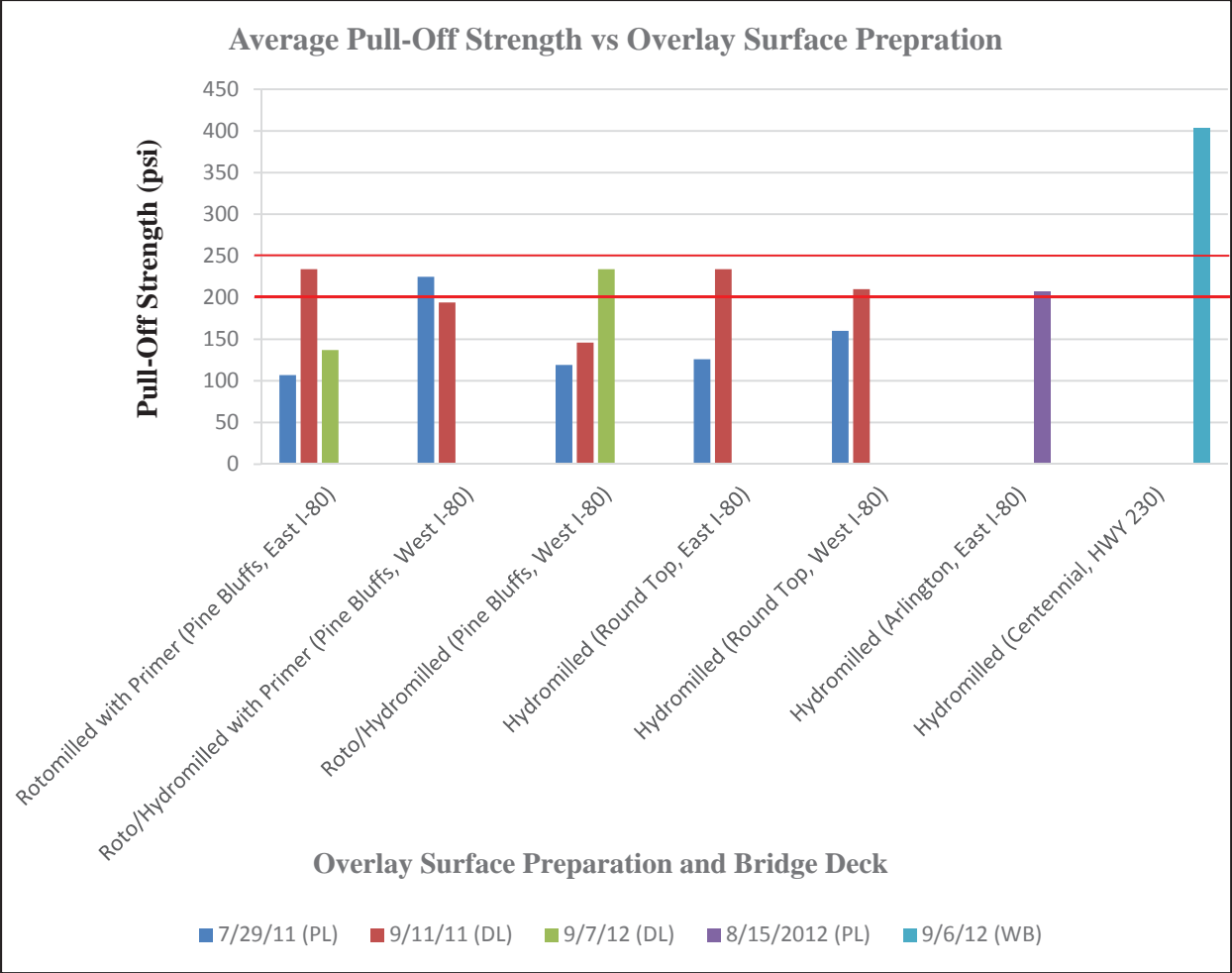
Figure 2.9. Bar chart for average pull-off strength versus overlay surface preparation.

2.4   PULL-OFF STRENGTH CONCLUSIONS

As shown in Figure 2.7 above, the overall average pull-off strengths for the old or existing overlays was 95 psi. Specifically, average pull-off strengths (Figure 2.8) for the Pine Bluffs I-80 and Round Top I-80 East and West bound lanes were 85, 36, 98 and 159 psi (586, 248, 676 and 1096 kPa), respectively.   All values were less than the 250 psi (1724 kPa) and the 200 psi (1379 kPa) bond strength recommended by the American Concrete Pavement Association for 3 inch overlays or thicker. In fact, all bond strengths were less than the 175 psi (1207 kPa) indicating a damaged or inadequate bond surface.

As shown in Figure 2.7 above, the overall average pull-off strengths for all of the new overlays were 147, 204, 186, 207 and 404 psi (1014, 1407, 1282, 1427, and 2786 kPa). For the Pine Bluffs and Round Top bridge decks and as shown in Figure 2.8, pull-off strengths for new overlays varied from a low of 107 psi (738 kPa) to a high of 234 psi (1613 kPa) with an average value of 177 psi (1220 kPa). All bond strengths for the Pine Bluffs and Round Top bridges were

24

less than 250 psi (1724 kPa). At 404 psi (2786 kPa), only the average strength for the Centennial bridge exceeded the 250 psi (1724 kPa) value.

As shown in Figure 2.8, only five out of the 12 data sets had bond strengths exceeding the recommended minimum 200 psi (1379 kPa) strength. Bond strength for seven of the data sets fell below the 200 psi (1379 kPa) value and six of those fell below 175 psi (1207 kPa). Most of the pull-off tests for the Pine Bluffs and Round Top bridges indicate the bond strength of the new overlays was inadequate to ensure proper bonding or to maintain bonding of the overlays.

In general, the failure zone for the pull-off tests occurred superficially within the concrete substrate for the new overlays installed on the Pine Bluffs and Round Top bridges followed by failure at the bond interface. Photo 2.5 above shows the common failure mode for the Pine Bluffs and Round Top pull-off tests.

As shown above in Figures 2.2 – 2.4, the average pull-off strengths for the Arlington (East I-80) and Centennial (HWY 130, MP 22.04) were 207 psi (1427 kPa) and 404 psi (2786 kPa), respectively. Majority of the pull-off failures occurred superficially within the concrete substrate followed by failure at the bond interface similar to the failure modes of the Pine Bluffs and Round Top bridges.

The Centennial bridge is located on a seasonable road with limited traffic as compared to the other bridges located on I-80 with heavy truck traffic. It is unclear why the pull-off strengths for the Centennial bridge were substantially higher.

In conclusion, it appears all the bond strengths except for the Centennial bridge fall below the 250 psi (1724 kPa) strength recognized as achievable value. Results indicate the bond strengths for the overlays tested, except for the Centennial bridge, are low and in some cases extremely low.

2.4.1   Questions and Answers

As part of the research, WYDOT wanted to evaluate the bond strength resulting from rotomilling versus hydroblasting with and without a portland cement mortar primer. To summarize the findings related to the surface preparation technique and primer, the following questions were answered using unpaired t tests with a 95 percent confidence interval as shown below in Table 2.10.

1. Did the rotomilling/hydroblasting surface preparation technique with a mortar primer increase the overlay bond strength as compared to just rotomilling with a mortar primer?

   Answer: No

As shown below in Table 2.3.1, the difference in the pull-off strengths for the different surface preparation techniques (210 psi versus 158 psi, 1448 kPa versus 1089 kPa) was not statistically different.

2. Did the rotomilling/hydroblasting surface preparation technique without a mortar primer increase the overlay bond strength as compared to rotomilling with a mortar primer?

   Answer: No
   The difference between the pull-off strengths for the different surface preparation techniques (186 psi versus 158 psi, 1282 kPa versus 1089 kPa) was not statistically significant.

3. For the rotomilling/hydroblasting, did using a mortar primer increase the bond strength of the overlay?

   Answer: No
   The difference between the pull-off strengths with and without a mortar primer (210 psi versus 186 psi, 1448 kPa versus 1282 kPa) was not statistically significant.

4. For the rotomilling with a mortar primer, did the time of the pull-off testing (9 and 16 days versus 378 days) affect the bond strength of the overlay?

   Answer: No
   Although the pull-off strength for the nine and 16-day testing was 176 psi (1214 kPa) and 137 psi (945 kPa) for testing at 378 days, the unpaired t test shows the difference was not statistically significant.

5. For the rotomilling/hydroblasting without a mortar primer, did the time of the pull-off testing (10 days versus 372 days) affect the bond strength of the overlay?

   Answer: Yes
   The unpaired t test shows the difference between the 10-day versus the 372-day pull-off strengths (126 versus 234 psi, 869 kPa versus 1613 kPa) was extremely statistically significant.

Therefore, there was no statistically difference between the bond strengths achieved from rotomilling versus hydroblasting with or without a portland cement primer.

For question number 4 above, it appears the bond strengths for the Pine Bluffs bridge (BAH, I-80 East) may have deteriorated after a year of service and exposure to traffic and winter. It is unclear why the bond strengths of the Pine Bluffs bridge (BAI, I-80 West) as referenced in question number 5 were higher than the earlier tests.

Table 2.10. Unpaired t Test Results (95 Percent CI)

Question	Group 1			Group 2			Statistically Significance	
	Avg.	Std.	n	Avg.	Std.	n	P Value*	Difference
1	Rotomilling/Hydroblasting with primer – BAI (7/29/11 & 9/11/11)			Rotomilling with primer - BAH (7/29/11, 9/11/11 & 9/7/12)			0.1541	Not statistically significant
	210 psi	44 psi	6	158 psi	83.9 psi	33		
2	Rotomilling/Hydroblasting without primer – BAI (7/29/11, 9/11/11 & 9/7/12)			Rotomilling with primer - BAH (7/29/11, 9/11/11 & 9/7/12)			0.1972	Not statistically significant
	186 psi	84 psi	28	158 psi	83 psi	34		
3	Rotomilling/Hydroblasting with primer – BAI (7/29/11 & 9/11/11)			Rotomilling/Hydroblasting without primer – BAI (7/29/11, 9/11/11 & 9/7/12)			0.5096	Not statistically significant
	210 psi	44 psi	6	186 psi	84 psi	28		
4	Rotomilling with primer – BAH (7/29/11 & 9/11/11) tested 9 & 16 days after placing overlay			Rotomilling with primer – BAH (9/7/12) tested 378 days after placing overlay			0.1835	Not statistically significant
	176 psi	101 psi	18	137 psi	54 psi	15		
5	Rotomilling/Hydroblasting without primer – BAI (7/29/11 & 9/11/11) tested 10 days after placing overlay			Rotomilling/Hydroblasting without primer – BAI (9/7/12) tested 372 days after placing overlay			0.0003	Extremely statistically significant
	126 psi	32 psi	13	234 psi	87 psi	15		

3.0   LABORATORY INVESTIGATION

To understand the properties of the silica fume concrete overlay mixtures commonly used by the Wyoming Department of Transportation (WYDOT) for bridge deck overlays, the WYDOT Materials Laboratory located in Cheyenne, WY, performed plastic and hardened concrete tests on twelve overlay mixtures as summarized below in Table 3.1. Using laboratory mixtures, WYDOT technicians performed plastic concrete testing that included slump, total air content and unit weight. [10,11,12] Table 3.2 shows the coarse and fine aggregate gradations for the mixtures.

Table 3.1. Overlay Laboratory Mixes - Proportions and Plastic Properties

Mix No.	Mix Proportions (lbs/yd³)					Plastic Properties			
	Coarse Aggr.	Fine Aggr.	Portland Cement	Silica Fume	Net Water	w/cm	Slump (inch)	Total Air (percent)	Unit Weight (lbs/ft³)
1	1,800	1,200	658	60	287	0.40	7.75	6.5	141.7
2	1,795	1,245	705	60	306	0.40	5.75	12.0	135.2
3	1,690	1,139	658	53	284	0.40	2.25	4.9	140.9
4	1,693	1,131	658	53	284	0.40	8.50	13.0	130.6
5	1,760	1,062	709	53	300	0.39	3.25	7.7	140.9
6	1,680	1,320	658	55	270	0.38	2.00	4.5	147.1
7	1,749	1,167	600	48	258	0.40	1.00	4.8	140.9
8	1,790	1,196	600	48	258	0.40	1.00	4.3	147.1
9	1,810	1,295	600	49	247	0.39	7.25	5.6	139.5
10	1,768	1,280	590	48	255	0.40	2.50	7.0	139.3
11	1,748	1,200	600	48	259	0.40	9.50	13.0	133.0
12	1,911	1,075	590	48	255	0.40	6.50	8.5	139.9

Table 3.2. Overlay Laboratory Mixes – Aggregate Gradations

Mix No.	Coarse Aggregates (Percent Passing)									Fine Aggregates (Percent Passing)							
	1/2”	3/8”	#4	#8	#16	#30	#50	#100	#200	3/8”	#4	#8	#16	#30	#50	#100	#200
1	100	87	22	3	1	0	0	0	0.0	100	99	90	68	45	22	7	0.4
2	100	98	20	2	1	1	1	0	0.4	100	97	82	63	38	13	4	1.0
3	100	92	24	4	2	2	1	1	0.3	100	95	78	56	33	12	5	2.3
4	100	100	10	3	2	2	2	2	0.8	100	99	87	66	41	18	6	1.7
5	100	94	16	4	2	2	2	2	1.3	100	100	86	60	34	10	4	1.0
6	100	97	12	2	2	1	1	1	0.9	100	100	92	70	43	16	6	2.7
7	100	100	10	3	2	2	2	2	0.8	100	99	87	66	41	18	6	1.7
8	100	94	16	4	2	2	2	2	1.3	100	100	86	60	34	10	4	1.0
9	100	99	42	6	5	5	4	3	1.8	100	99	94	72	42	15	6	3.0
10	100	90	60	6	5	5	4	3	1.9	100	99	94	72	42	15	6	3.0
11	95	58	15	5	3	2	2	1	0.5	100	99	94	72	42	15	6	3.0
12	90	60	25	8	4	4	4	3	1.5	100	99	94	72	42	15	6	3.0

As shown above in Table 3.1, the silica fume overlay mixtures on an average contained 1,766 lbs/yd³ (1048 kg/m³) of coarse aggregates, 1,193 lbs/yd³ (708 kg/m³) of fine aggregates, 636 lbs/yd³ (377 kg/m³) of portland cement, 52 lbs/yd³ (31 kg/m³) of silica fume and 272 lbs/yd³ (161 kg/m³) of net water. In general, the water to cementitious materials (w/cm) ratio was 0.40.

As shown above in Table 3.2, the overlay mixes were essentially pea-gravel mixes where 10 of the 12 mixtures had 100 percent of the coarse aggregate passing the ½-inch size sieve.

3.1   HARDENED CONCRETE PROPERTIES INCLUDING SHRINKAGE RESULTS

For the silica fume overlay mixtures created in the laboratory, WYDOT technicians also performed the following hardened concrete tests: compressive strength, resistance to chloride penetration (RCP), concrete shrinkage (bar length change) and concrete restrained ring shrinkage. [8,9,13,14] Table 3.3 below summarizes the hardened concrete test results.

Table 3.3. Overlay Laboratory Mixes – Hardened Concrete Properties

Mix No.	Strength (psi)		RCP (Coulombs)		Shrinkage – Bar Length Change (Percent)						Restrained Ring Shrinkage
	Days		Days		Days After Casting (Days of Air Storage)						Days to 1st Crack
	14	28	28	45	11 (4)	14 (7)	21 (14)	35 (28)	63 (56)	119 (112)	
1	8,880	11,620	602	617	0.013	0.049	0.061	0.074	0.083	0.103	9
2	6,200	7,760	460	518	0.015	0.042	0.053	0.064	0.069	0.080	10
3	7,880	10,230	886	665	0.014	0.028	0.039	0.048	0.060	0.063	21+
4	6,450	8,170	927	603	0.012	0.029	0.039	0.052	0.061	0.066	13
5	6,100	7,740	1,445	817	0.017	0.039	0.051	0.058	0.075	0.076	14
6	7,020	9,750	835	576	0.020	0.037	0.055	0.062	0.077	0.093	21+
7	7,340	10,930	273	436	0.019	0.027	0.040	0.052	0.054	0.077	21+
8	6,220	8,780	1,180	775	0.033	0.040	0.055	0.072	0.075	0.100	10
9	5,160	11,520	719	862	0.051	0.072	0.099	0.116	0.134	0.110	6
10	7,590	10,250	1,066	651	0.033	0.053	0.077	0.114	0.123	0.096	5.5
11	7,060	9230	3,044	3043	0.026	0.072	0.089	0.095	0.074	0.097	7
12	7,820	9540	1,451	984	0.025	0.058	0.073	0.080	0.077	0.085	3.5
AVG	6,980	9,630	1,074	879	0.023	0.046	0.061	0.074	0.080	0.087	-

As shown above, the 28-day compressive strengths varied from 7,740 psi (53.4 MPa) to 11,620 psi (80.1 MPa) with an average strength of 9,960 psi (68.7 MPa) for the overlay mixtures evaluated.

With an average 1,074 coulombs, the 28-day chloride penetration resistances were low as defined by ASTM C1202. In general, resistances varied from 719 to 1451 coulombs with one moderate value of 3,044 coulombs. WYDOT does not specify a maximum resistance but accepts overlay mixtures with values approaching and less than 1,000 coulombs.

3.1.1 ASTM C157 Shrinkage Results

As shown below in Figure 3.1, ASTM C157 or bar length changes were measured at 11, 14, 21, 35, 63 and 119 days after mixing and casting the specimens. Table 3.3 above summarizes the ASTM C157 test results.

In accordance with the requirements of ASTM C157, specimens were cast and then cured in a moist room for 23½ ± ½ hours. Then, technicians demolded and placed the specimens in lime-saturated water maintained at 73 ± 1 °F for a minimum of 30 minutes. At the age of 24 ± ½ hours after the mixing operations, specimens were removed from the water, wiped with a damp cloth and the length was measured to obtain the initial comparator reading.

Figure 3.1. Photo - Length comparator used to measure shrinkage of 4" x 4" x 11¼" concrete bars in accordance with ASTM C157/C157M - 08(2014) Standard Test Method for Length Change of Hardened Hydraulic-Cement Mortar and Concrete.

After the initial comparator reading, technicians stored the specimens in lime-saturated water at 73 ± 3 °F until they reached an age of seven days including the time period in the molds. At the end of the curing period, technicians performed the second comparator reading and placed the specimens in the air storage within the concrete laboratory. Technicians performed comparator readings after periods of 4, 7, 14, 28, 56 and 112 days of air storage.

In accordance with ASTM C157, length change of the specimens was computed as shown below:

$$\Delta Lx = \frac{CRD - initial\ CRD}{G}\ x\ 100$$

where:

ΔLx = length change of specimens at any age, (percent),

CRD = difference between the comparator reading of the specimen and the reference bar at any age, and

G = the gage length.

Table 3.3 above summarizes the 4, 7, 14, 28, 56 and 122-day (air-dried) concrete shrinkages for the 12 silica fume concrete mixtures evaluated. As shown in Table 3.3, the average 28-day (air-dried) shrinkage was 0.074 percent with values varying from 0.048 percent (Mix No. 3) to 0.166 percent (Mix No. 9).

As discussed in Section 6.5, the measured ASTM C157 concrete shrinkages shown in Table 3.3 are excessive for a bonded concrete overlay with a thickness equal to or less than 5 inches for relative humidities that commonly occur in Wyoming. Chapter 5 shows the shrinkage potential of the concrete overlay mixtures significantly influences the stresses along the bond line between the overlay and substrate concrete. Large shrinkage of the overlay concrete mixture can cause bond line failures and curling of the overlay concrete.

3.1.2   ASTM C157 Restrained Ring versus ASTM C157 Concrete Shrinkage

As shown above in Table 3.3, the days until the appearance of the first restrained-shrinkage crack as determined by ASTM C1581 (restrained ring shrinkage) varied from 3.5 to 21+ days. The time to first cracking is a function of the fresh and hardened concrete properties including the rate and magnitude of the shrinkage and tensile capacity versus time relationship for the overlay concrete mixtures. Figure 3.2 below shows the relationship between days to first cracking as determined by ASTM C1581 and 28-day shrinkage as determined by ASTM C157.
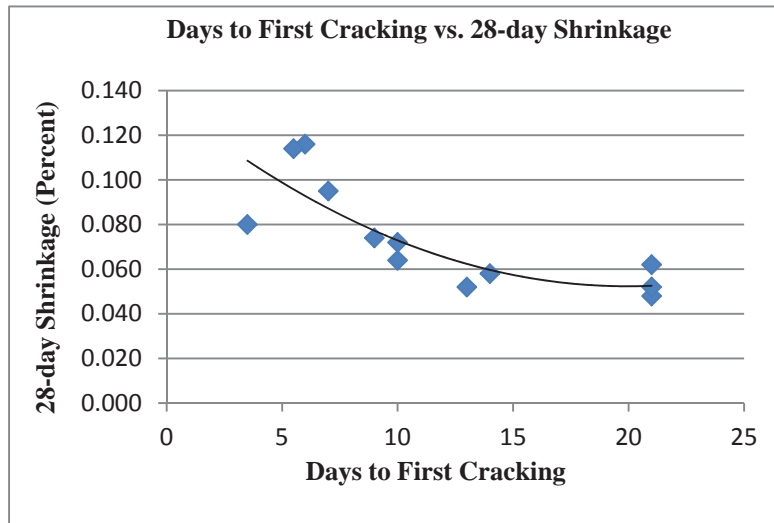
Figure 3.2. Days to First Cracking versus 28-day Air-dried Shrinkage for Silica Fume Concrete Overlay Mixtures.

As shown in Figure 3.2, there was a non-linear relationship between the measured 28-day (air-dried) shrinkage and the number of days to first cracking. In general, reducing the rate and magnitude of the concrete shrinkage reduces the risk of cracking. Therefore, reducing the shrinkage potential of the silica fume concrete overlay mixtures should reduce the potential for cracking, curling and subsequent debonding of the bridge deck overlays.

4.0   PETROGRAPHIC EXAMINATIONS

As part of the research project, DRP Consulting, Inc. (DRP) conducted petrographic examinations on cores extracted from bridge decks with bonded silica fume overlays constructed by the Wyoming Department of Transportation (WYDOT). The main purpose of the requested petrographic investigation was to help determine potential causes for premature cracking and deterioration of the overlays, which in several cases involved failures at or near the bonding surface.

4.1   INTRODUCTION

On January 12, 2012, DRP received fourteen (14) cores from KB Engineering, LLC (KBE). On December 7, 2012 DRP received two additional cores from KBE as listed in Table 4.1. On March 7, 2013 DRP received an additional fifteen (15) cores from KBE as listed in Table 4.2.

Table 4.1. Summary of Identifications and Locations of Cores Received in 2012

KBE No.	DRP No.	WYDOT Core ID	Comments
1	16YD5222	Core BAH-C3	Vertical crack through core; overlay not cracked
2	16YD5223	Core BAH-C4D	Delaminated; Broke at overlay interface
3	16YD5224	Core BAI-C2	Intact core
4	16YD5225	Core BAI-C5D	Delaminated; Broke at overlay interface
5	16YD5226	Core BAI-PBW	Intact core
6	16YD5227	Core AYS-C4D	Broke just below overlay interface; cracked overlay
7	16YD5228	Core AYS-C7D	Broke just below overlay interface; cracked overlay
8	16YD5229	Core AYS-C8	Intact core
9	16YD5230	Core BAH-N3-4A	Rotomilled and mortar slurried prior to overlay (old WYTDOT method); Intact core
10	16YD5231	Core Pine Bluffs BAH-EBDL West	Rotomilled and mortar slurried prior to overlay (old WYTDOT method); Intact core
11	16YD5232	Core BAI-2N-4	FAST TRACK (rotomilled and then hydromilled prior to overlay); intact core
12	16YD5233	Pine Bluffs BAI-WBDL West end	FAST TRACK (rotomilled and then hydromilled prior to overlay); intact core
13	16YD5234	Roundtop AYR-EBDL West end	Only hydromilled prior to overlay; intact core
14	16YD5235	Core AYS-2N-4	Only hydromilled prior to overlay; intact core
15	16YD5665	NA	Shorter of two cores
15	16YD5666	NA	Longer of two cores

Table 4.2. Summary of Identifications and Locations of Cores Received in 2013

KBE No.	DRP No.	WYDOT Core ID	Comments/Testing
16	17YD5932	Pine Bluffs 400.58 E Bound	Middle (95 mm); ASTM C856 Petrography
17	17YD5933	Pine Bluffs 400.58 E Bound	Middle A (50 mm)
18	17YD5934	Pine Bluffs 400.58 E Bound	Middle B (50 mm)
19	17YD5935	Pine Bluffs 400.58 E Bound	Middle C (50 mm)
20	17YD5936	Pine Bluffs 400.58 E Bound	Middle D (50 mm)
21	17YD5937	Pine Bluffs - East End	95 mm; ASTM C856 Petrography
22	17YD5938	Pine Bluffs – W Bound	Middle (95 mm); ASTM C856 Petrography
23	17YD5939	Pine Bluffs East - West End A	BAH (95 mm); ASTM C856 Petrography
24	17YD5940	Pine Bluffs East - West End A	BAH A (50 mm)
25	17YD5941	Pine Bluffs East - West End A	BAH B (50 mm)
26	17YD5942	Pine Bluffs East - West End A	BAH C (50 mm)
27	17YD5943	Pine Bluffs - East Bound	East End BAH (95 mm); ASTM C856 Petrography
28	17YD5944	2204 A – Arlington- East I80	Aug 4 (95 mm)
29	17YD5945	2204 B – Arlington East I80	Aug 4 (95 mm)
30	17YD5946	2204 C – Arlington East I80	Aug 4 (95 mm); ASTM C856 Petrography

4.2   SCOPE OF WORK

The work involved petrographic analysis of the cores according to ASTM C856. [15] The investigation focused on the nature of the contact between the original bonded deck concrete (BDC) and the silica fume overlays (SFO) and any cracking or microcracking in the cores. The scope of work did not include thin section microscopy so detailed studies of the paste fraction of the materials were not done. The scope of work did not include microscopical analyses of the air void systems so air void analyses were not done. During the initial investigation of the cores received in 2012, evidence of alkali-silica reaction (ASR) was observed and reported.

A second round of sampling was done in 2013 and subsequent work focused on documenting the nature and extent of ASR in the 2012 and 2013 cores listed in Table 4.1 and Table 4.2. These cores were exposed to elevated temperature (T = 104°F, 40ºC) and relative humidity (RH = 100 percent) conditions for several days and then examined visually and microscopically to determine if exudations of ASR gel were present. Analyses of these exudations were done using SEM/EDS to determine the composition of the exudations.

This chapter summarizes the main findings from the petrographic examinations. Appendices to this report are organized as follows.

Appendix A   Photographs of cores in as-received condition

Appendix B   Photographs of prepared surfaces from cores

Appendix C   Concrete components

Appendix D   Cracking and microcracking

Appendix E   Alkali-silica reaction

Appendix F   Petrographic worksheets

Appendix G   Procedures

4.3   GENERAL FINDINGS

The following general findings are relevant to the concrete represented by the cores.

4.3.1   Core Orientation, Dimensions & As-received Condition

All the cores are vertical in orientation. The cores that are subjects of petrographic examinations measured 95 mm (3 ¾ in.) in diameter. The cores span from textured surfaces on top that display variable degrees of wear to fractured surfaces on the bottom such that the cores represent partial thicknesses of the deck slabs (Figure 4.1). The cores were all hard and compact. None of the cores contained embedded objects such as steel reinforcement but synthetic fibers were observed in some of the SFO concrete.

(a)   (b)

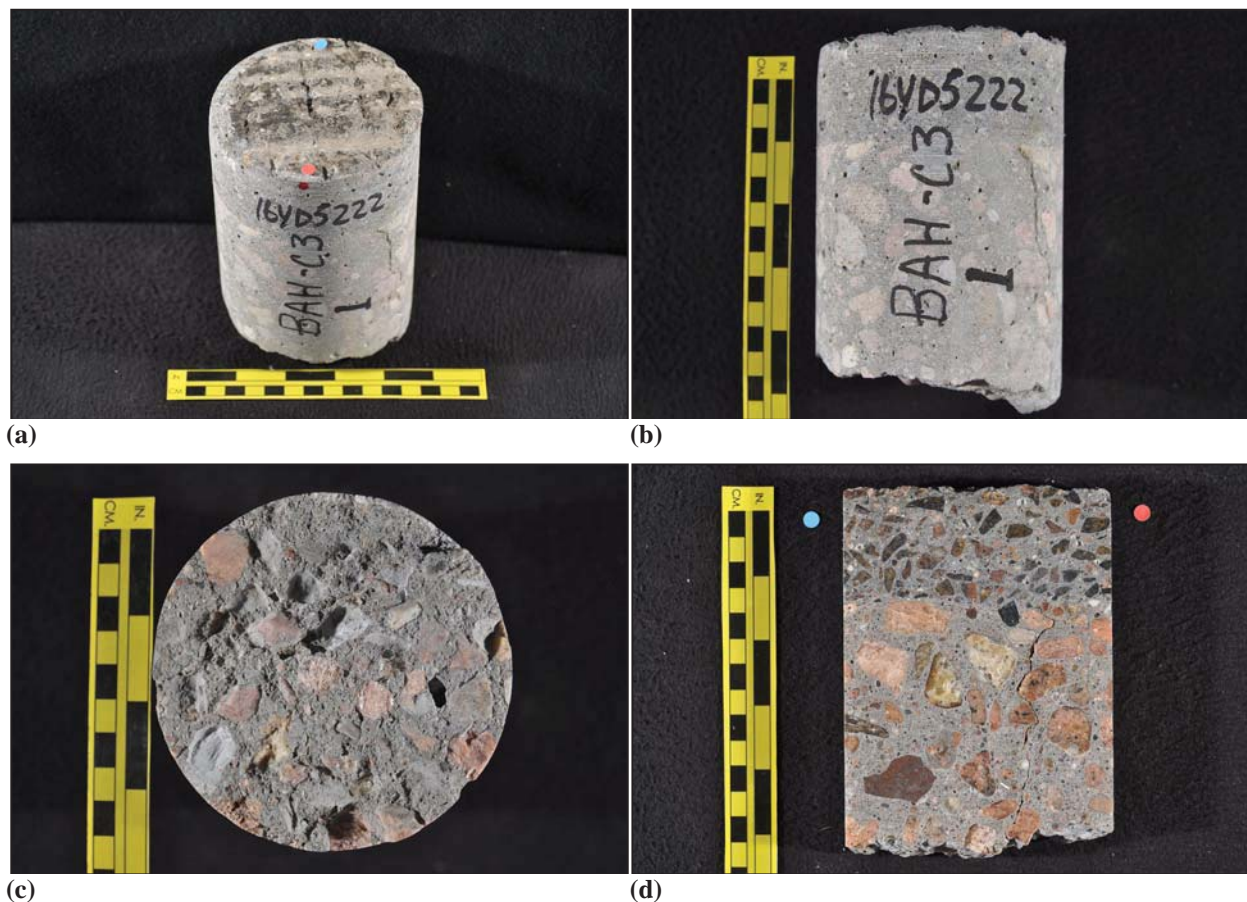(c)   (d)

Figure 4.1. Photographs showing example of typical core. (a) Oblique view of the core showing top and side; the red and blue dots indicate the orientation of the saw-cuts used to prepare the sample. (b) The side of the core showing markings used to identify the core. (c) The bottom fracture surface. (d) Polished surface of the core. The yellow scale bar is ~ 150 mm (6 in.) long.
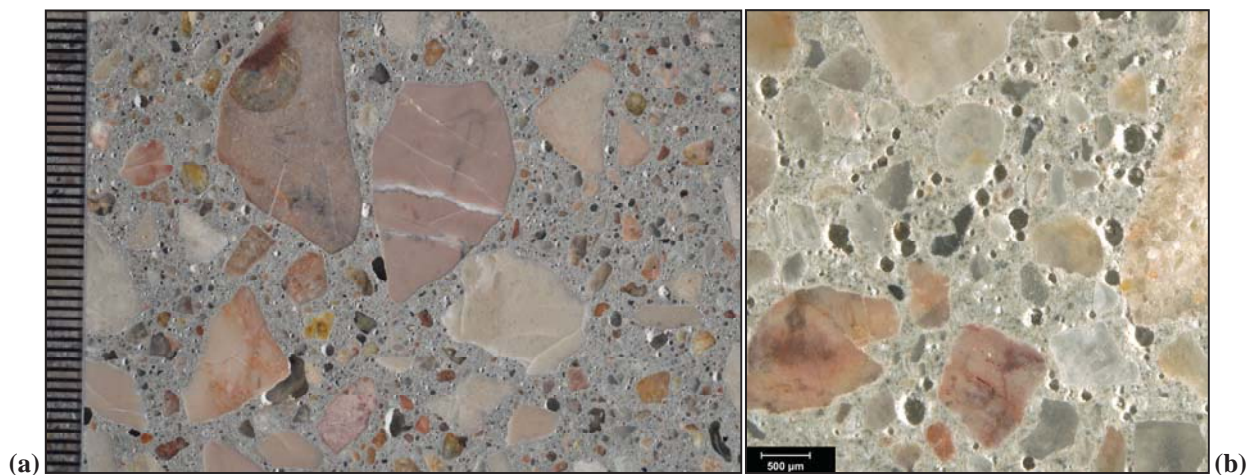
4.3.2 Concrete Components: BDC Aggregates

The BDC was made with two distinct types of aggregates. In the cores from Pine Bluffs, the BDC contains natural gravels that are siliceous in composition and consist primarily of granitic rocks (Figure 4.2). The nominal top size of the coarse aggregate ranges from 19-25 mm (¾-1 in.). The fine aggregate in the Pine Bluffs BDC is a natural sand that is siliceous in composition and consists primarily of granitic rocks, quartz and feldspar. In the Roundtop cores the BDC contains crushed quarried rocks that are carbonate in composition and consist of limestone (Figure 4.3). The nominal top size of the coarse aggregate is 19 mm (¾ in.). The fine aggregate in the Roundtop cores is a natural sand that is siliceous in composition and consists primarily of granitic rocks.
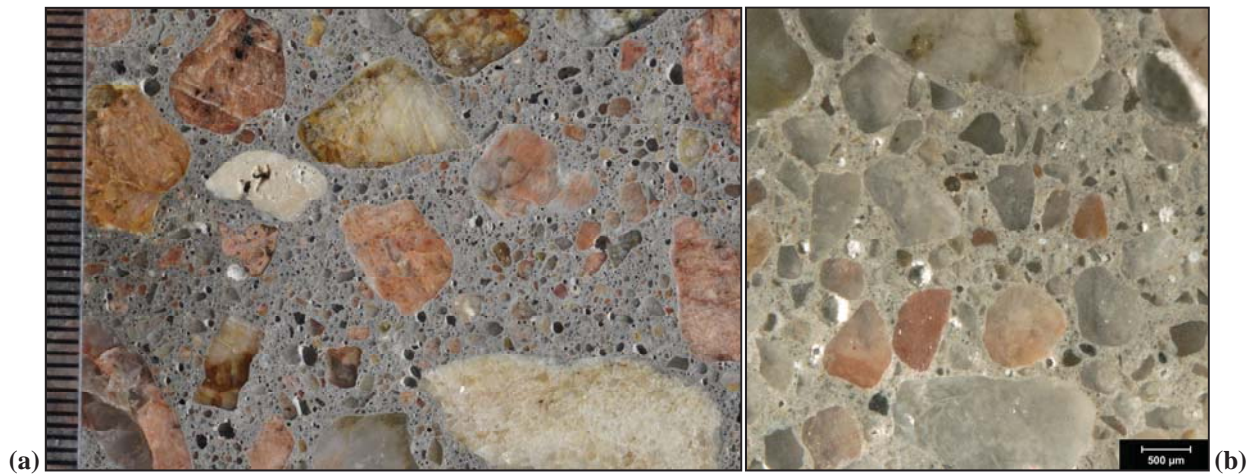
Figure 4.2. Aggregate in Pine Bluffs BDC. (a) Photograph and (b) reflected light photomicrograph of polished surface of Core 2 showing coarse aggregate and sand, respectively. Scale in millimeters in (a).

Figure 4.3. Aggregate in Roundtop BDC (a) Photograph and (b) reflected light photomicrograph of polished surface of Core 7 showing coarse aggregate and sand, respectively. Scale in millimeters in (a).

4.3.3   Concrete Components: SFO Aggregates

The SFO concrete was made with similar aggregates in all the cores. The coarse aggregate is a crushed gravel with a 9.5 mm (⅜ in.) nominal top size and the fine aggregate is a natural sand (Figure 4.4). The coarse and fine aggregates are siliceous in composition and consist primarily of granitic rocks, albeit different granites than were used in the production of the Pine Bluffs BDC.
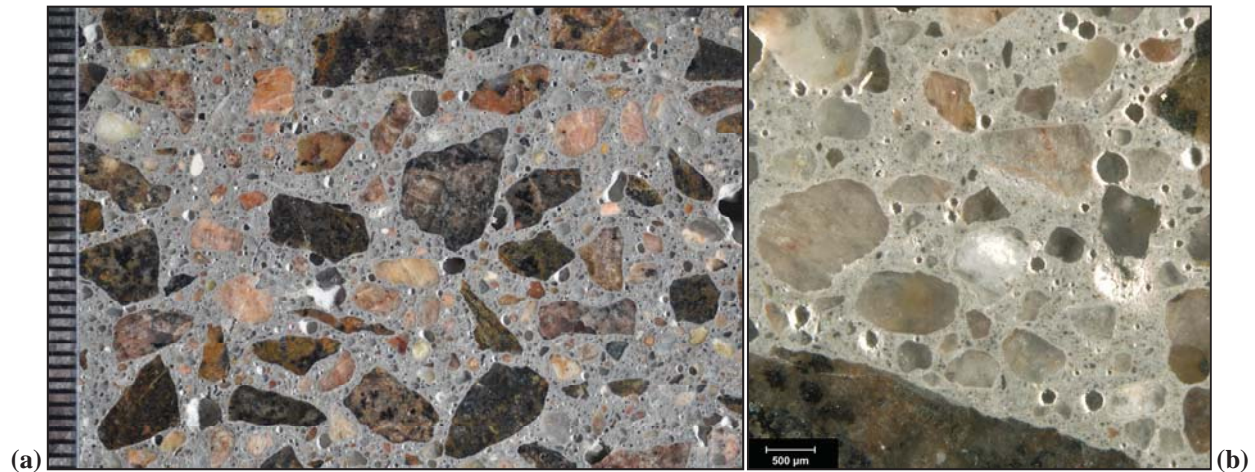

Figure 4.4. Aggregate in Pine Bluffs SFO. (a) Photograph and (b) reflected light photomicrograph of polished surface of Core 2 showing coarse aggregate and sand, respectively. Scale in millimeters in (a).

4.3.4   Concrete Components: Paste

Detailed studies of the paste in the BDC and SFO were not within the scope of work outlined for the project. The BDC in the Pine Bluffs and Roundtop cores have medium-gray paste that is smooth, has a sub-vitreous luster and is moderately hard. No grains of fly ash were observed. The SFO in the Pine Bluffs and Roundtop cores has gray paste that is smooth, has a sub-vitreous luster and is hard. No grains of fly ash were observed in the SFO samples.

4.3.5 Voids

Estimations of air contents were done from visual and microscopical observation; no quantitative point count work was done. The BDC in all the cores is air entrained; a few cores show SFO showing with low air and marginal air entrainment (Figure 4.5).

The BDC in the Pine Bluffs cores has estimated air contents that range from 5-8 percent. The air content of the SFO in the Pine Bluffs cores shows much more variability. Some cores show marginal air entrainment with 2-4 percent estimated air whereas others are air-entrained with air contents that range from 4-5 percent and 6-7 percent. The BDC in the Roundtop cores has estimated air contents that range from 4-7 percent. The SFO in the Roundtop cores has estimated air contents that range from 3-5 percent and 4-6 percent.
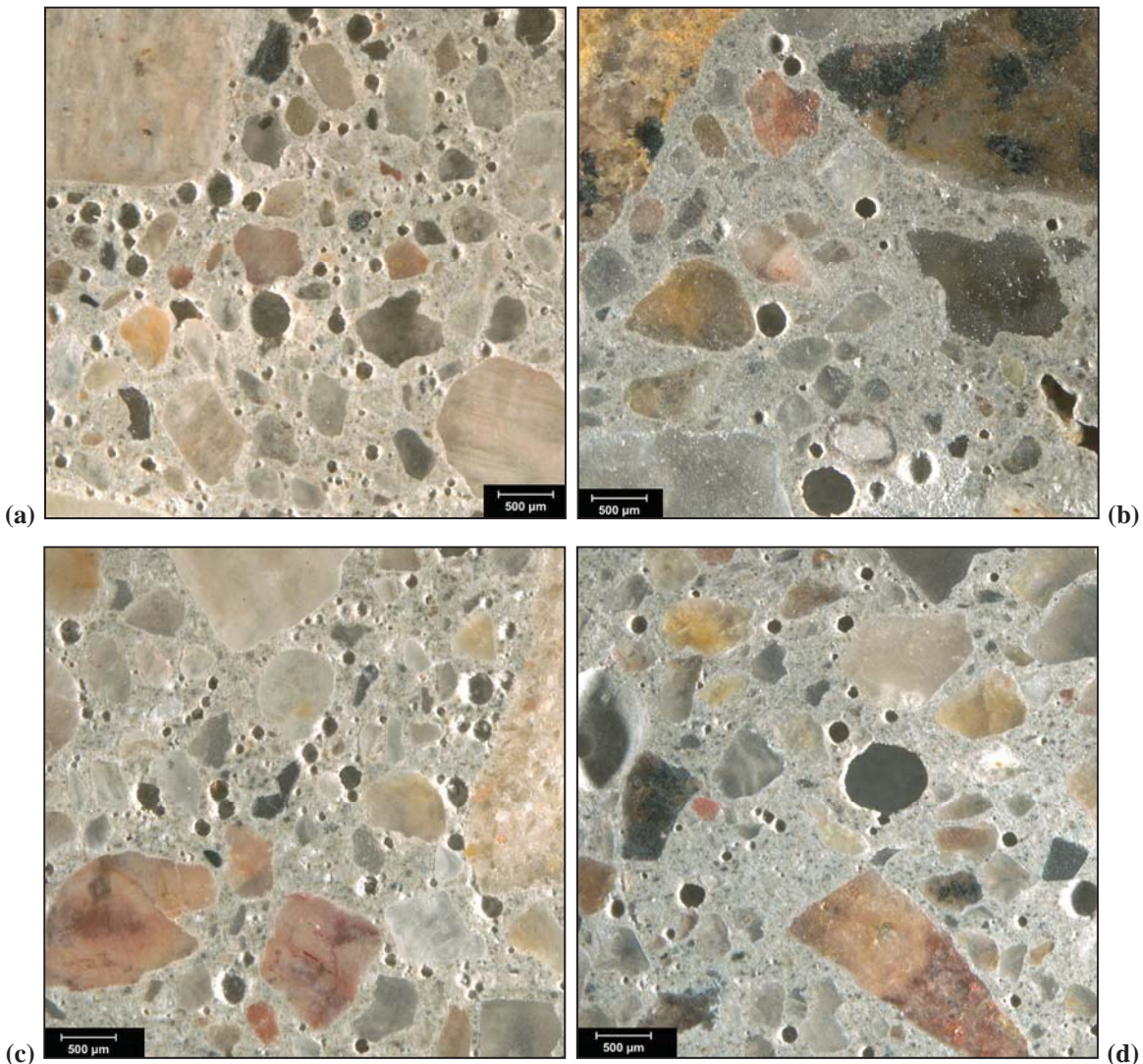
Figure 4.5. Photomicrographs showing examples of air void systems. (a) BDC in Core 3 (Pine Bluffs). (b) SFO in Core 3. This area of the overlay had low air (2-4 percent estimated) in the top of the overlay. (c) BDC in Core 7 (Roundtop). (d) SFO in Core 7. Note that all the photomicrographs are of polished slabs using oblique reflected light at the same magnification.

39

4.3.6 Cracking & Microcracking

Several different types of cracks were observed in the cores. The SFO in cores from both Pine Bluffs and Roundtop commonly show sub-vertical cracks and microcracks. Examples were observed that wrap around aggregate particles and lack secondary deposits, which are typical of drying shrinkage, and cracks that cut through aggregate particles, which are typical of other mechanisms (Figure 4.6). Such cracks are typical of drying shrinkage and were observed only very rarely in the BDC in these cores. The BDC in the cores show sub-horizontal cracks and microcracks near the contact with the SFO (Figure 4.7). These cracks and microcracks are also free of secondary deposits but cut both around and through aggregate particles. Section 3.4 and Appendix *D* provide details regarding these cracks. Cracking and microcracking related to ASR in both SFO and BDC was also observed and is discussed in more detail below.

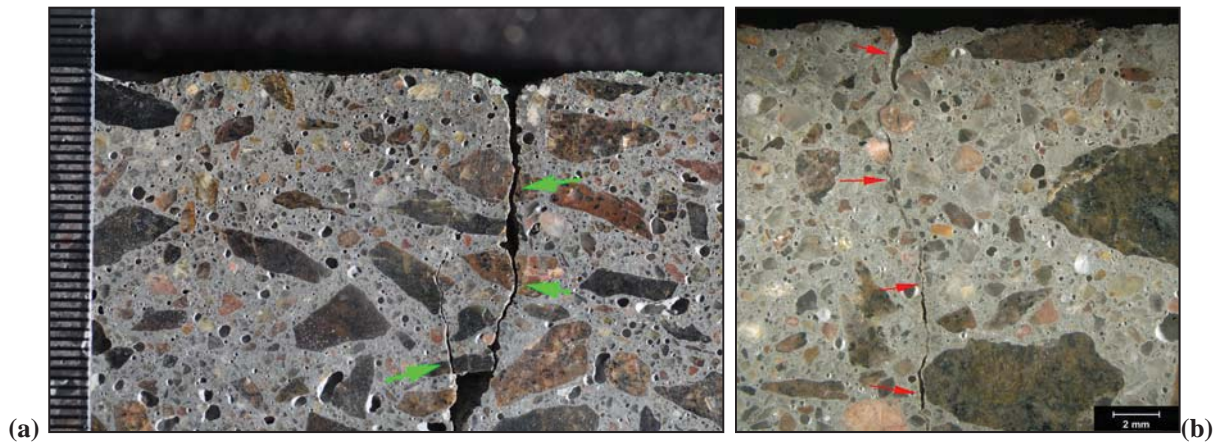(a)   (b)

Figure 4.6. Sub-vertical cracks and microcracks in SFO. (a) Photograph and (b) reflected light photomicrograph of polished surface of Core 6 and Core 7, respectively showing sub-vertical cracks and microcrack in the SFO. Note the crack in (a) cuts through aggregate particles.

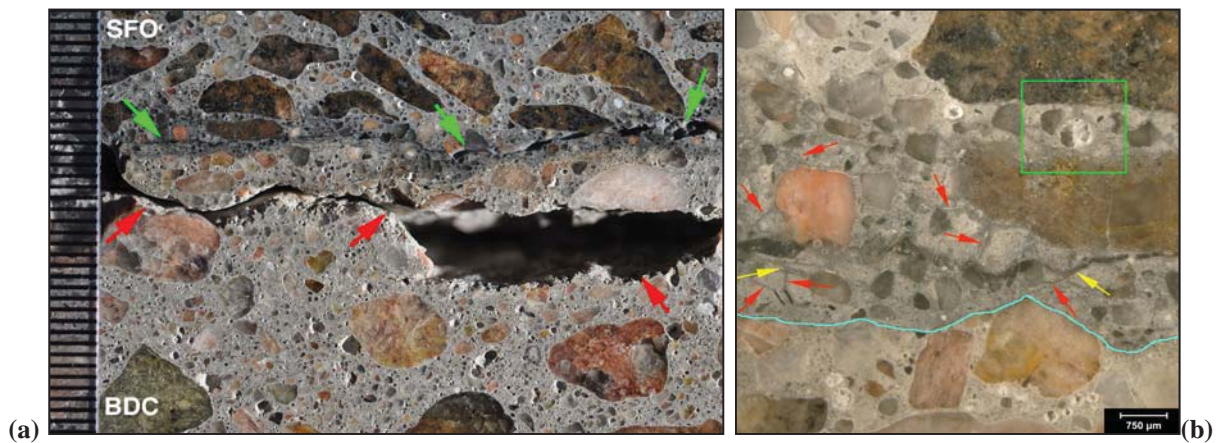(a)   (b)

Figure 4.7. Sub-horizontal cracking near the BDC/SFO contact (Core 4). (a) Photograph of the polished surface where the green arrows show a sub-horizontal crack in the SFO and the red arrows show a crack in the BDC. (b) Reflected light photomicrograph of the polished surface where the red and yellow arrows highlight oblique and sub-horizontal microcracks, respectively, in the SFO. The blue line marks the contact between the BDC and SFO and the green box indicates a void with deposits of ettringite and gel.

4.3.7 ASR

Variable levels of ASR were observed in the SFO and the BDC in many cores (Figure 4.8) but in general no significant cracking due to ASR was observed. Microcracking due to ASR was observed in many cores; *Appendix E* provides details of these observations. The reactive components in the SFO typically consist of rhyolite and occasionally granitic rocks in the fine aggregate. Exudations of gel were observed in the SFO in association with particles of granitic rocks and rhyolite after exposure of many cores to elevated T/RH conditions. In the BDC the reactive components include rhyolite and granitic rocks in the fine aggregate in both Roundtop and Pine Bluffs cores. The limestone aggregates that make up the coarse aggregate in the Roundtop cores showed no evidence of alkali-aggregate reactions. The granitic rocks present in the coarse aggregate in the Pine Bluffs cores occasionally showed evidence of ASR. SEM/EDS analysis of gels collected before and after exposure to elevated T/RH conditions show variable compositions (Figure 4.9).

(a)   (b)   (c)

(d)   (e)   (f)
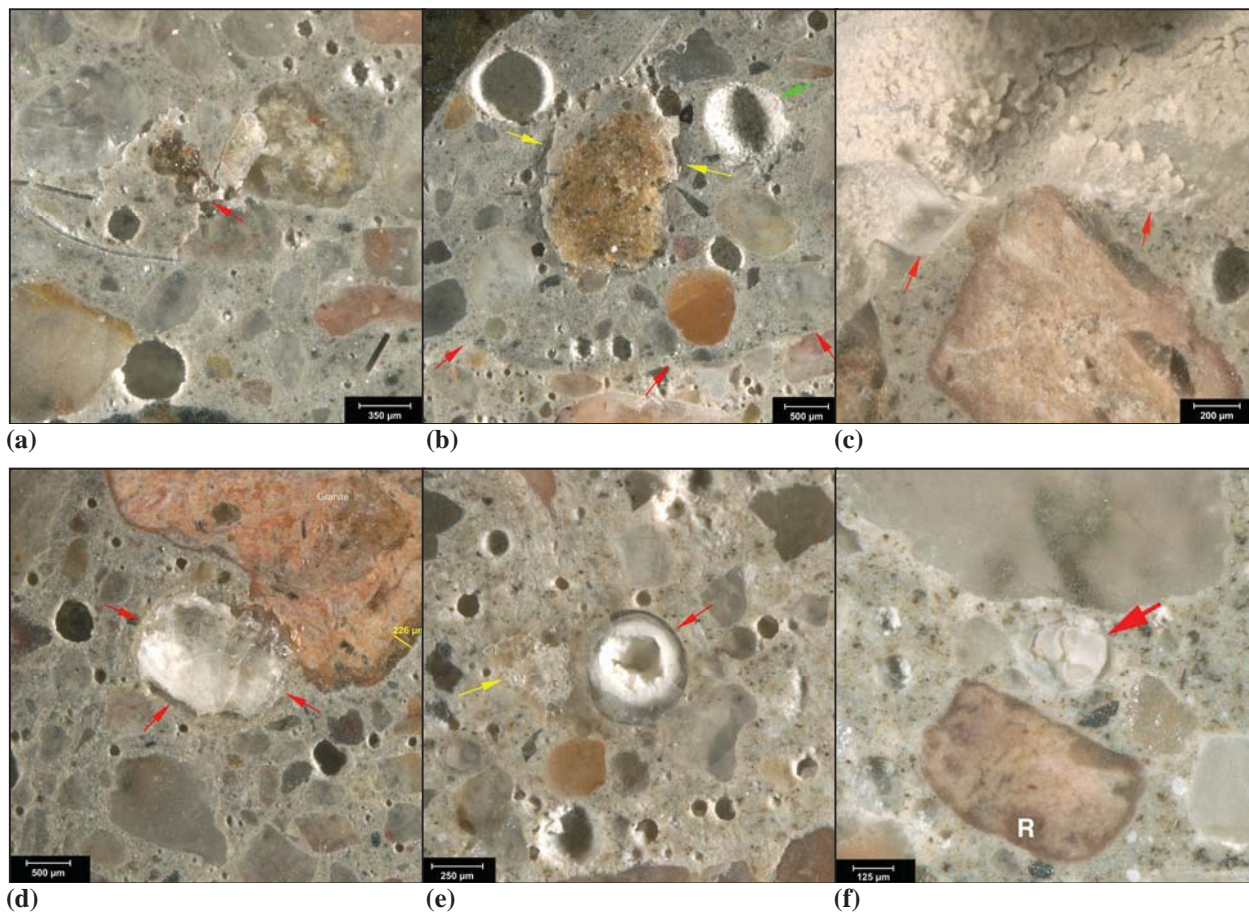
Figure 4.8. Examples of ASR in the SFO and BDC. Reflected light, polished surfaces showing (a)-(c) the SFO and (d)-(f) the BDC. (a) Core 2; the red arrow indicates a swollen siliceous volcanic rock. (b) Core 3; yellow arrows indicate margins of swollen granite particle, the green arrow indicates a void with deposits of ettringite and red arrows indicate the SFO/BDC contact. (c) Core 7; red arrows indicate gel lining void next to a rhyolite particle. (d) Core 2; red arrows highlight gel in void next to a granitic aggregate particle with a distinct reaction rim (yellow bar). (e) Core 4; red arrow highlights void with clear to white gel and yellow arrow indicates fractured aggregate particle. (f) Core 7; red arrow highlights deposit of gel in a void next to a rhyolite particle (R).

(a)

(b)

**(c)** Lsec: 10.0 0 Cnts 0.000 keV Det: Apollo X-SDD Det
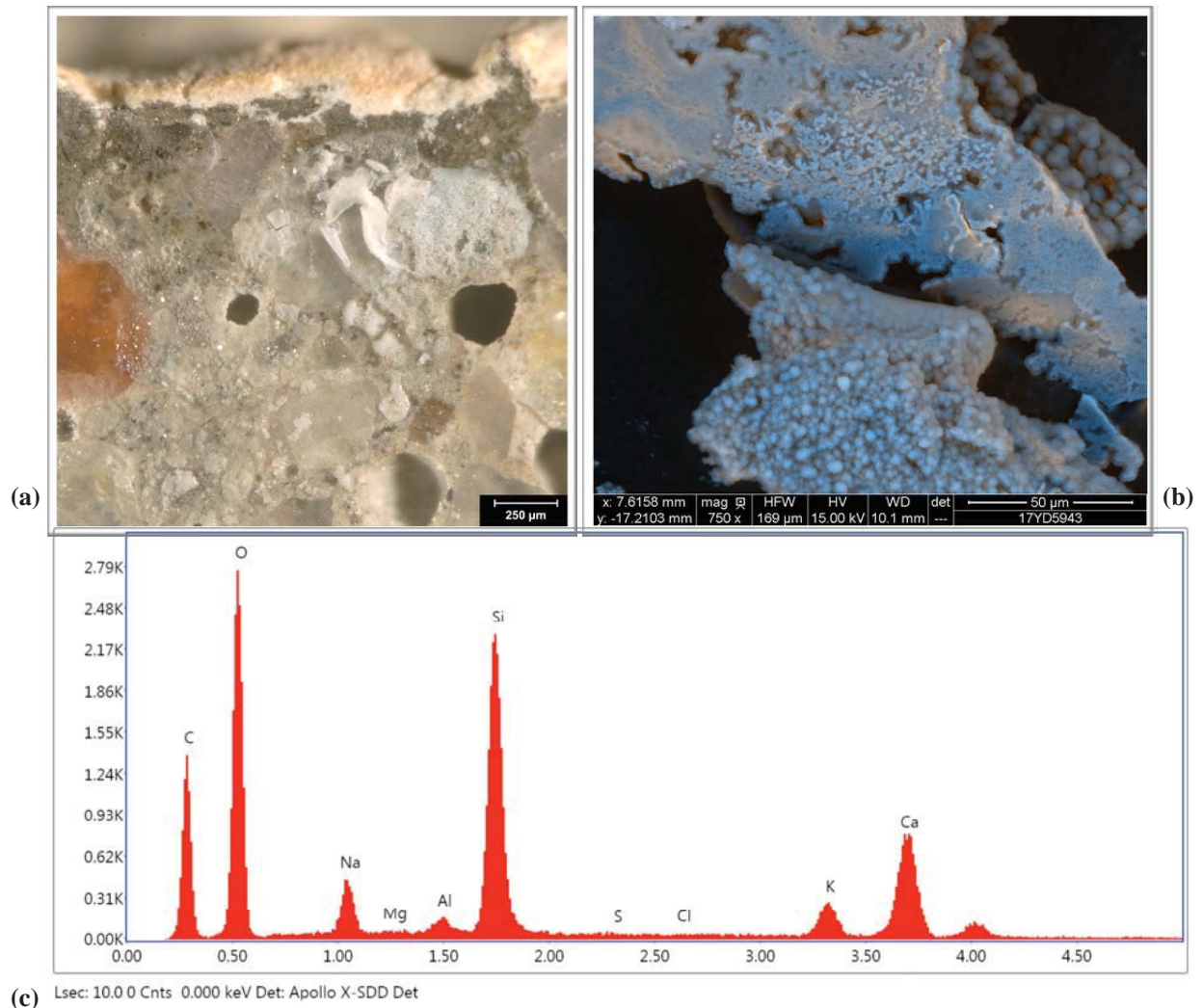
Figure 4.9. SEM/EDS analysis of gel exudation. (a) Reflected light photomicrograph of polished surface showing exudation in SFO after exposure to elevated T/RH conditions. (b) Combined backscatter and secondary electron micrograph of gel that was scraped from the surface and placed on a carbon tape. (c) EDS spectrum obtained from gel that indicates a composition consistent with alkali-silica reaction.

4.3.8 Carbonation/Ettringite

In general the cores show negligible levels of carbonation as detected from phenolphthalein staining (Figure 4.10); also see *Appendix B, Prepared Surfaces).* Deposits of ettringite are commonly observed in voids in both SFO and BDC from both Pine Bluffs and Roundtop cores (Figure 4.11). No cracking or microcracking due to ettringite mineralization was observed in any core.
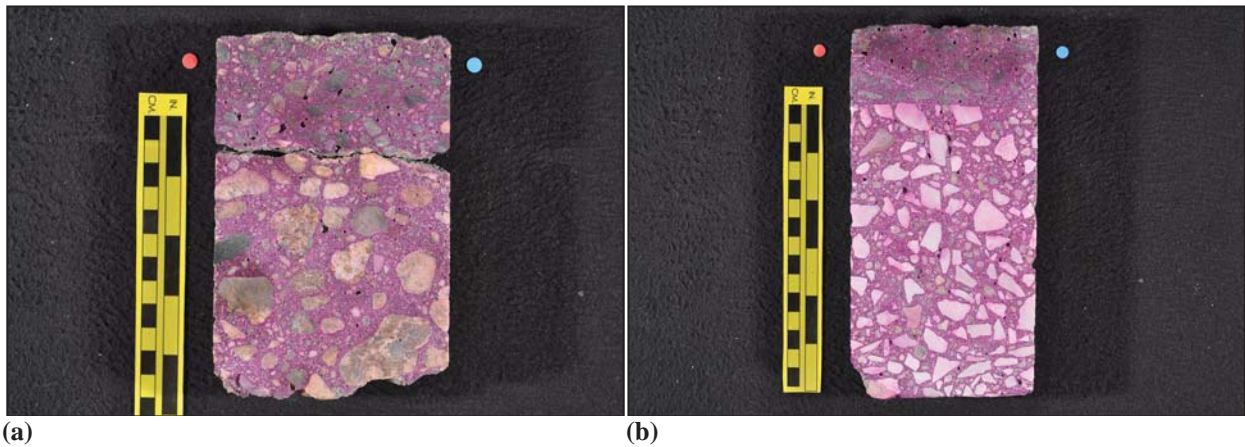
(a)   (b)

Figure 4.10. Carbonation determined from phenolphthalein. Photographs showing examples of phenolphthalein stained surfaces in (a) Core 2 and (b) Core 8. The yellow scale bar is ~ 150 mm (6 in.) long.
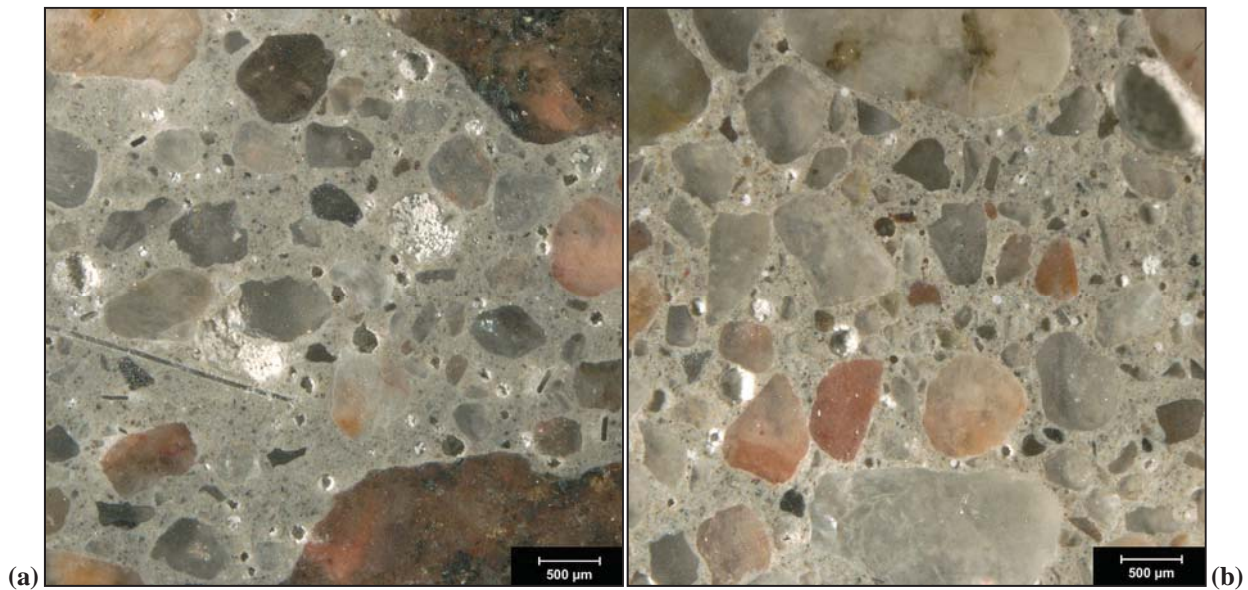
(a)   (b)

Figure 4.11. Deposits of ettringite in voids. Reflected light photomicrographs of polished slab from Core 2 showing examples of voids with deposits of ettringite in (a) the SFO and (b) the BDC.

4.4 FINDINGS REGARDING CRACKING & ASR BY CORE LOCATION

See *Appendix D* for photographs and photomicrographs that document details regarding the cracking and microcracking observed in the cores. Table 4.3 below summarizes information regarding cracking around the SFO/BDC contact in cores that were studied in detail. See *Appendix E* for photographs and photomicrographs that document details regarding ASR. Table 4.4 below summarizes information regarding ASR in cores that were studied in detail.

Table 4.3. Summary of Findings Regarding Cracking

WYDOT Core ID	Comments Regarding Cracking
Core BAH-C3	Sub-vertical drying shrinkage crack observed in SFO. Full depth drying shrinkage crack with deposits of ASR gel and ettringite along segments observed in BDC. Sub-horizontal cracks with microcrack splays observed in BDC subjacent to SFO contact.
Core BAH-C4D	Sub-vertical hairline shrinkage crack cuts through full thickness of SFO. Sub-horizontal microcracks observed near top surface of SFO. No cracking observed in the BDC.
Core BAI-C2	No cracks observed in SFO. Minor shrinkage microcrack in SFO. Sub-horizontal cracking and microcracking observed in BDC subjacent to SFO contact. ASR gel observed in these cracks and microcracks.
Core BAI-C5D	Sub-horizontal crack and microcracks with secondary deposits observed in SFO superjacent to the BDC contact. Sub-horizontal crack that cuts core in two observed in upper part of BDC subjacent to contact with SFO. Sub-horizontal hairline cracks and microcracks present at top of BDC that are free of secondary deposits. Microcracks filled with ASR gel observed near top of BDC; one microcrack with gel cuts across contact with SFO.
Core BAI-PBW	No cracking or significant microcracking observed in SFO. Sub-horizontal cracks and microcracks that are free of secondary deposits observed in BDC subjacent to SFO contact.
Core AYS-C4D	Shrinkage cracks and microcracks observed in SFO. Sub-horizontal crack occurs in BDC about 9.5-19 mm (⅜-¾ in.) below contact with SFO. Minor sub-horizontal microcracking observed in BDC subjacent to SFO contact.
Core AYS-C7D	Full depth shrinkage crack cuts through SFO. Sub-horizontal crack occurs *along* contact between SFO and BDC and then cuts obliquely through BDC. En echelon sub-horizontal cracks and microcracks observed in BDC subjacent to SFO contact and in BDC up to 12.5 mm (½ in.) below main sub-horizontal crack at SFO/BDC contact.
Core AYS-C8	No cracks observed in SFO. Minor shrinkage microcrack in SFO. Sub-horizontal cracking and microcracking observed in BDC subjacent to SFO contact. No secondary deposits observed in these cracks and microcracks. Sub-vertical microcracks typical of drying shrinkage observed at the top of the BDC.

Table 4.3. Summary of Findings Regarding Cracking

WYDOT Core ID	Comments Regarding Cracking
Core BAH-N3-4A[a]	No cracking or significant microcracking observed in SFO. Sub-horizontal microcracks that are free of secondary deposits observed in BDC along and subjacent to SFO contact along a 28 mm (1 ⅛ in.) long segment of the contact between the BDC and SFO.
Core Pine Bluffs BAH-EBDL West Bound[a]	No cracking or significant microcracking observed in SFO. Sub-horizontal microcracks that are free of secondary deposits observed only along a 28 mm (1 ⅛ in.) segment in BDC subjacent to SFO contact.
Core BAI-2N-4[b]	No cracking or significant microcracking observed in SFO. No cracks or microcracks observed near SFO/BDC contact. Rare, minor microcracks with ASR gel observed in BDC.
Cr Pine Bluffs BAI-WBDL West Bound End[b]	No cracks observed in SFO. Minor shrinkage microcracks and sub-horizontal microcracks observed at top of SFO. No cracks or significant microcracks observed in BDC.
Cr Roundtop AYR-EBDL West Bound End[c]	No cracks observed in SFO. Minor shrinkage microcracks and sub-horizontal microcracks observed at top of SFO. No cracks or significant microcracks observed in BDC.
Core AYS-2N-4[c]	No cracks observed in SFO. Minor shrinkage microcracks and sub-horizontal microcracks observed at top of SFO. Minor sub-horizontal to oblique microcracks observed in SFO superjacent to the BDC contact. The microcracks lack secondary deposits. No cracks or significant microcracks observed in BDC.
Longer of two cores	No cracking or significant microcracking observed in SFO. Sub-horizontal microcracks that are free of secondary deposits observed in BDC subjacent to SFO contact.
Pine Bluffs 400.58 East Bound Middle	No cracking or significant microcracking observed in SFO. Sub-horizontal microcracks that are free of secondary deposits observed in BDC subjacent to SFO contact.
Pine Bluffs East Bound End	Sub-vertical hairline shrinkage crack at top of SFO. No cracks in BDC. Minor sub-horizontal to oblique microcracks observed in BDC subjacent to the SFO contact.
Pine Bluffs West Bound	Sub-vertical plastic cracks observed in SFO. No cracks or significant microcracks in BDC. No cracking or microcracking at BDC/SFO contact.
East-West Bound End A	No cracking or significant microcracking observed in SFO. Sub-horizontal to oblique microcracks that are free of secondary deposits observed in BDC and mortar slurry subjacent to SFO contact.

Table 4.3. Summary of Findings Regarding Cracking

WYDOT Core ID	Comments Regarding Cracking
East Bound End BAH	No cracking or significant microcracking observed in SFO or BDC.
2204 C	No cracking or significant microcracking observed in SFO. Plastic microcracks that are free of secondary deposits observed in SFO superjacent to BDC contact.

[a] Old WYDOT surface preparation method involving rotomilling and then using a mortar slurry prior to placement of the overlay.

[b] FAST TRACK method involving rotomilling and then hydromilling prior to the placement of the overlay.

[c] Only hydromilling prior to placement of overlay.

Table 4.4. Summary of Findings Regarding ASR

WYDOT Core ID	Evidence Regarding ASR
Core BAH-C3	ASR gel observed lining main crack in BDC and in voids in BDC. Gel exudations observed in BDC and SFO after elevated T/RH exposure.
Core BAH-C4D	ASR gel observed in BDC and swollen fine aggregate observed in SFO. Gel exudations observed in SFO after elevated T/RH exposure.
Core BAI-C2	Swollen fine aggregate observed in SFO. Gel-filled microcracks observed in BDC. Gel exudations observed in BDC and SFO after elevated T/RH exposure.
Core BAI-C5D	Gel-filled microcracks and voids observed in BDC. Gel exudations observed in BDC and SFO after elevated T/RH exposure.
Core BAI-PBW	Gel-filled voids observed in SFO. Gel exudations observed in BDC and SFO after elevated T/RH exposure.
Core AYS-C4D	ASR gel in void in SFO and in microcracks in BDC. Gel exudations observed in SFO after elevated T/RH exposure.
Core AYS-C7D	ASR gel in voids in SFO and BDC. No exudations observed after elevated T/RH exposure.
Core AYS-C8	ASR gel in void in BDC. No exudations observed after elevated T/RH exposure.
Core BAH-N3-4A[a]	Gel-filled voids observed in BDC. No exudations observed after elevated T/RH exposure.
Core PineBluffs BAH-EBDL West[a]	Gel-filled microcracks and swollen fine aggregate observed in BDC. Gel exudations observed in BDC after elevated T/RH exposure.
Core BAI-2N-4[b]	Gel-filled microcracks and swollen fine aggregate observed in BDC. Gel exudations observed in BDC after elevated T/RH exposure.
Cr PineBluffs BAI-WBDL West End[b]	Gel in voids and as exudation on polished surface in BDC without elevated T/RH exposure. Gel exudations observed in BDC after elevated T/RH exposure.
Cr Roundtop AYR-EBDL West end[c]	Gel observed in BDC. Gel exudations observed in BDC after elevated T/RH exposure.
Core AYS-2N-4[c]	Gel exudations on polished surface in BDC without elevated T/RH exposure. No gel exudations observed after elevated T/RH exposure.
Longer of two cores	No gel observed in SFO or BDC. No exudations observed after elevated T/RH exposure.
Pine Bluffs 400.58 East Bound(Middle)	No gel observed in SFO or BDC. No exudations observed after elevated T/RH exposure.

Table 4.4. Summary of Findings Regarding ASR

WYDOT Core ID	Evidence Regarding ASR
Pine Bluffs East End	No gel observed in SFO or BDC. Gel exudations observed in SFO and BDC after elevated T/RH exposure.
Pine Bluffs West Bound	ASR gel observed in voids in BDC. Gel exudations observed in SFO and BDC after elevated T/RH exposure.
East-West End A	No gel observed in SFO or BDC. Gel exudations observed in SFO and BDC after elevated T/RH exposure.
East End BAH (95 mm)	No gel observed in SFO or BDC. Gel exudations observed in SFO after elevated T/RH exposure.
2204 C	No gel observed in SFO or BDC. Gel exudations observed in SFO after elevated T/RH exposure.

[a] Old WYDOT surface preparation method involving rotomilling and then using a mortar slurry prior to placement of the overlay.

[b] FAST TRACK method involving rotomilling and then hydromilling prior to the placement of the overlay.

[c] Only hydromilling prior to placement of overlay.

4.5   CONCLUSIONS

The findings from this work indicate there is not clear evidence of surface preparation affecting bonding or causing distress or deterioration on the BDC. Although cracking and microcracking was observed near the BDC/SFO contacts, and most commonly in the BDC concrete, it is not clear that these cracks are due to surface preparation.

Six (6) cores were identified as representing three (3) different methods of surface preparation. Details regarding the relationship between the condition of the contact and the known surface preparation method are as follows.

1. The two cores from Pine Bluffs where the old WYDOT surface preparation method (rotomilling followed by a bonding slurry) showed no systematic deterioration or distress near the SFO/BDC contact.

2. The two cores from Pine Bluffs where the FAST TRACK surface preparation method (rotomilling followed by hydromilling) showed no cracking or significant microcracking in the BDC.

3. The cores from Roundtop where surface preparation involved only hydromilling showed no cracking or significant microcracking in the BDC.

Two (2) cores were present where there is a separation of the SFO from the BDC. The method(s) used for surface preparation of these cores was not indicated. The cracking observed in these cores as follows.

1. In Core BAH-C4D, a sub-vertical crack cuts through the full thickness of the SFO, which is cleanly separated from the underlying BDC. No cracks or significant microcracking was observed in the BDC, indicating that damage related to surface preparation is not a factor in the delamination of the SFO.

2. In Core BAI-C5D the separation occurs within the upper portion of the BDC, about 3-9.5 mm ($\frac{1}{8}$-$\frac{3}{8}$ in.) below the contact between the BDC and SFO. Sub-horizontal microcracking and hairline cracks are present in the upper 3-6 mm ($\frac{1}{8}$-$\frac{1}{4}$ in.) of the BDC. Some microcracks in this region contain deposits of ASR gel but it is not clear that the microcracking is due to ASR.

The most consistent observation regarding cracking and microcracking around the interface between the SFO and BDC is that it occurs within the BDC, subjacent to the SFO contact. Typically, the cracks are microcracks are within ~ 6 mm ($\frac{1}{4}$ in.) of the interface. The bond between the SFO and BDC remains tight and intact in almost all the cores. The cracks around the SFO/BDC interface are straight and linear and commonly cut through aggregate particles and lack secondary deposits. These observations suggest that the cracking occurred after tight bonding was achieved between the layers and that the cracking mechanism is an externally imposed stress.

Evidence of alkali-silica reaction (ASR) was observed in many cores, in both the SFO and the BDC. Deposits of gel were observed most commonly in the BDC whereas gel was observed more rarely in the SFO. The reactive components in all the cores are typically particles of rhyolite and granitic rocks in the fine aggregate in both BDC and SFO. Cores from Roundtop, which were made with a crushed limestone coarse aggregate and a siliceous sand, showed evidence of ASR involving rhyolite in the sand. No cracking or significant microcracking that affected the bonding between the BDC and SFO was observed in association with ASR in any core. Exudations of ASR gel were observed commonly in both BDC and SFO after the prepared concrete slabs were exposed to elevated T/RH conditions. SEM/EDS analysis of the gels indicated a range of compositions regarding the relative abundance of sodium, potassium and calcium in the gel.

5.0   FINITE ELEMENT ANALYSES

As part of this research project, GES TECH GROUP has conducted a non-linear Mechanical Event Simulation FEA (finite element analysis). The formulations used in this study were analyzed using Autodesk Simulation Mechanical 2014.[1]

The non-linear FEA method employed is defined as a Mechanical Event Simulation using a special concrete materials model that is treated as statistically homogeneous with different tensile and compressive behaviors. The FEA formulation uses a smeared crack model where cracking and crushing are simulated via a degeneration of elasticity at integration points. The model accounts for both compression under confinement and tensile crack formation but cracking is considered to be the most important aspect.

5.1   GENERAL ARRANGEMENT AND ASSUMPTIONS

The overall cross section of a typical bridge deck and overlay is illustrated below in Figure 5.1 reproduced from the project proposal.
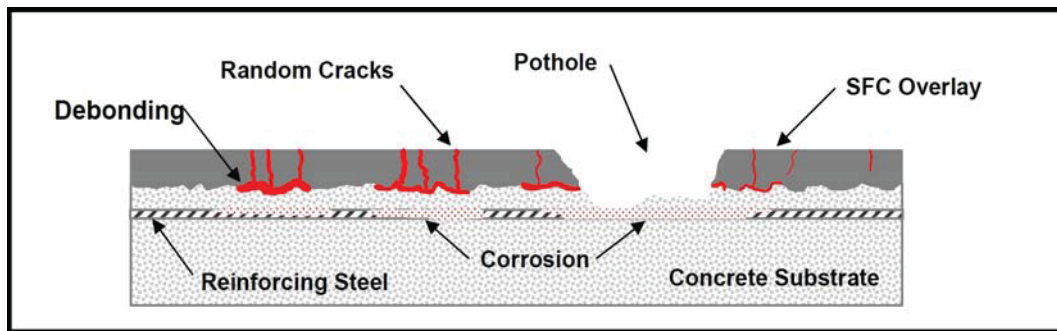
Figure 5.1. Cross section of bridge deck and overlay, description of issues.

Figure 5.2 below shows the basic FEA formulation or model used to investigate the overlay stresses including bond line stresses at the interface of the silica fume concrete overlay and bridge deck substrate. Overlay compressive stengths of 4,000 psi (27.6 MPa) to 10,000 psi (69.0 MPa) with E_c or modulus of elasticity values of 4.5 x 10^6 psi (31,026 MPa) and 6.5 x 10^6 psi (44,816 MPa) were investigated using concrete shrinkage values of 0.02, 0.03, 0.05, 0.07 and 0.09 percent.

We assumed that an 8 foot cross section would be representative of a road way overlay. Larger dimensions proved to simply yield repeating patterns of cracks so we compromised with a 48 inch (1219 mm) cross section and boundary conditions on the left of Figure 5.2 that simulate another 48 inch (1219 mm) section to the left, terminating in a free edge identical to the free edge on the right.

The overlay was bonded to the deck and then shrinkage factors were applied as illustrated in Figure 5.2. The expected total shrinkage in a 48 inch (1219 mm) section based on 0.03 percent

---

[1] http://www.autodesk.com/products/simulation-mechanical/overview

is thus 0.0003 x 48 = 0.014 inches (0.0003 x 1219 = 0.366 mm), as noted in the general arrangement in Figure 5.2.
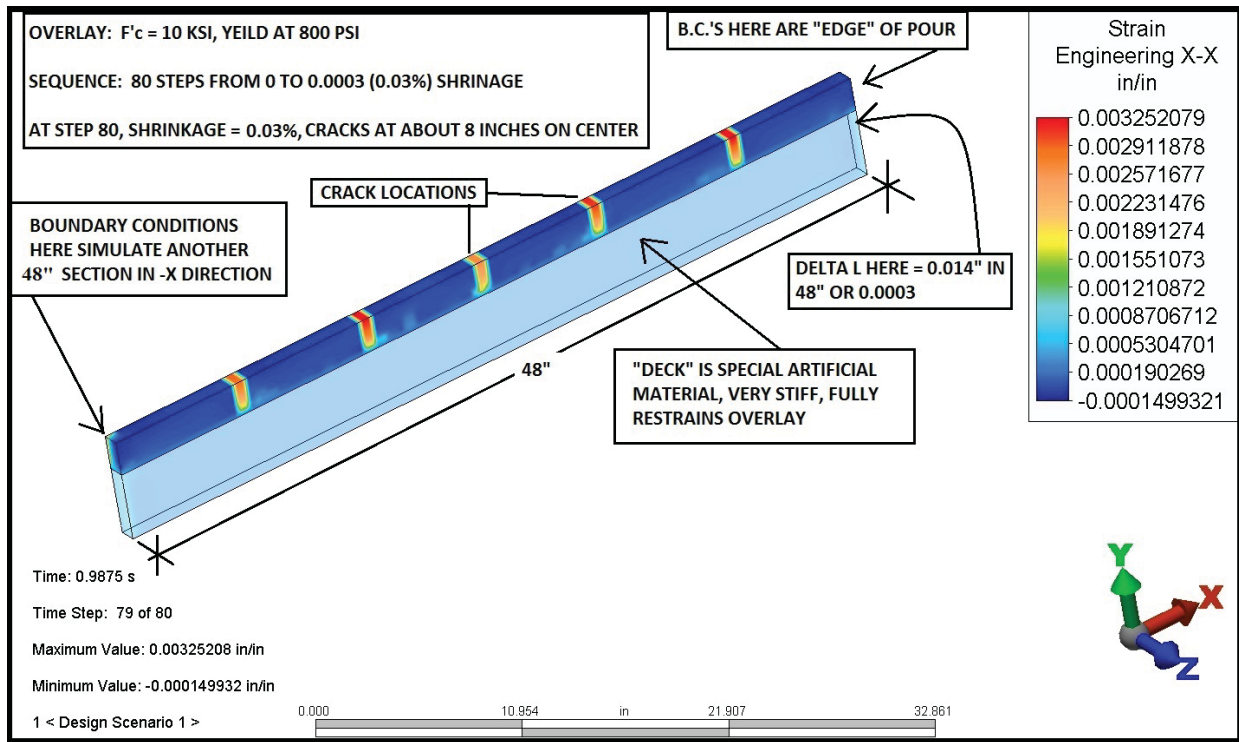
Figure 5.2. FEA formulation based on Figure 5.1 definitions.

Locations of cracks were indicated by plotting the strain tensor in the X vector direction. In general, strain values up to about 0.002 inch/inch (0.051 mm/mm) were considered to be microcracks and values from 0.003 inch/inch (0.076 mm/mm) to 0.005 inch/inch (0.127 mm/mm) and above were considered to be approaching visibility. All cracks including microcracks were considered to relieve tensile stresses but still retain some ability to transmit shear forces (rough fracture surface with mechanical interlock).

5.2   OVERLAY: 8,000 PSI COMPRESSIVE, 800 PSI TENSILE AND E = 4.5 x10⁶ PSI

The most sensitive variable is the tensile strength of the cured overlay since the overlay is not likely to experience compressive failure. Figures 5.3 – 5.10 describe our 8,000 psi (55.2 MPa) compressive and 800 psi (5.5 MPa) tensile strength results.

As shown in Figure 5.3 below, numerous microcracks appeared in this formulation with at least three larger cracks developing at the center and edge of the section. The strains of approximately 0.001 inch/inch (0.025 mm/mm) would not likely be visible but would admit moisture unless the overlay were sealed.

52

The plot in Figure 5.4 illustrates the conditions within the overlay as cracks begin to form near the bond line with the deck. Zones of tensile failure are indicated with corresponding zones of compressive stress as the overlay flexes under eccentric tensile forces within the layer.
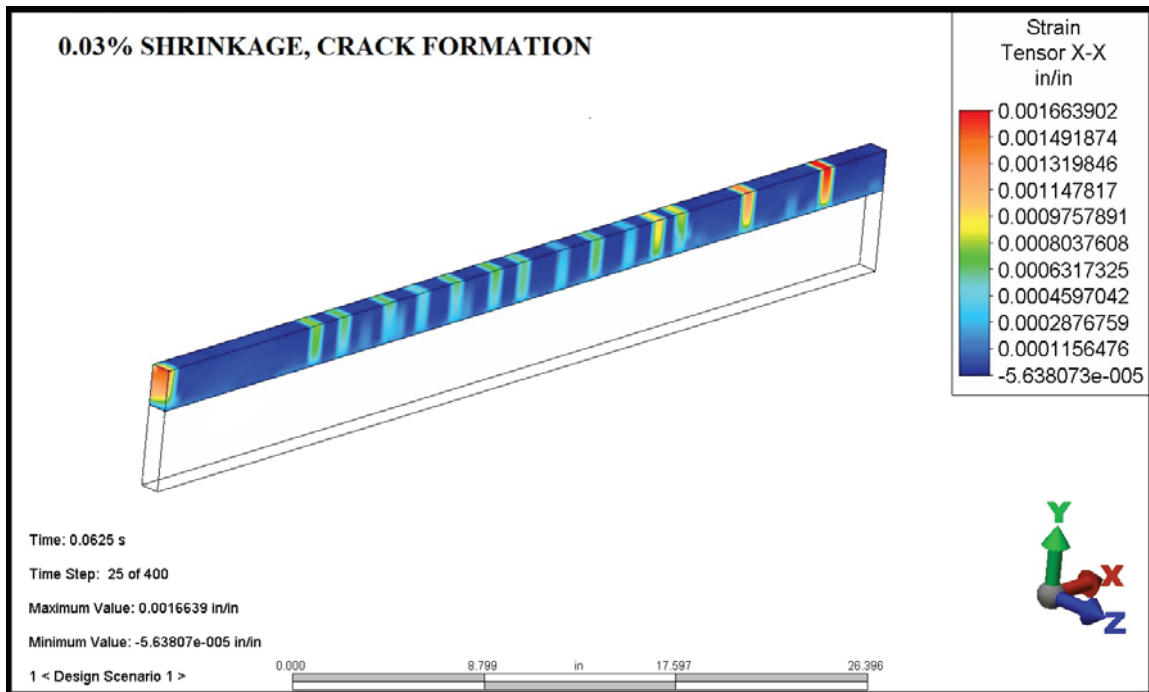
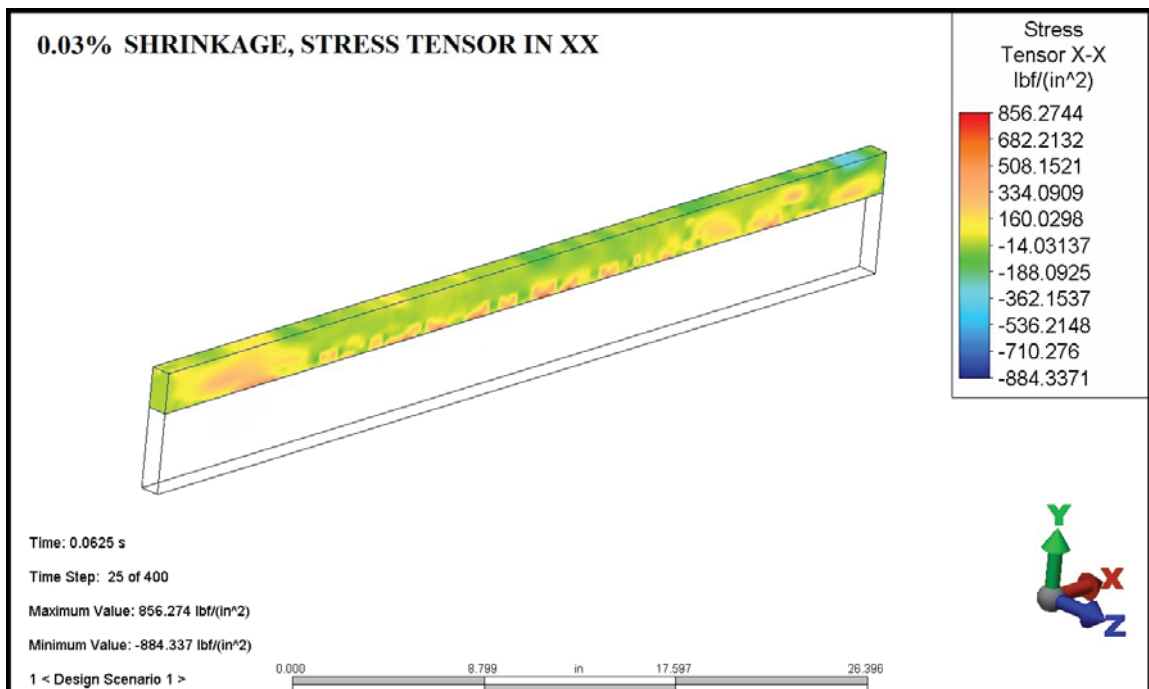**Figure 5.3. 8,000 psi/800 psi FEA formulation at 0.03% shrinkage condition.**

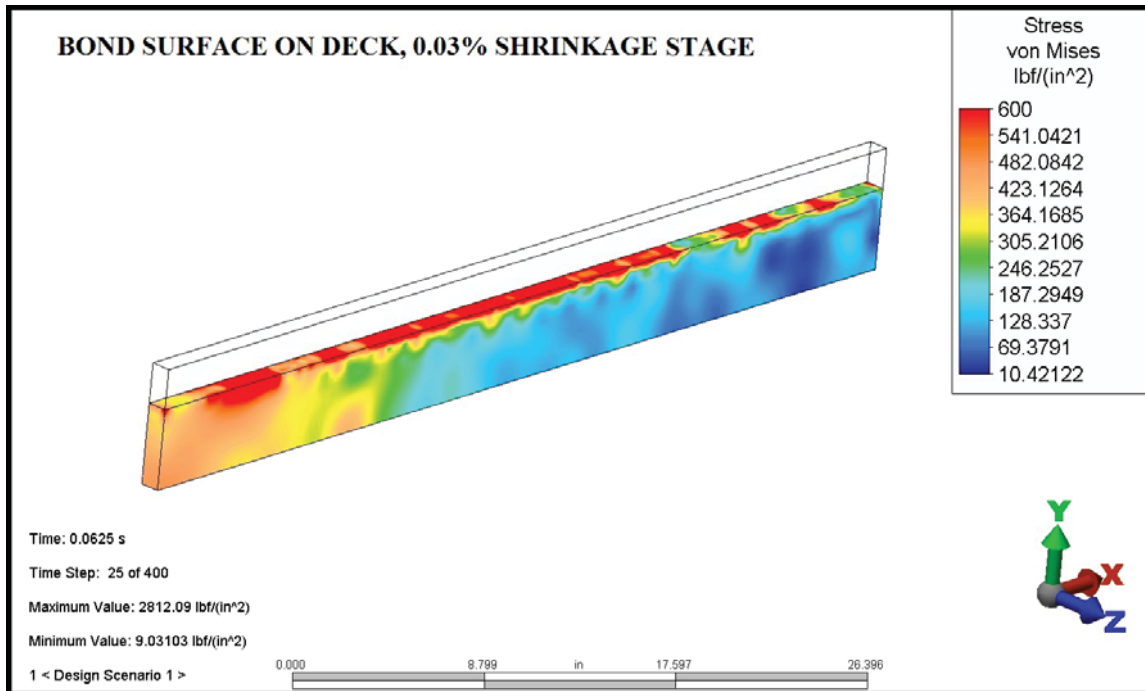**Figure 5.4. Stress tensor in X-X, with compressive zones above insipient crack locations at 0.03% shrinkage**

Figure 5.5. Stress at overlay to deck bond surface at 0.03% shrinkage condition.

Figure 5.5 shows the stresses in the substrate concrete at the bond line for the 0.03 percent shrinkage condition. Figures 5.6 and 5.7 illustrate that early cracks that form at 0.03 percent shrinkage simply grow larger along with the formation and growth of additional microcracks as the shrinkage increases.
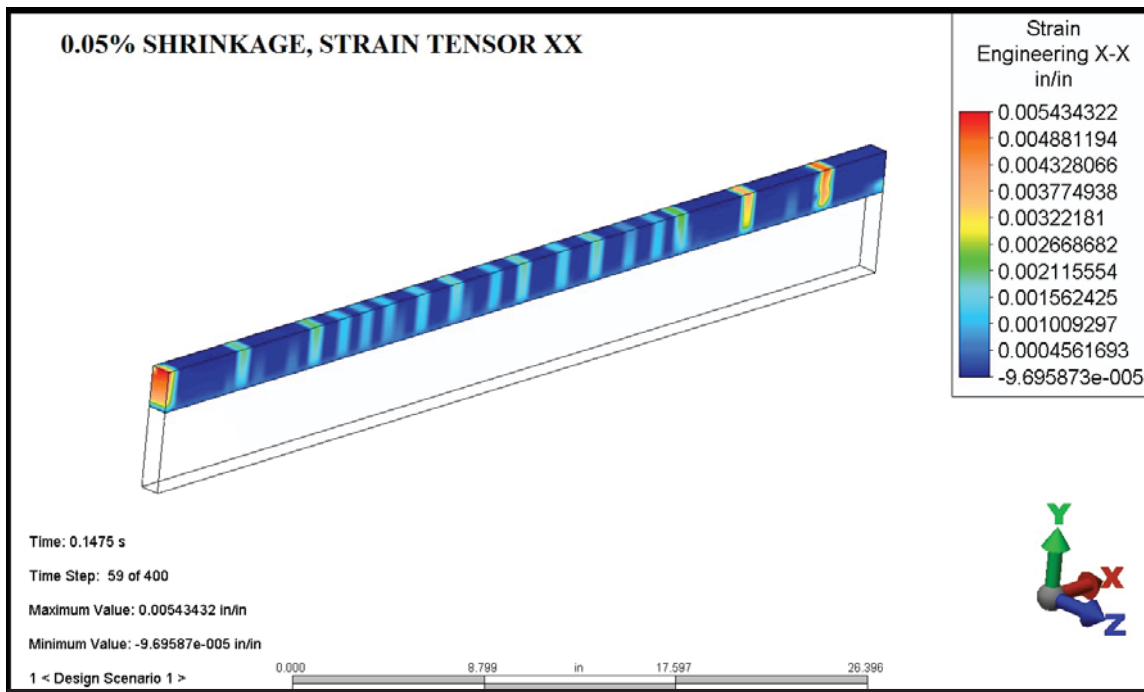
Figure 5.6. Strain tensor X-X, increased strain due to 0.05% shrinkage condition.

54
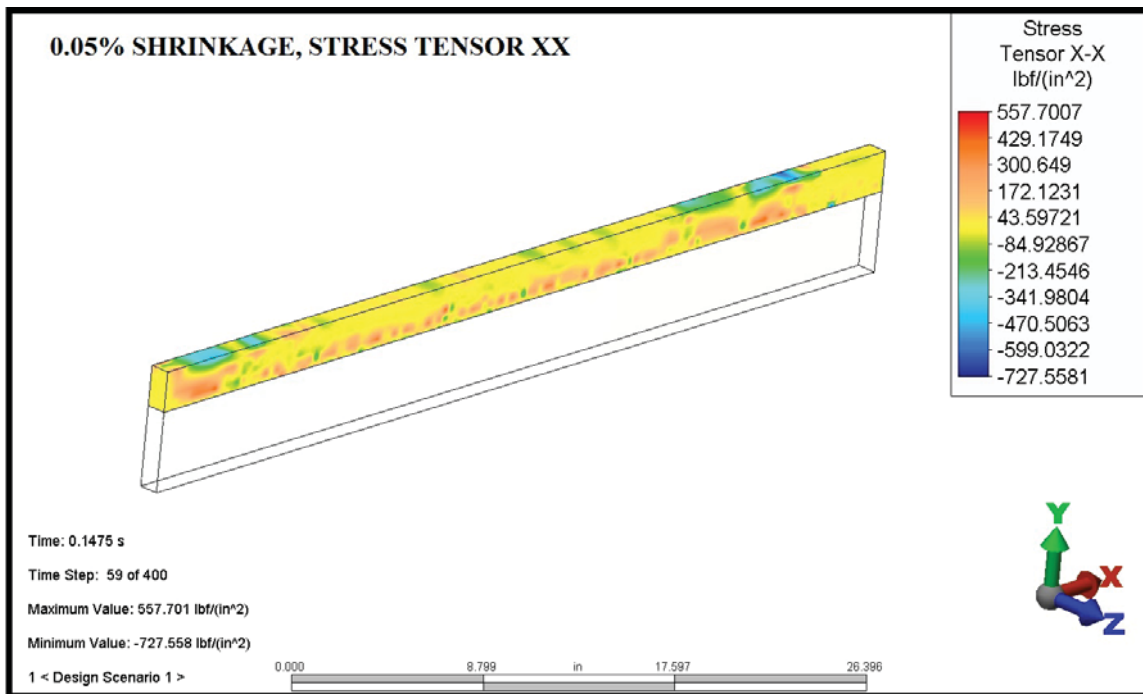
Figure 5.7. Stress tensor X-X at 0.05% shrinkage condition.

Figures 5.8, 5.9 and 5.10 illustrate that at 0.09 percent shrinkage the formation of additional stress relieving microcracks may in some cases result in the relaxation of some cracks that formed earlier in the sequence.
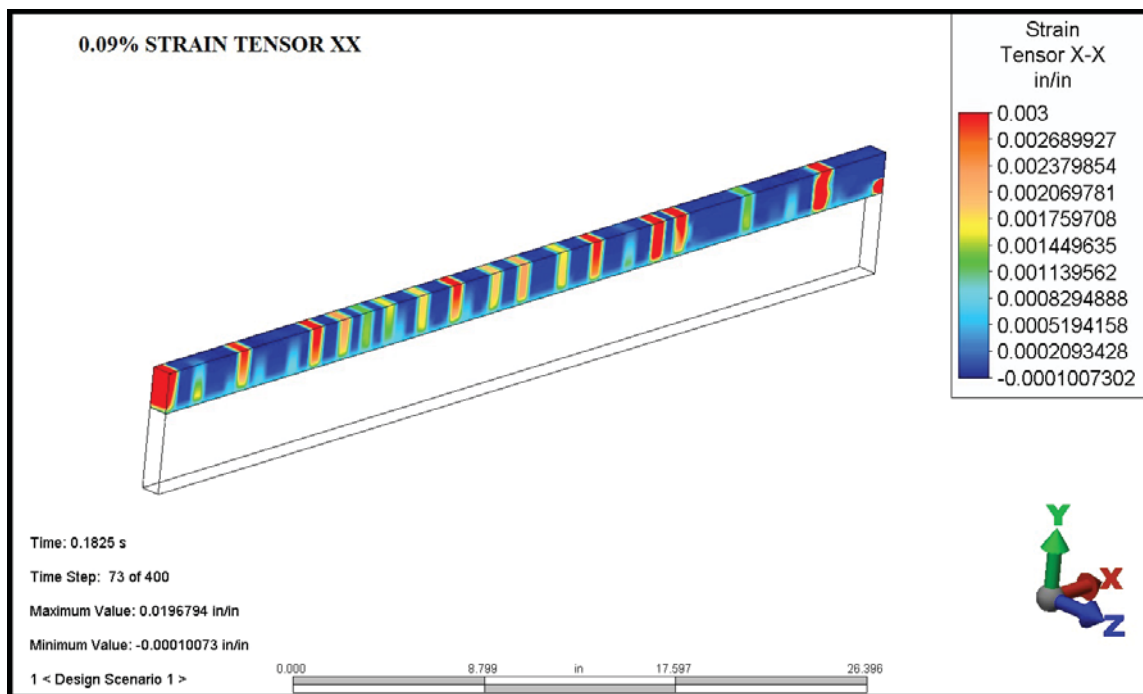
**Figure 5.8. Strain tensor X-X at maximum at 0.09% shrinkage condition.**
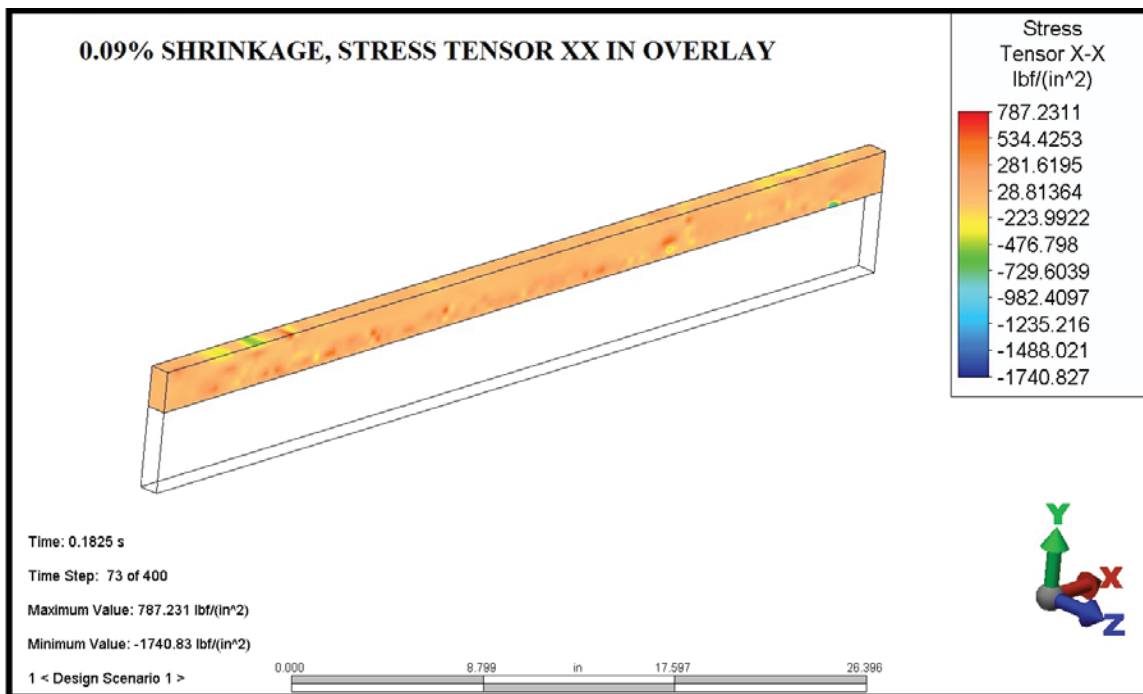
Figure 5.9. Stress tensor X-X, with tensile yield level at 800 psi; overlay section approaches 800 psi at 0.09% shrinkage condition.
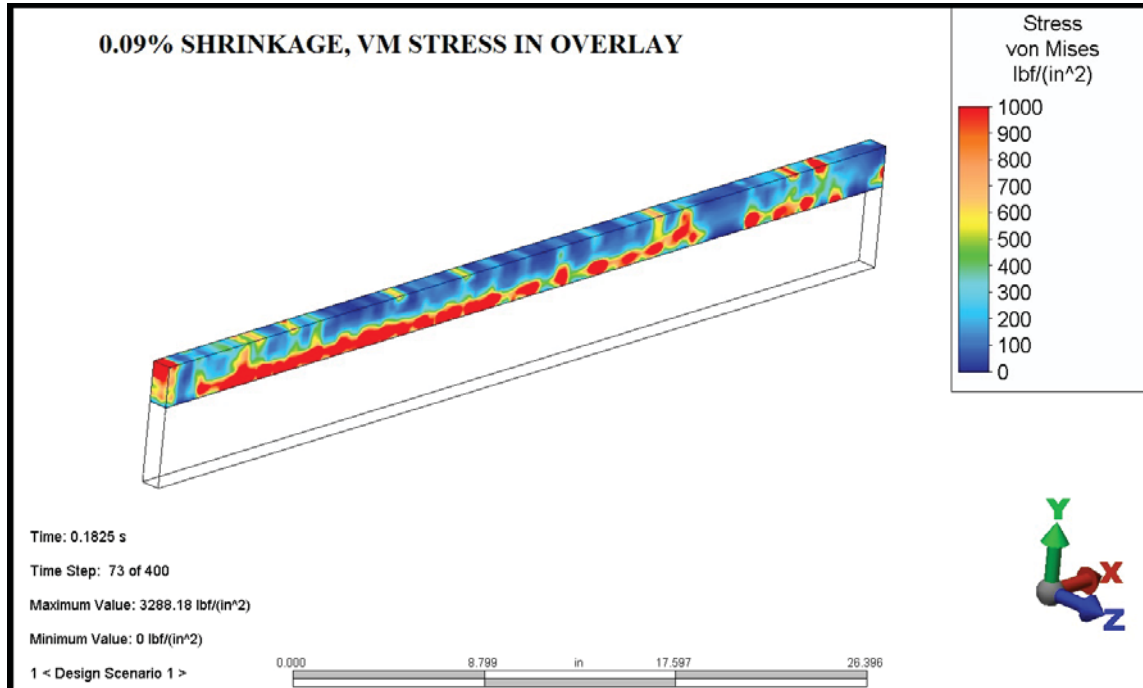
Figure 5.10. Von Mises Stress Formulation (includes shear component) in overlay at 0.09% shrinkage condition.

5.3 OVERLAY: 8,000 PSI COMPRESSIVE, 800 PSI TENSILE AND E = 6.5 x 10⁶ PSI

The 8,000 psi (55.2 MPa) compressive and 800 psi (5.5 MPa) tensile formulation was selected as representative of the variables we investigated. We found that the patterns and timing of crack formation varied with the other compressive strengths but the final results were similar. The following sequence describes a formulation using $E = 6.5 \times 10^6$ psi (44,816 MPa) concrete overlay. We have selected two crack locations and embedded graphs showing when and to what extent the crack opened. A horizontal trace indicated no crack formation. The conditions within the overlay and the bond surface stress pattern are also illustrated.
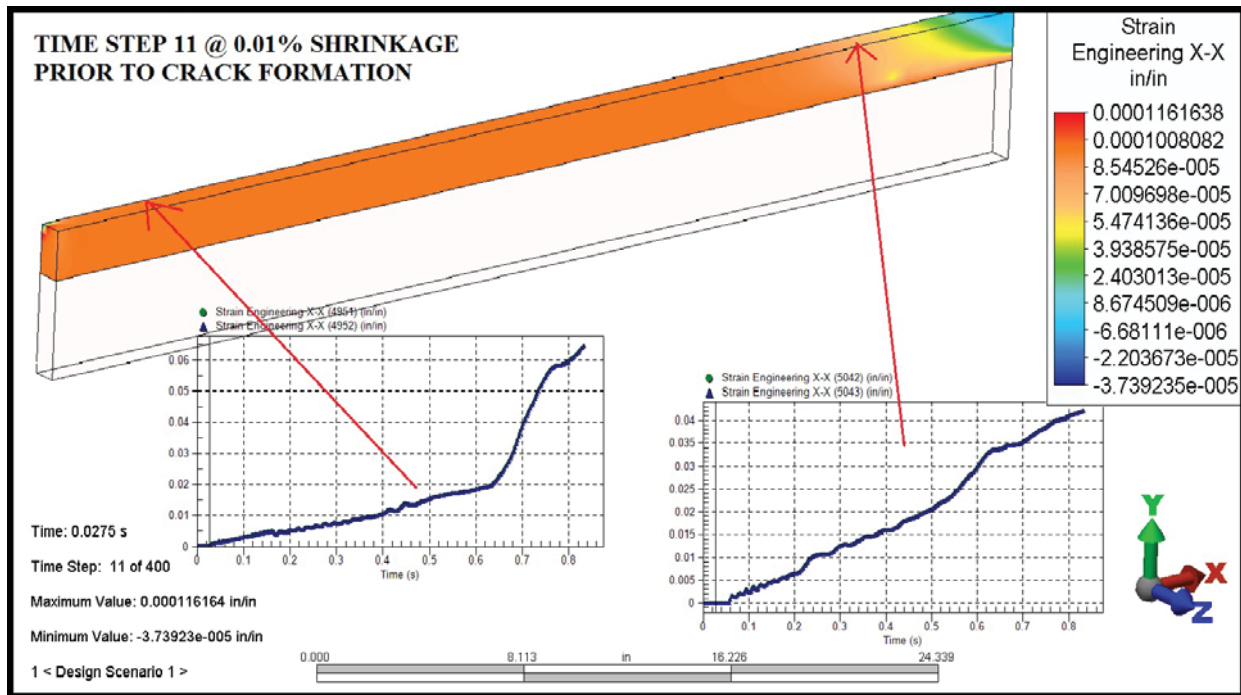
Figure 5.11. Two insipient crack locations prior to fracture (time step 11 at 0.01% shrinkage condition).

Figure 5.11 shows the strain tensor X-X due to 0.01 percent shrinkage pror to crack formation. As the shrinkage increases to 0.03 percent, cracks start to form as shown in Figures 5.12 and 5.13. Figure 5.14, shows the resulting stresses in the substrate concrete at the bond line. As the shrinkage increases to 0.07 percent, the number and size of the crack openings increase as shown in Figure 5.15.
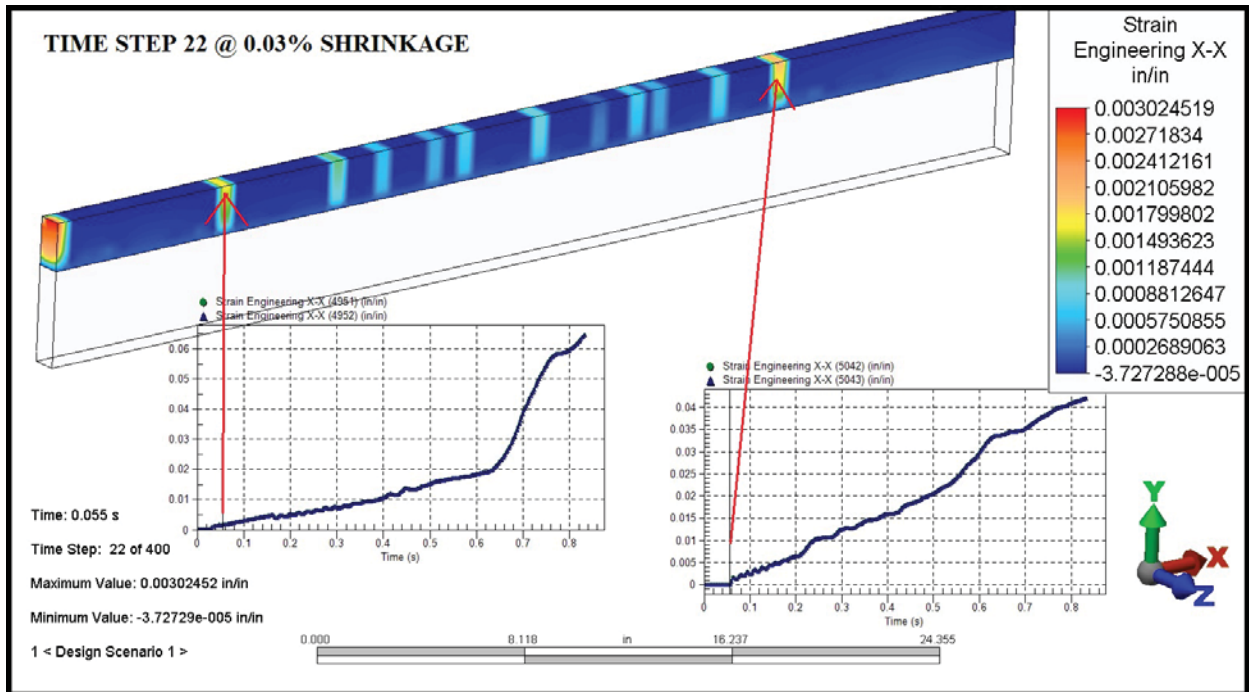
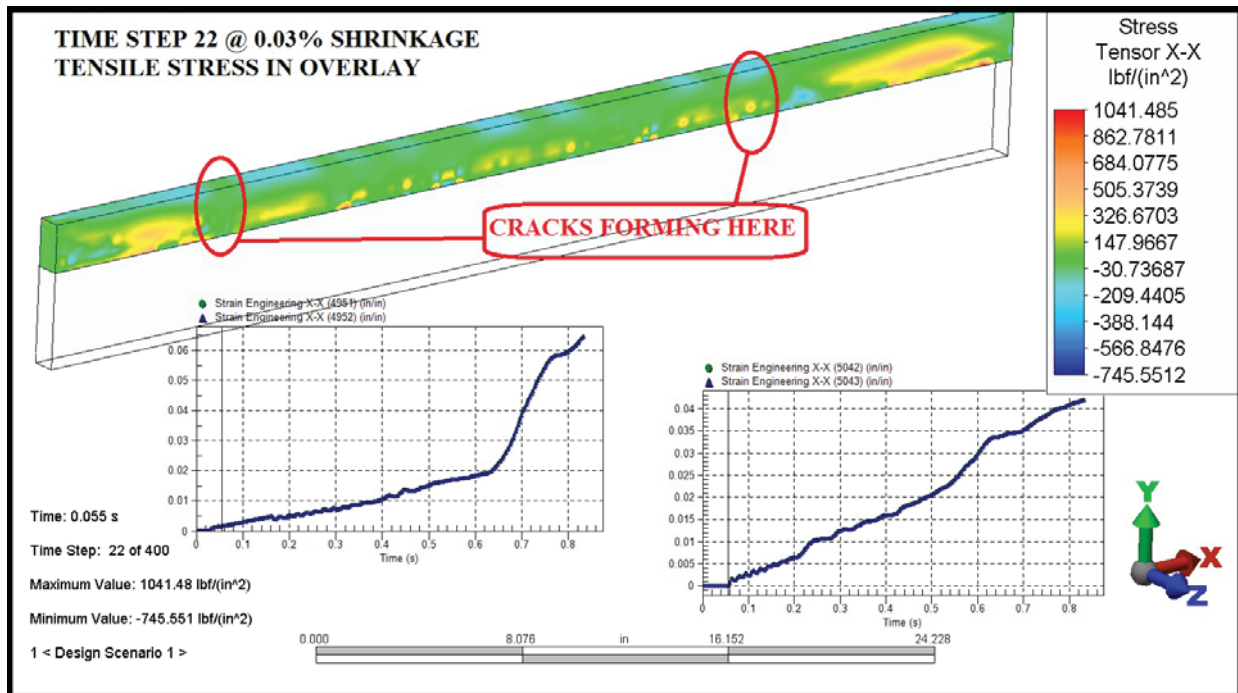**Figure 5.12. Cracks forming at time Step 22 at 0.03% shrinkage condition.**

Figure 5.13. Stress Condition within overlay at crack locations at time step 22 at 0.03% shrinkage condition.
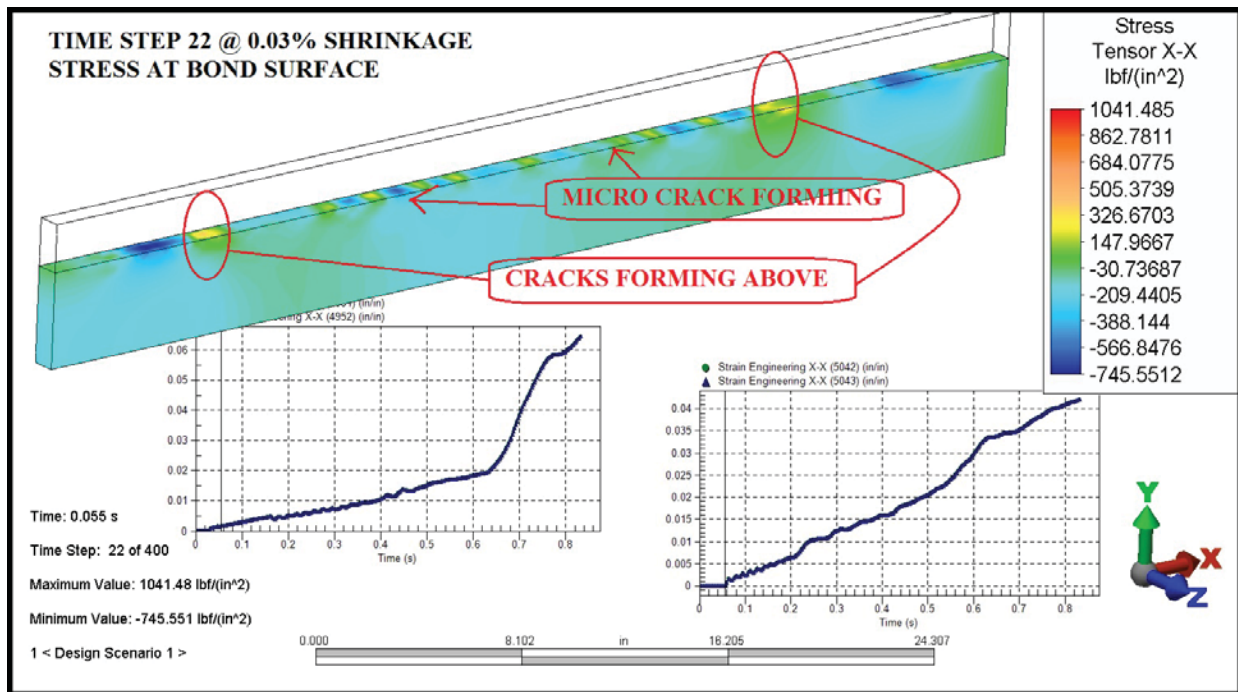
Figure 5.14. Conditions at bond surface at time step 22 at 0.03% shrinkage condition.
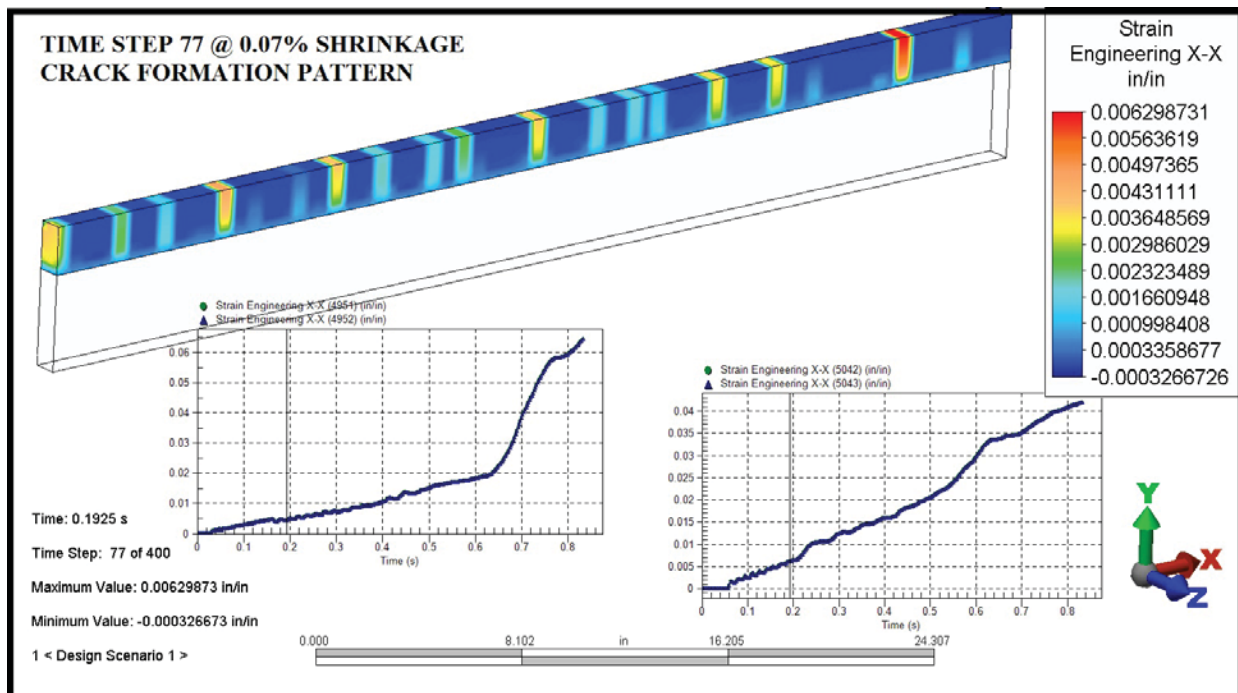

Figure 5.15. Crack pattern at 0.07% shrinkage condition with numerous microcracks and larger initial crack openings.

As shown in Figure 5.15, the crack pattern becomes more dense and previous cracks continue to open as the overlay shrinks relative to the bridge deck. Some cracks may also relax slightly as stresses are relieved in adjacent areas due to the formation of microcracks.

5.4   HIGH RESOLUTION SERIES

The formulations used in this study were analyzed using Autodesk Simulation Mechanical 2014. As noted previously, the analysis method is known as Mechanical Event Simulation. This technique uses a pseudo time framework to define the steps of the analysis. The high resolution version of the model presented in the following slides was divided into 400 steps from zero to 0.09 percent shrinkage within a pseudo time period of one second. The time steps are related to the shrinkage stages based on the following table:

Shrinkage (Percent)	Time Step	Delta-L (on 48 inches)
0.02	089/400	0.0096 inches
0.03	133/400	0.014 inches
0.05	222/400	0.024 inches
0.07	311/400	0.034 inches
0.09	400/400	0.043 inches

The following slides (Figures 5.16 – 5.32) are based on the five shrinkage steps noted above. In this series, we present a detailed view of the location of shrinkage cracks and the associated stress pattern in the deck overlay and at the bond to overlay interface. The time step resolution is approximately four times finer than the previous series. A tensor stress in the X-X vector was selected as the best representation of the shear stress at the interface.
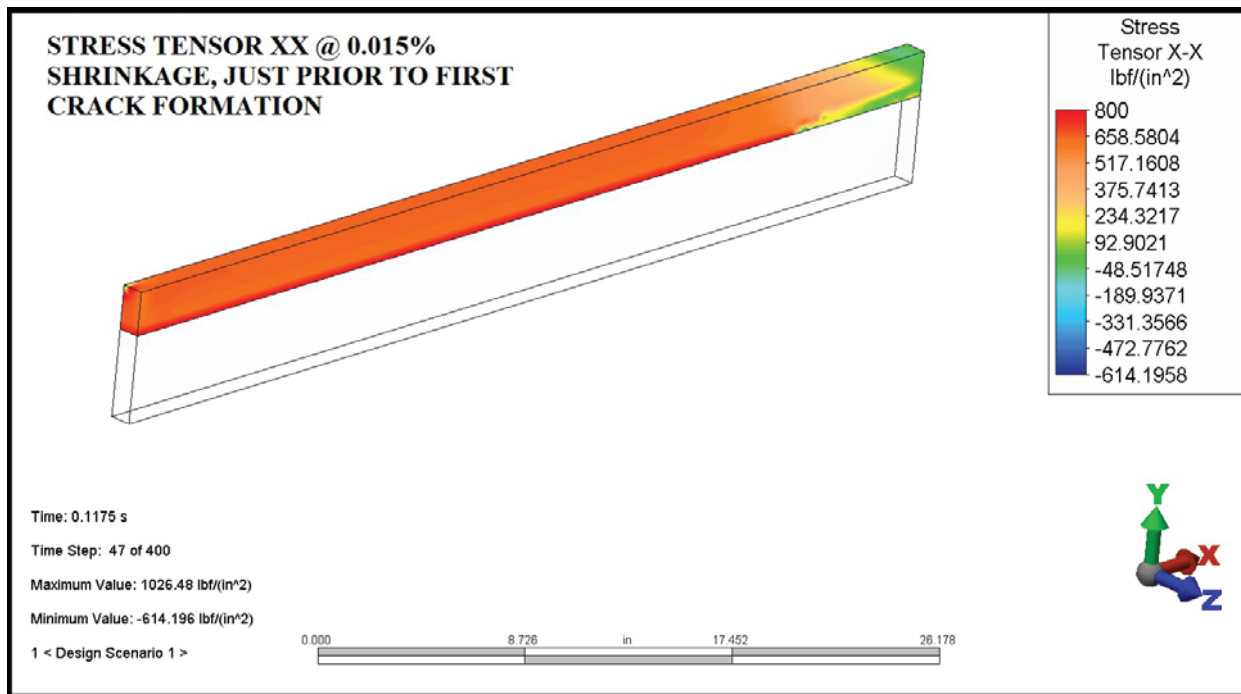
Figure 5.16.   Fine Time Step Model (higher resolution). Stress tensor X-X at 0.015% shrinkage just prior to first crack formation.
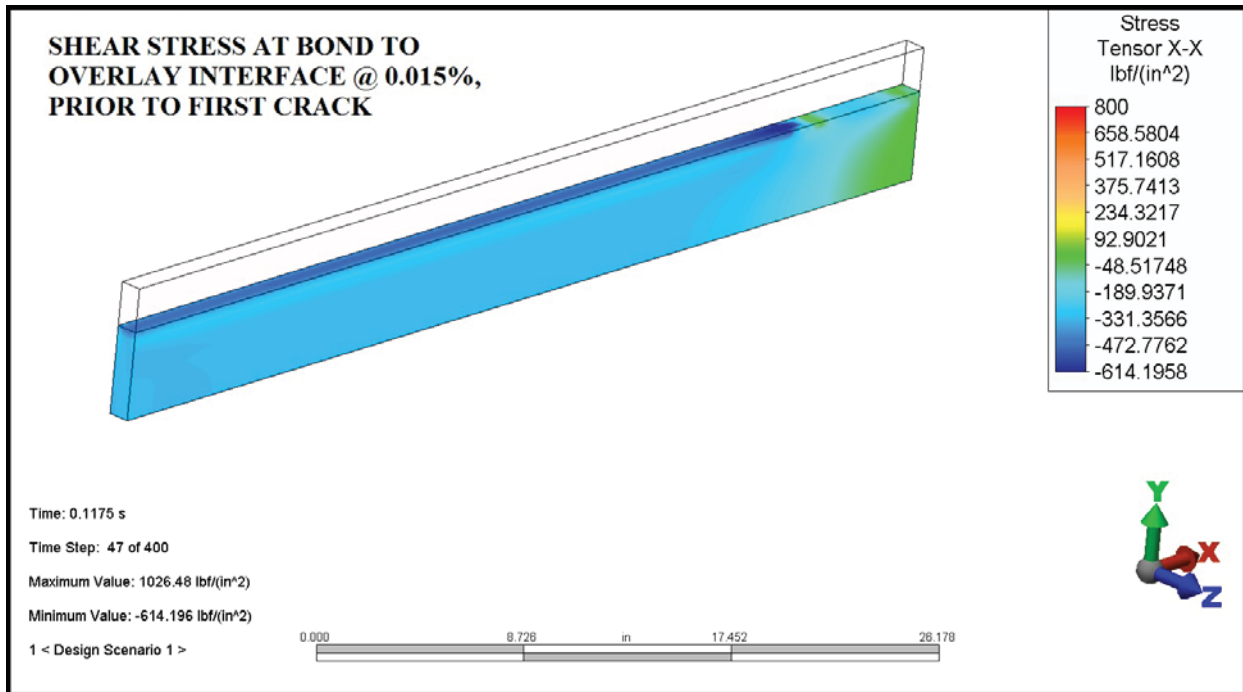
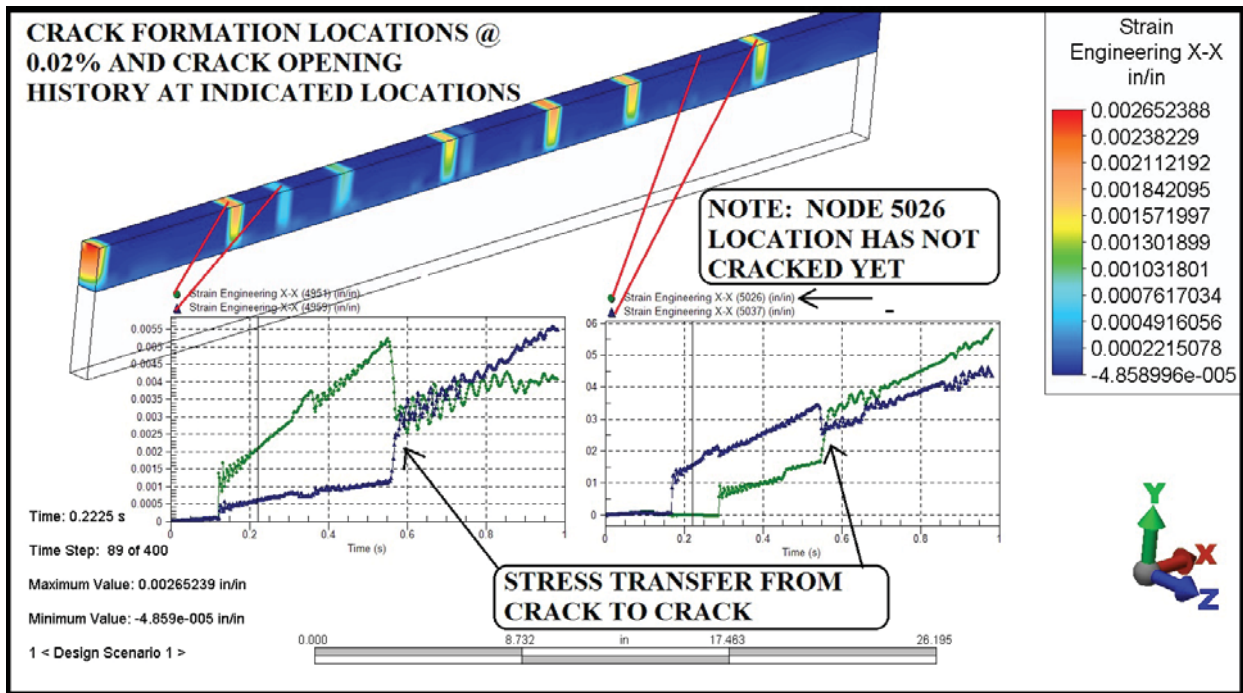**Figure 5.17. Shear stress at bond to overlay interface at 0.015% shrinkage just prior to first crack.**

Figure 5.18. Crack development in overlay for the 0.02% shrinkage condition and crack opening history plots.
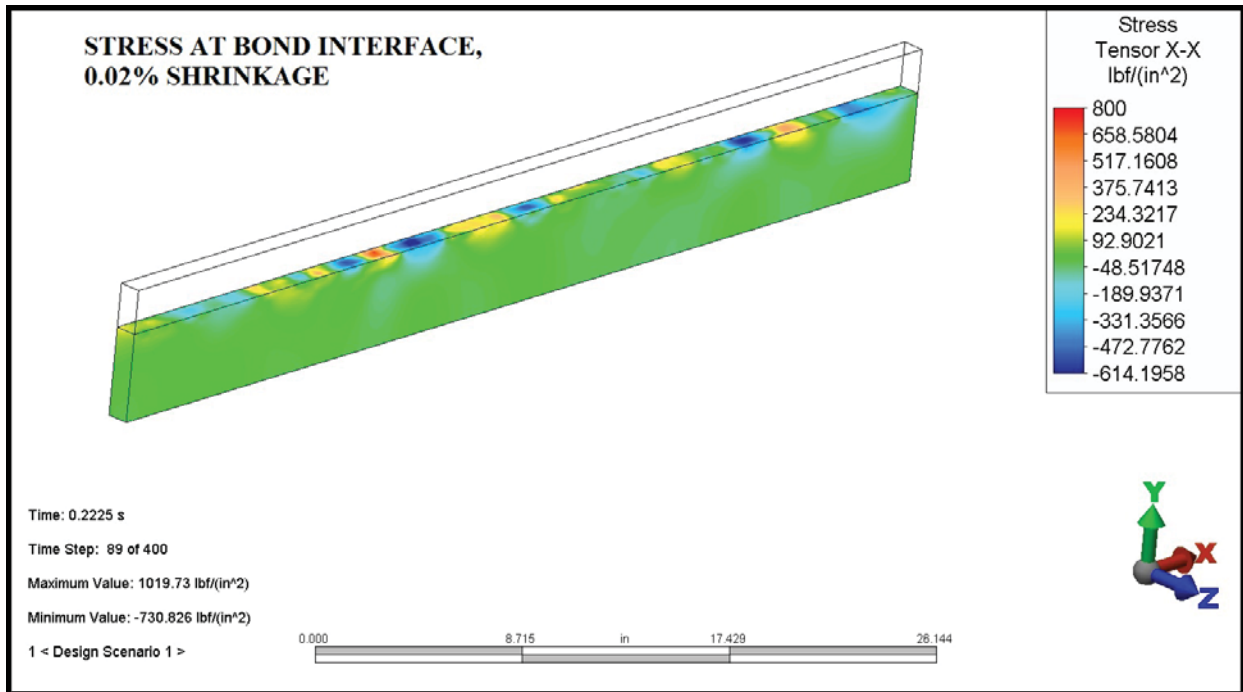
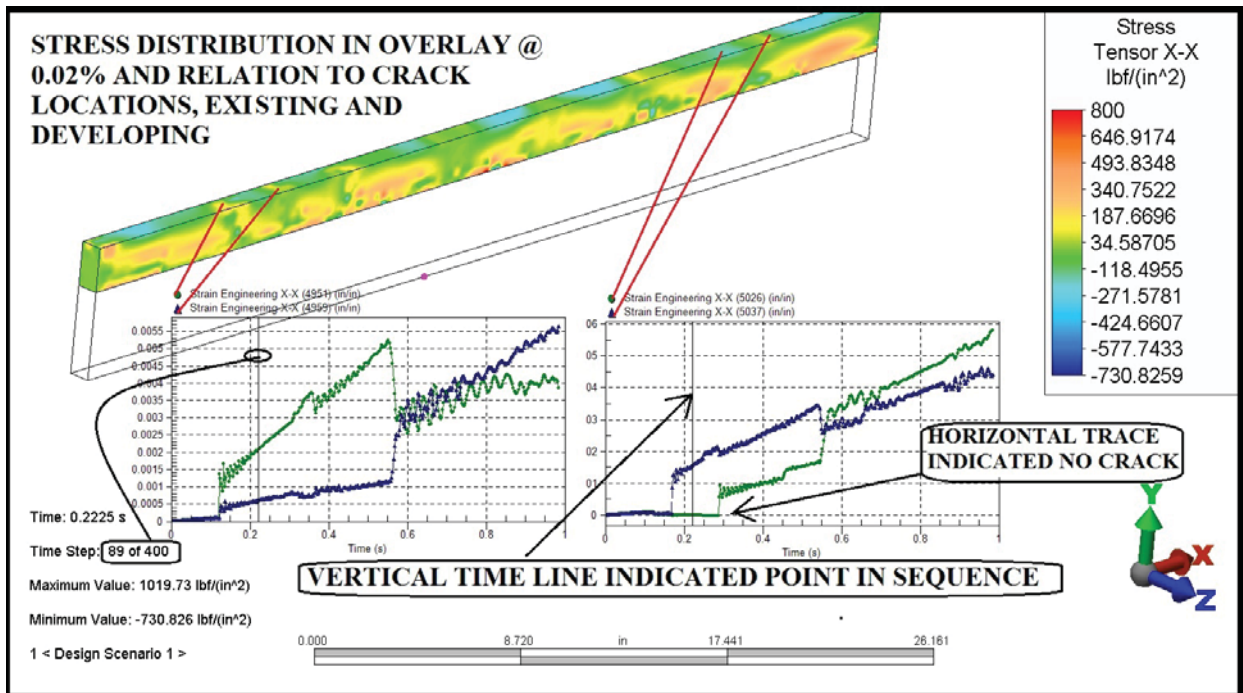**Figure 5.19. Stress tensor X-X at bond interface for at 0.02% shrinkage condition.**

Figure 5.20. Stress distribution in overlay at 0.02% shrinkage condition and relation to locations of existing and developing cracks with crack opening history plots.
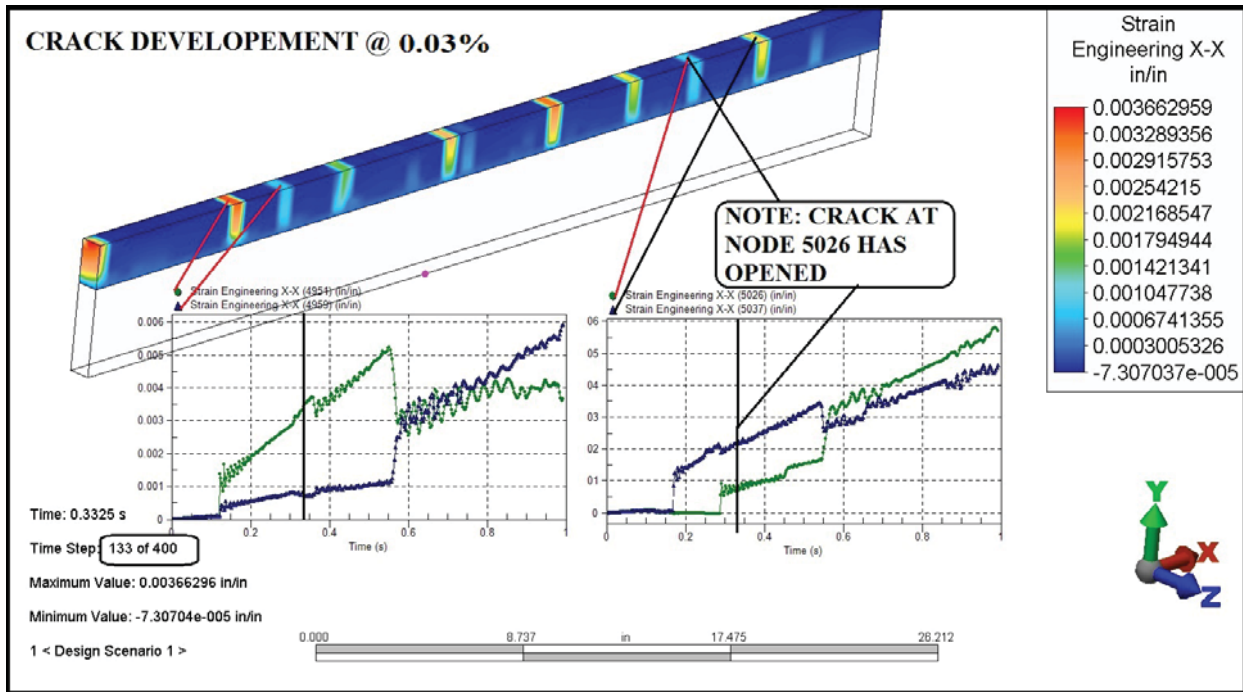
Figure 5.21. Crack development in overlay for the 0.03% shrinkage condition and crack opening history plots.

Figure 5.22. Stress tensor X-X at bond interface for at 0.03% shrinkage condition and crack opening history plots.

Figure 5.23. Stress distribution in overlay at 0.03% shrinkage and relation to locations of existing and developing cracks with crack opening history plots.

Figure 5.24. Crack development in overlay at 0.05% shrinkage condition and crack opening history plots.

64

Figure 5.25. Stress tensor X-X at bond interface for at 0.05% shrinkage condition and crack opening history plots.

Figure 5.26. Stress distribution in overlay at 0.05% shrinkage and relation to locations of existing and developing cracks with crack opening history plots.
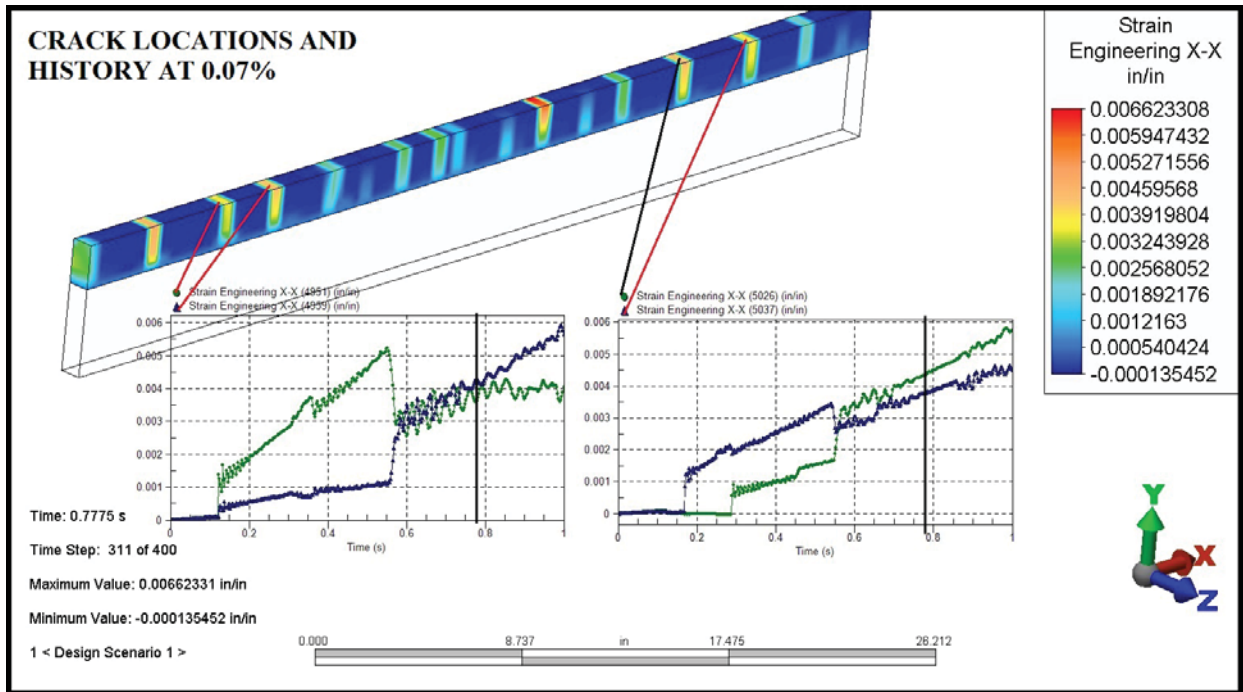
Figure 5.27. Crack development in overlay for the 0.07% shrinkage condition and crack opening history plots.
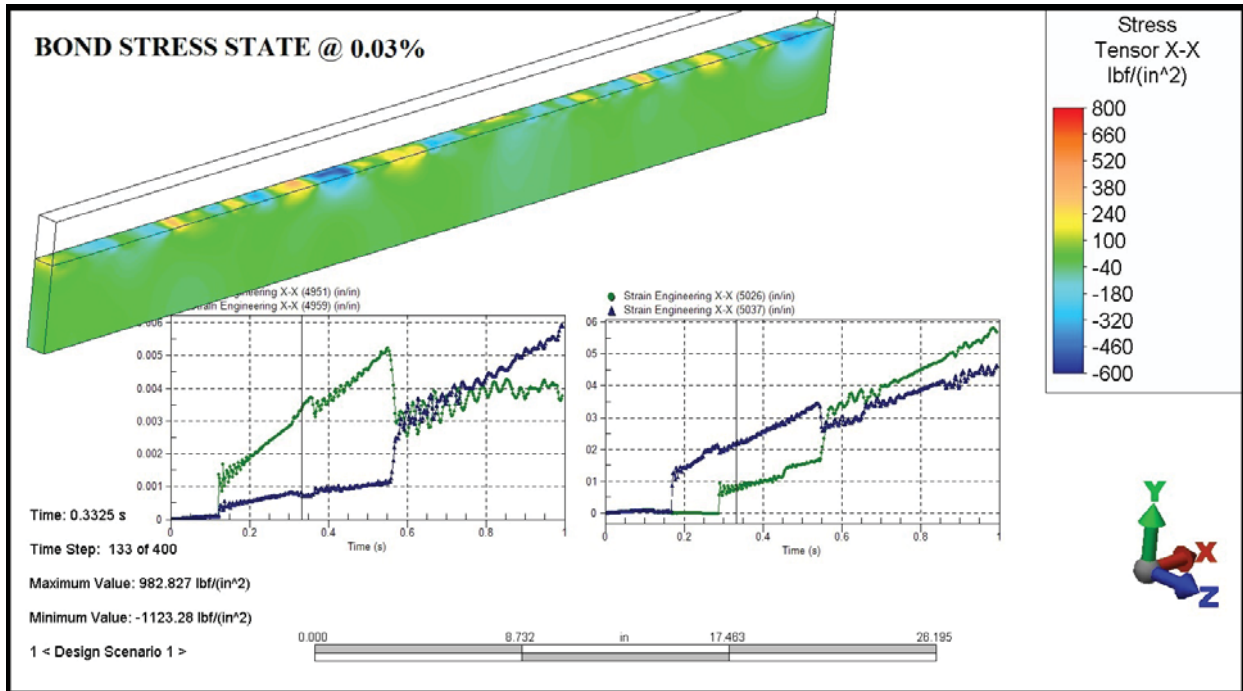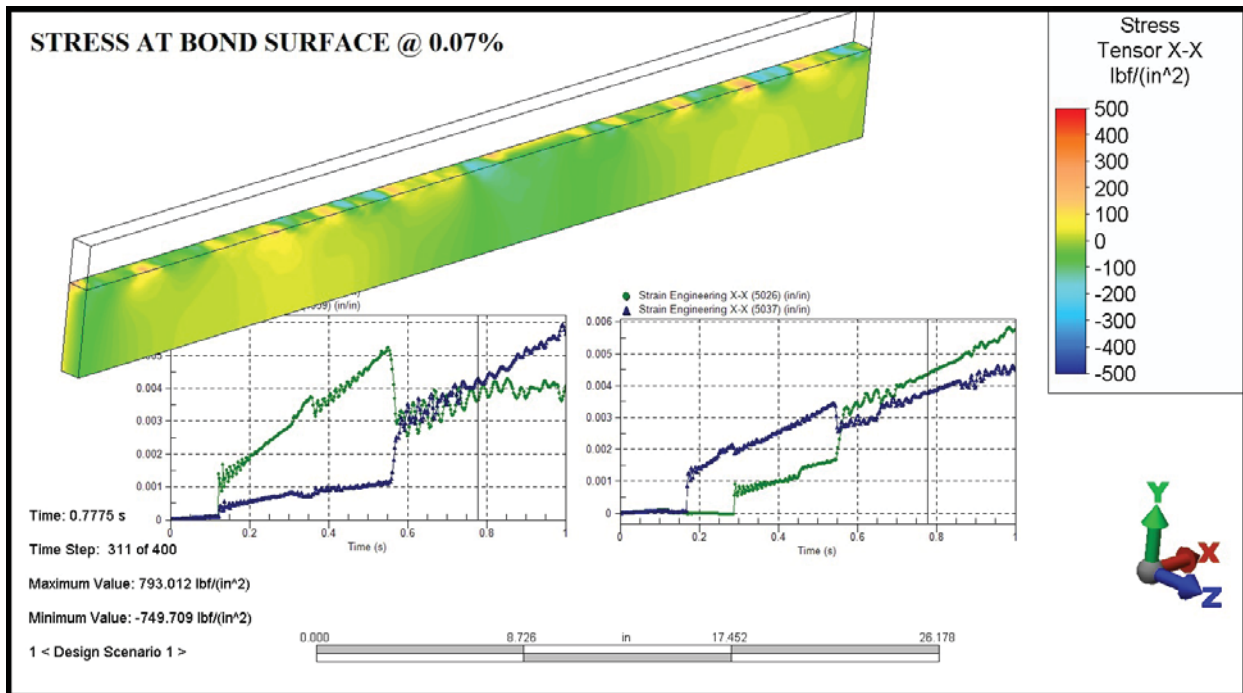

Figure 5.28. Stress tensor X-X at bond interface for at 0.07% shrinkage condition and crack opening history plots.
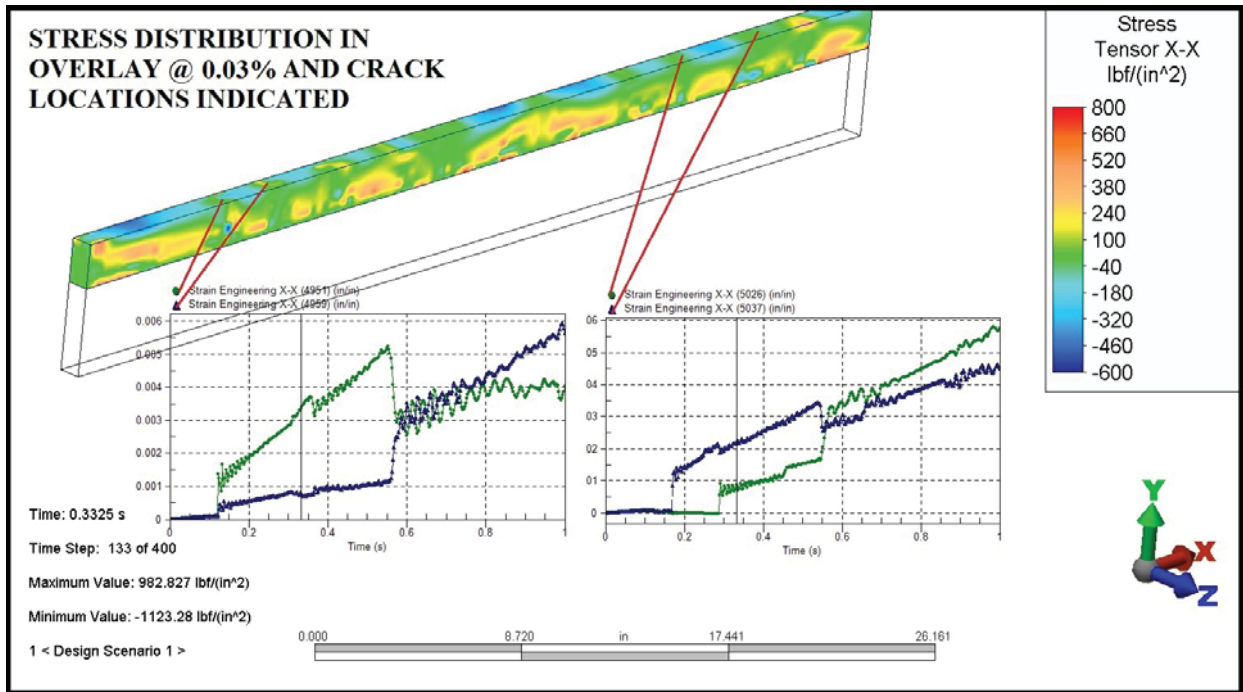
66

Figure 5.29. Stress distribution in overlay at 0.07% shrinkage and relation to locations of existing and developing cracks with crack opening history plots.
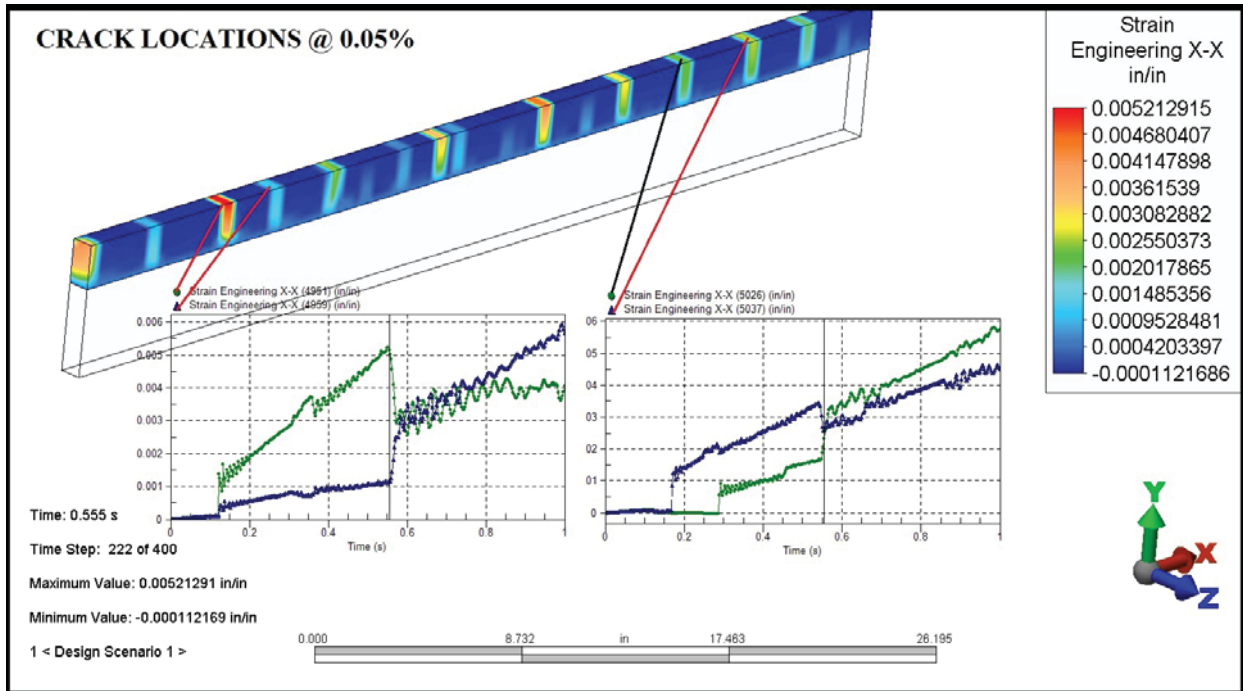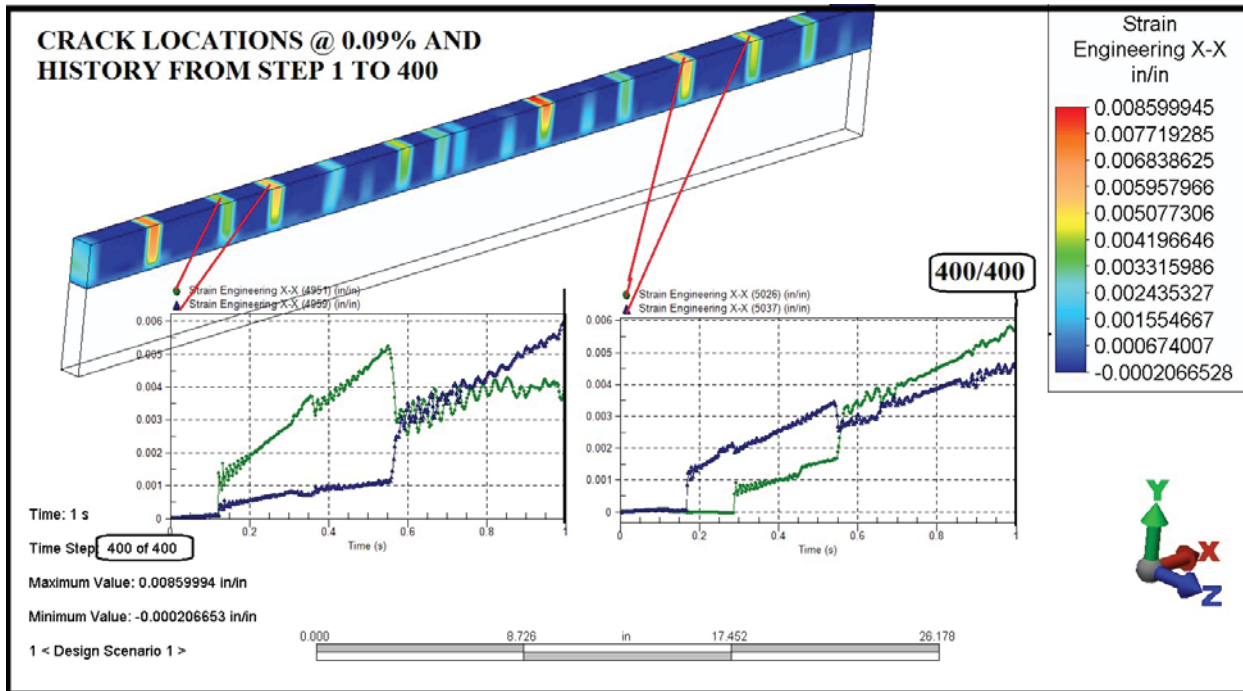

Figure 5.30. Crack development in overlay for the 0.09% shrinkage condition and crack opening history plots.
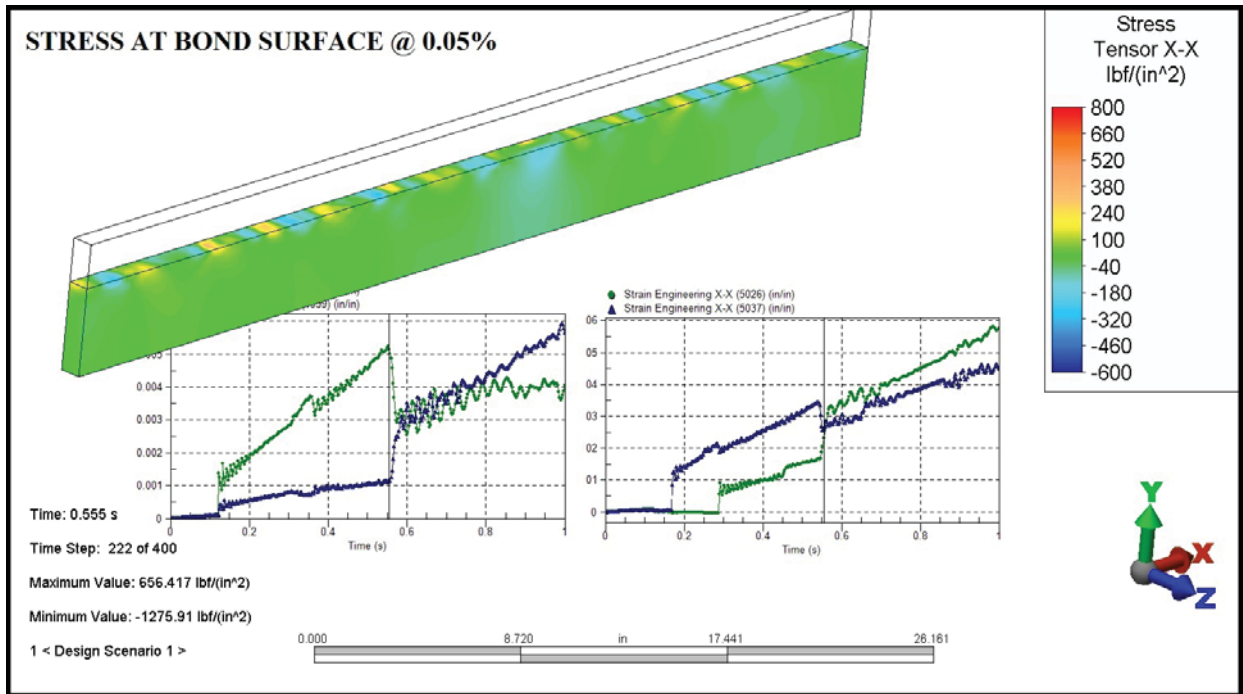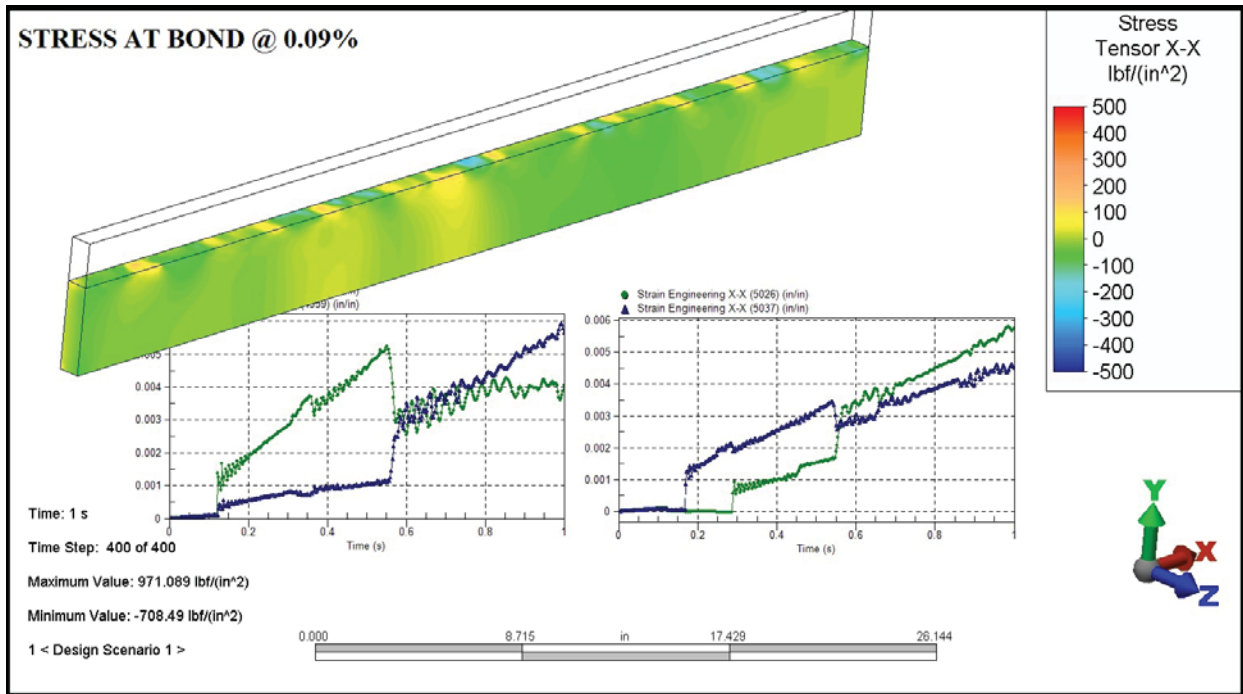
Figure 5.31. Stress tensor X-X at bond interface for at 0.09% shrinkage condition and crack opening history plots.
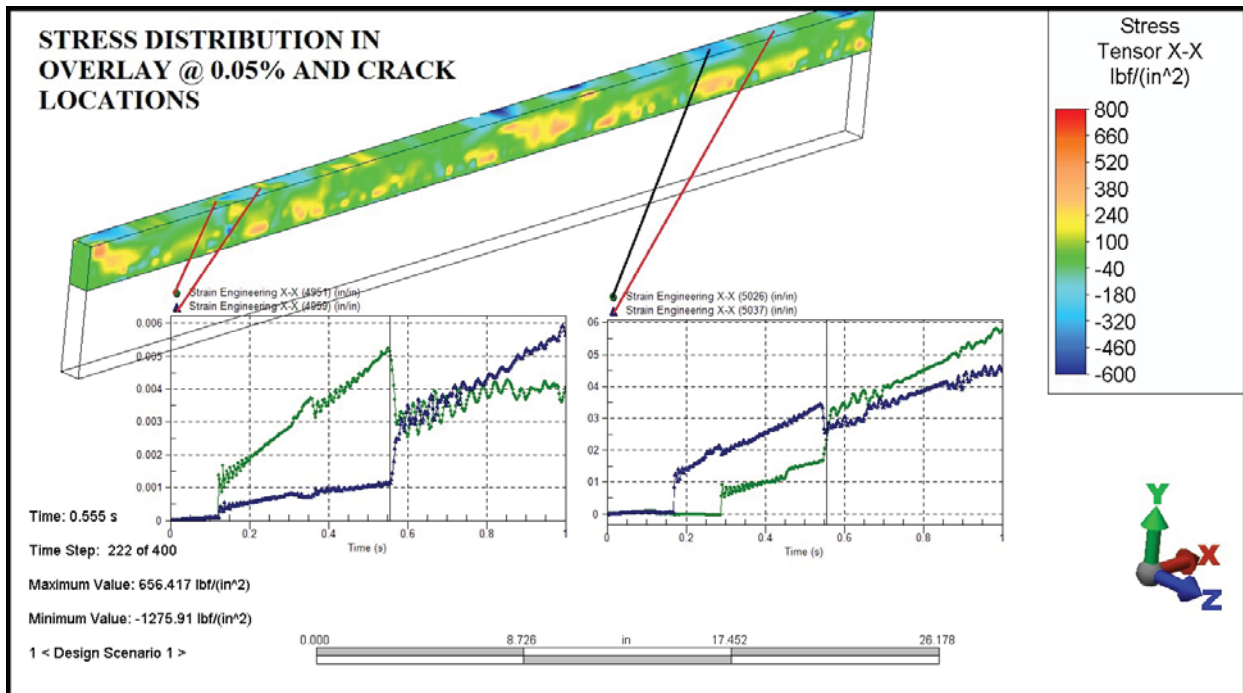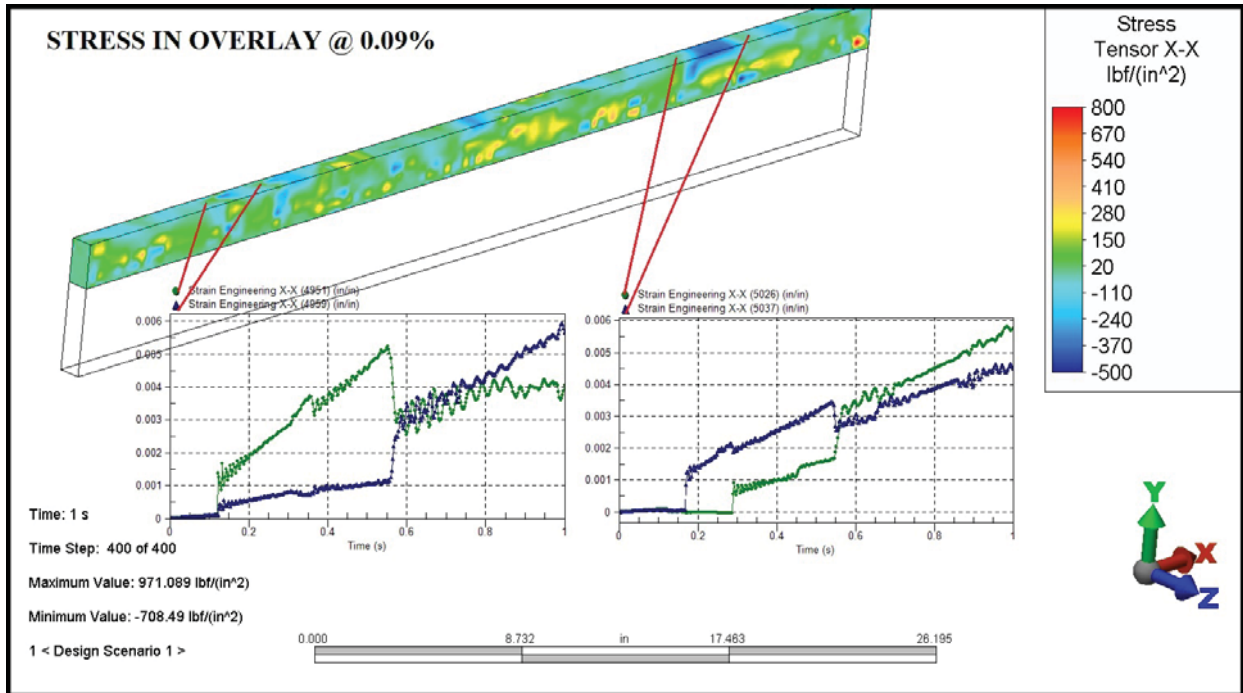

Figure 5.32. Stress distribution in overlay at 0.09% shrinkage and relation to locations of existing and developing cracks with crack opening history plots.
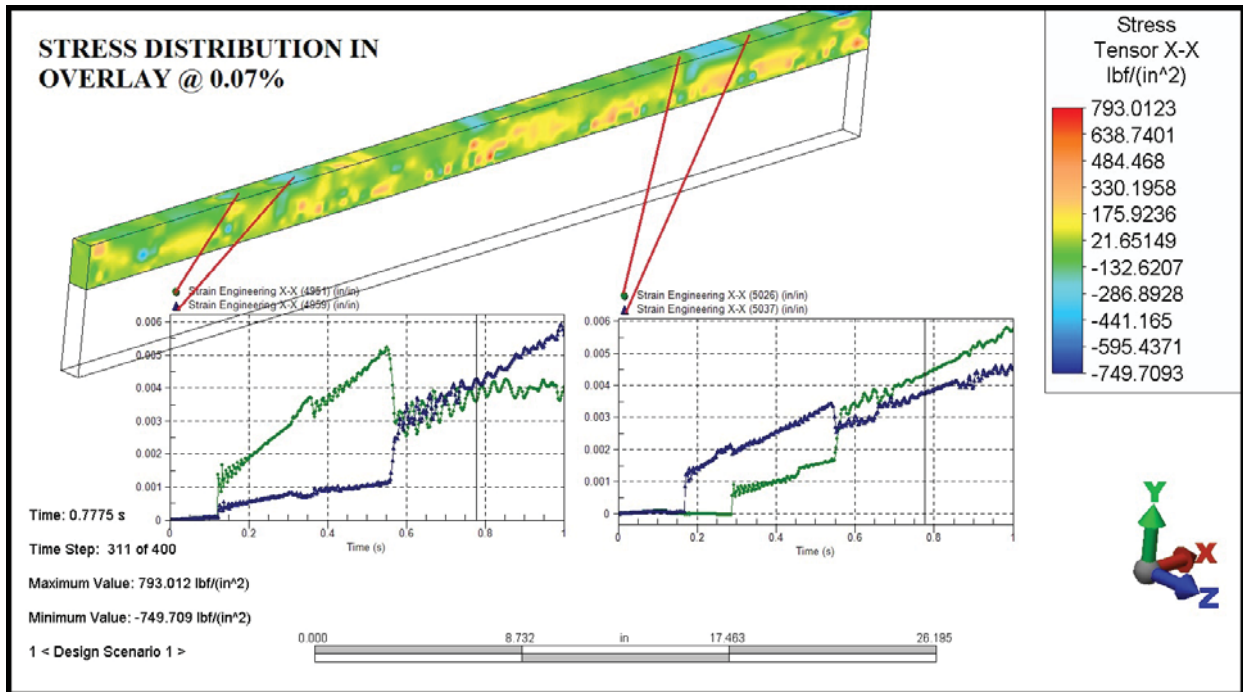
5.5   DECK FLEXURE DUE TO WHEEL LOADS

An analysis of bridge overlay flexure due to traffic loads suggested that the overlay would be subjected to positive or negative moments depending on the location of an overlay area relative to the bridge deck structural system. We suspected that a concave deflection downward of an overlay on top of a bridge deck would most likely result in largely compressive stresses developing in the overlay. Since the overlay is strong in compression, the expected crushing of a confined concrete element would occur at approximately the compressive strength of the mix. The following slides (Figures 5.33 – 5.35) illustrate this mechanism for our 8,000 psi/800 psi (55.2 MPa/5.5 MPa) model.
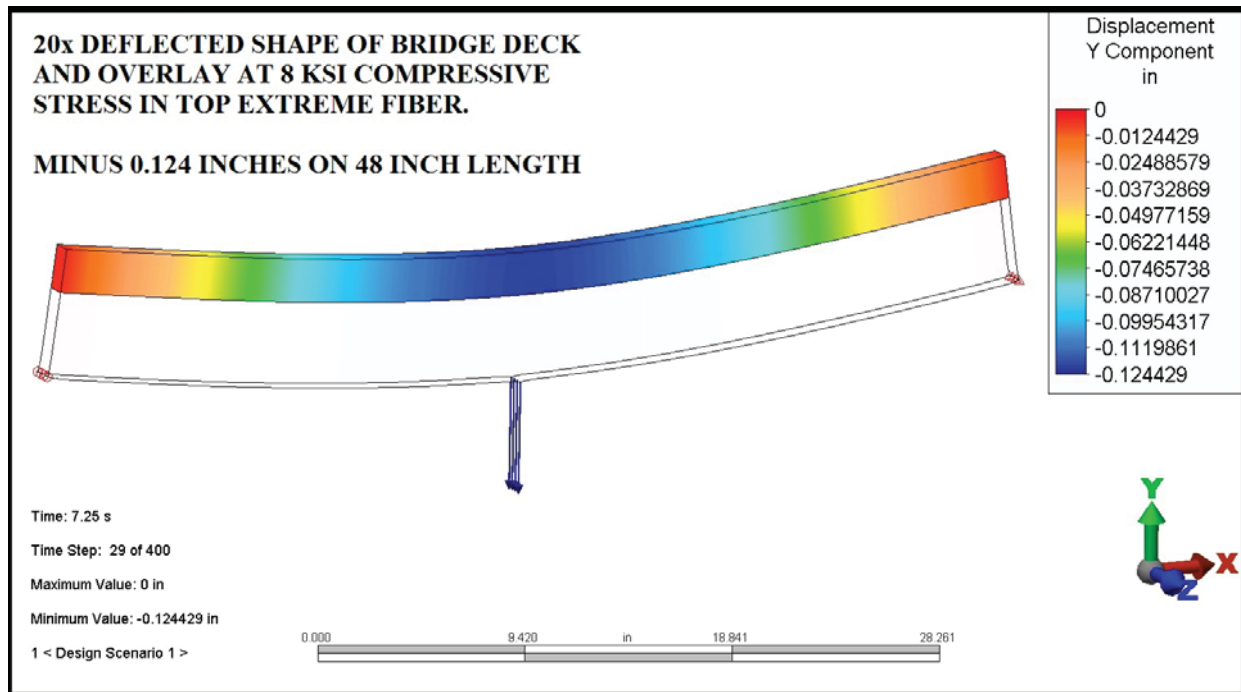
Figure 5.33. Deflected shape of bridge deck and overlay due to the positive bending moment .
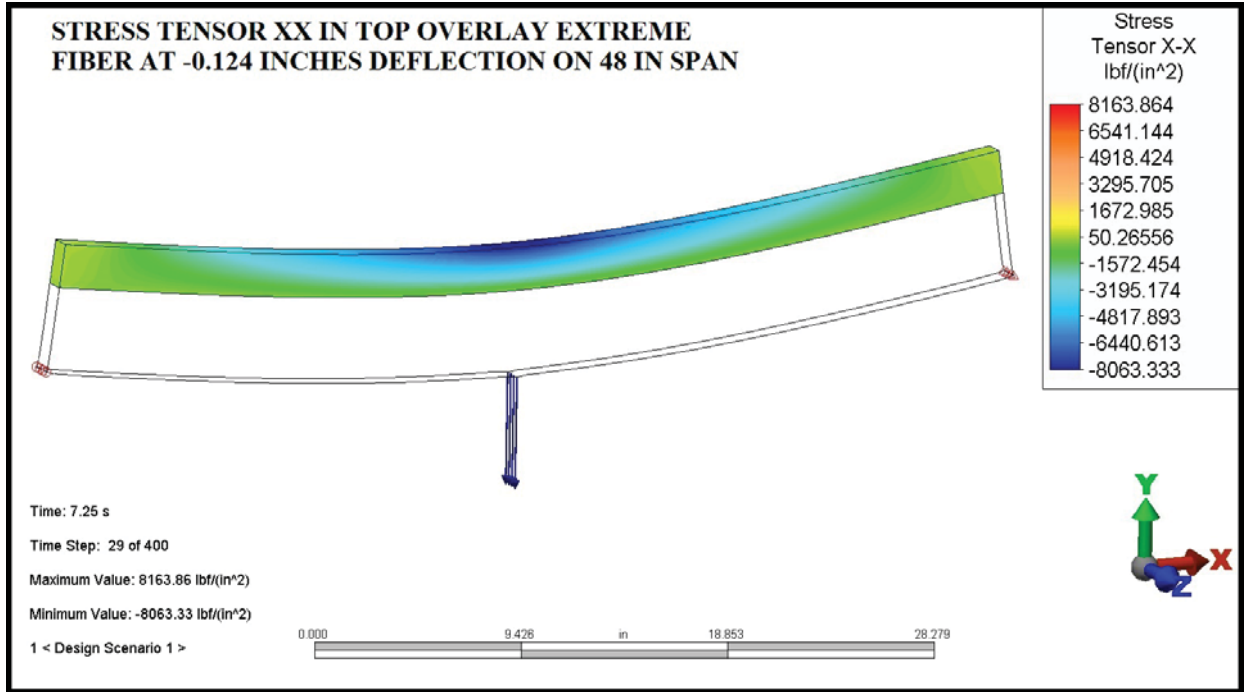
Figure 5.34. Stress tensor X-X at extreme fiber in top of overlay at -0.124 inch deflection.
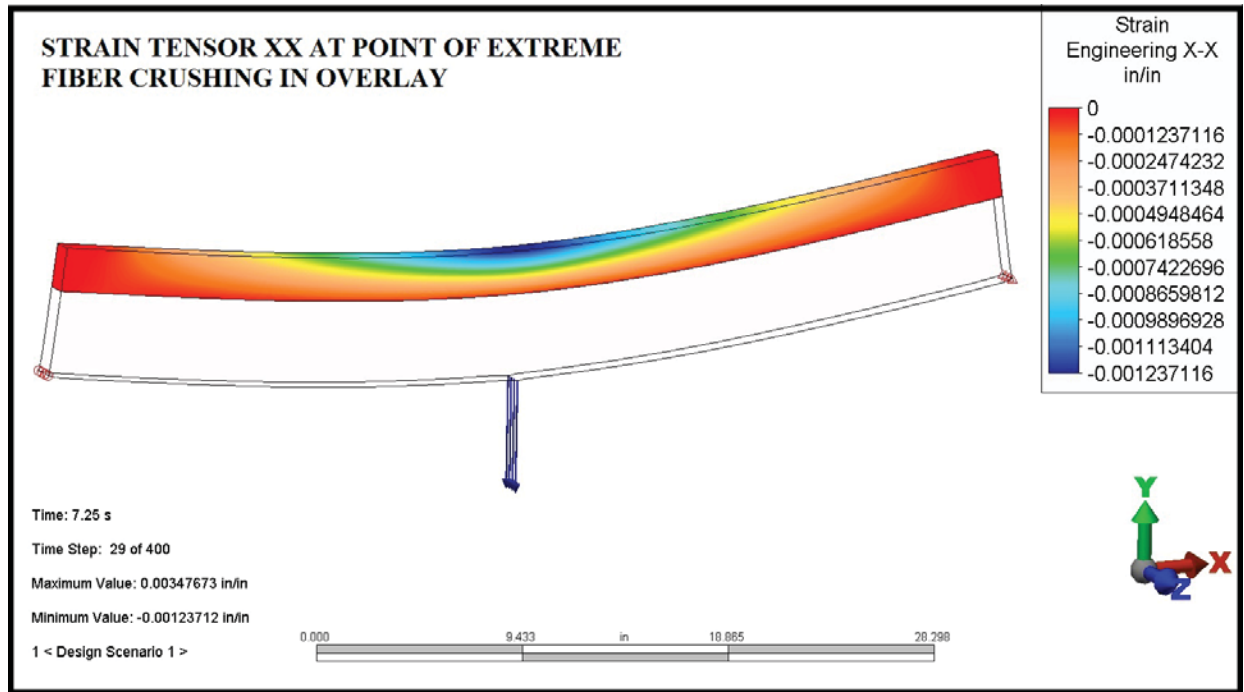
Figure 5.35. Stress tensor X-X at extreme fiber in top of overlay at extreme fiber crushing.

Negative moment due to an overlay section located directly above a bridge main or secondary structural member would tend to create a tensile stress in the overlay. Since cracks would form at the upper extreme fiber of the section, this cracking mechanism due to the negative moment was considered to be a likely cause of overlay damage as shown in Figures 5.36 – 5.42.
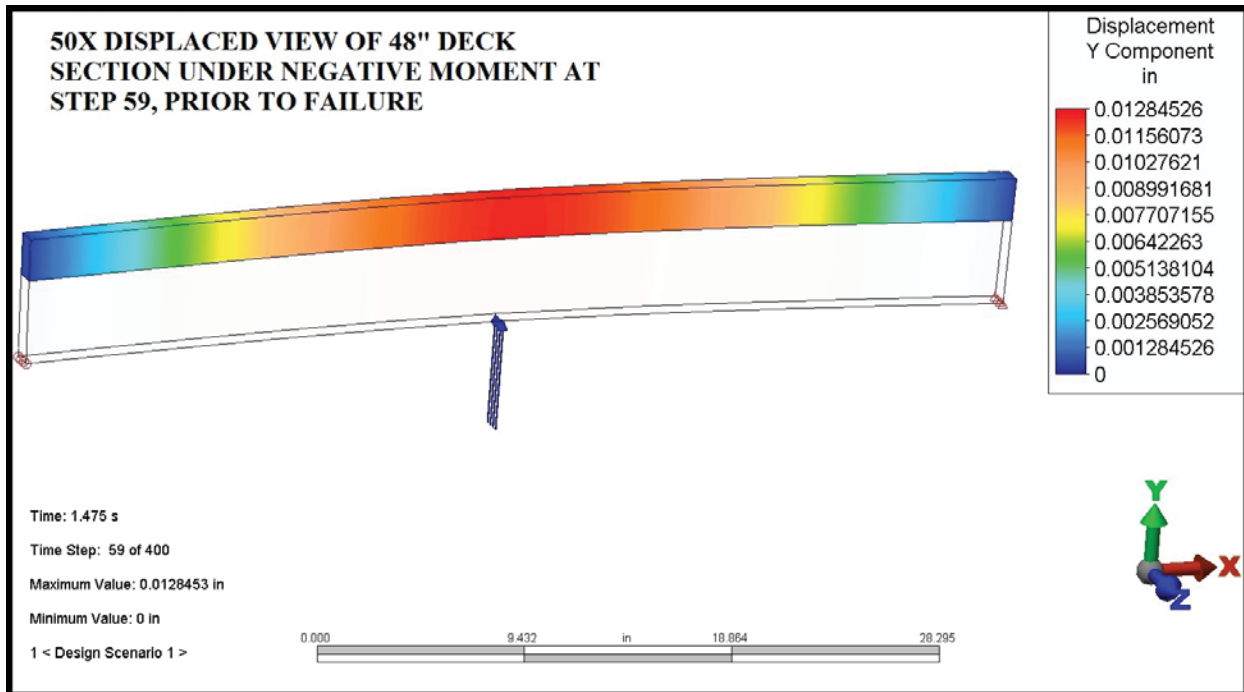
Figure 5.36. Deflected shape of bridge deck and overlay due to the negative bending moment prior to tensile failure.
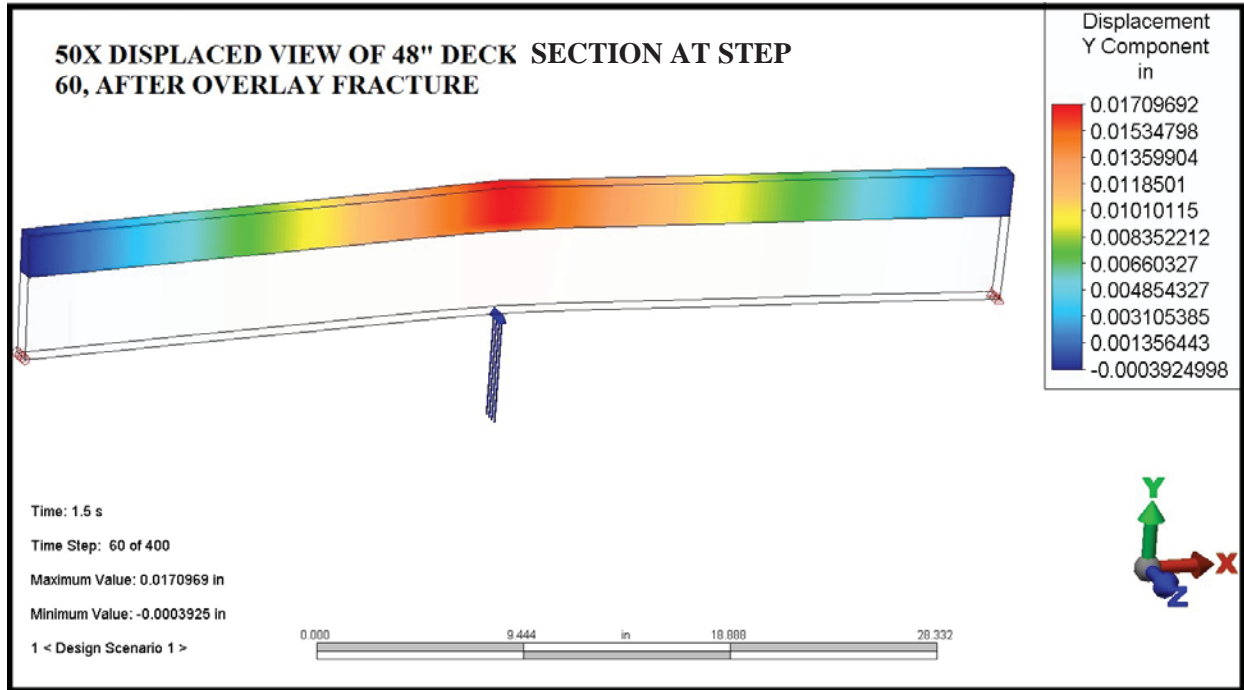
Figure 5.37. Stress tensor X-X at extreme top fiber of overlay prior to tensile failure.
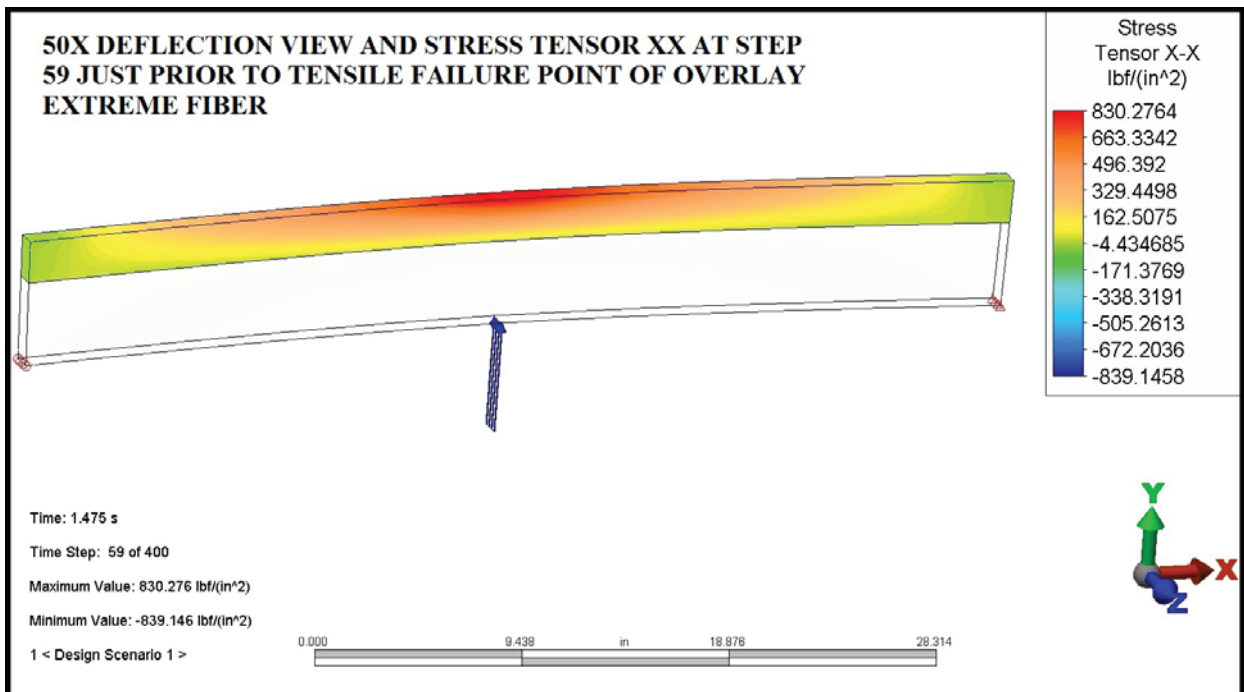
Figure 5.38. Deflected shape of bridge deck and overlay due to negative moment after tensile failure of overlay.
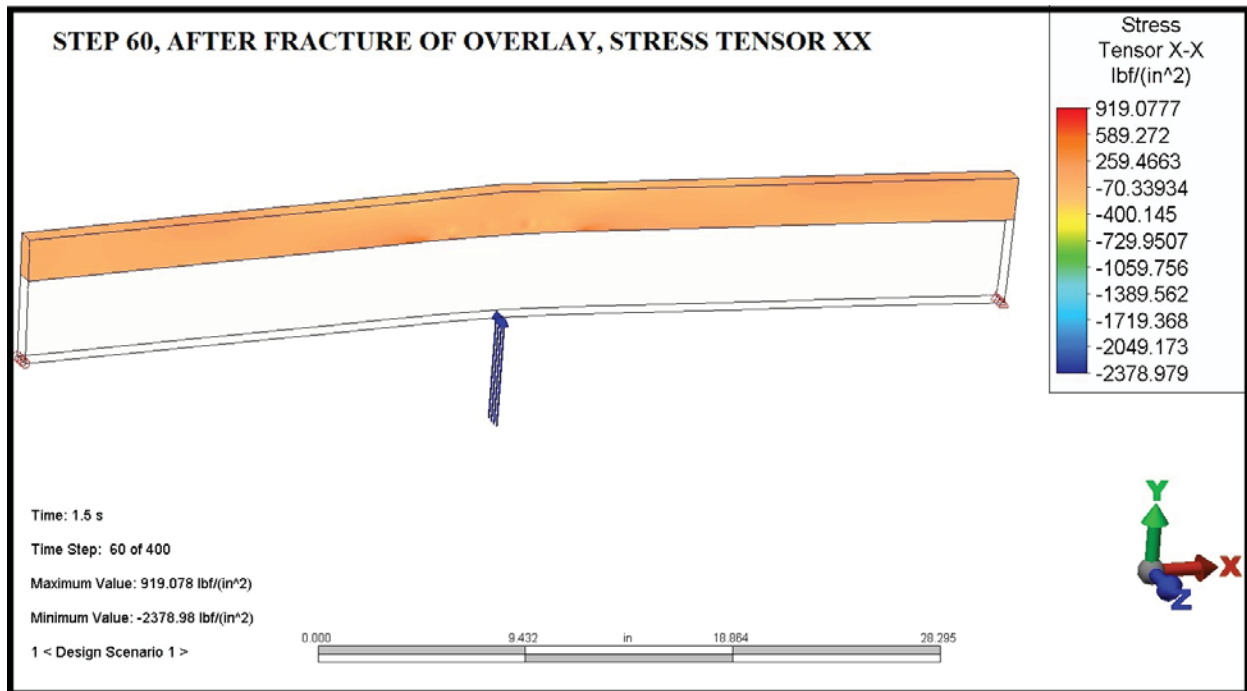
Figure 5.39. Stress tensor X-X at extreme top fiber of overlay after fracture.
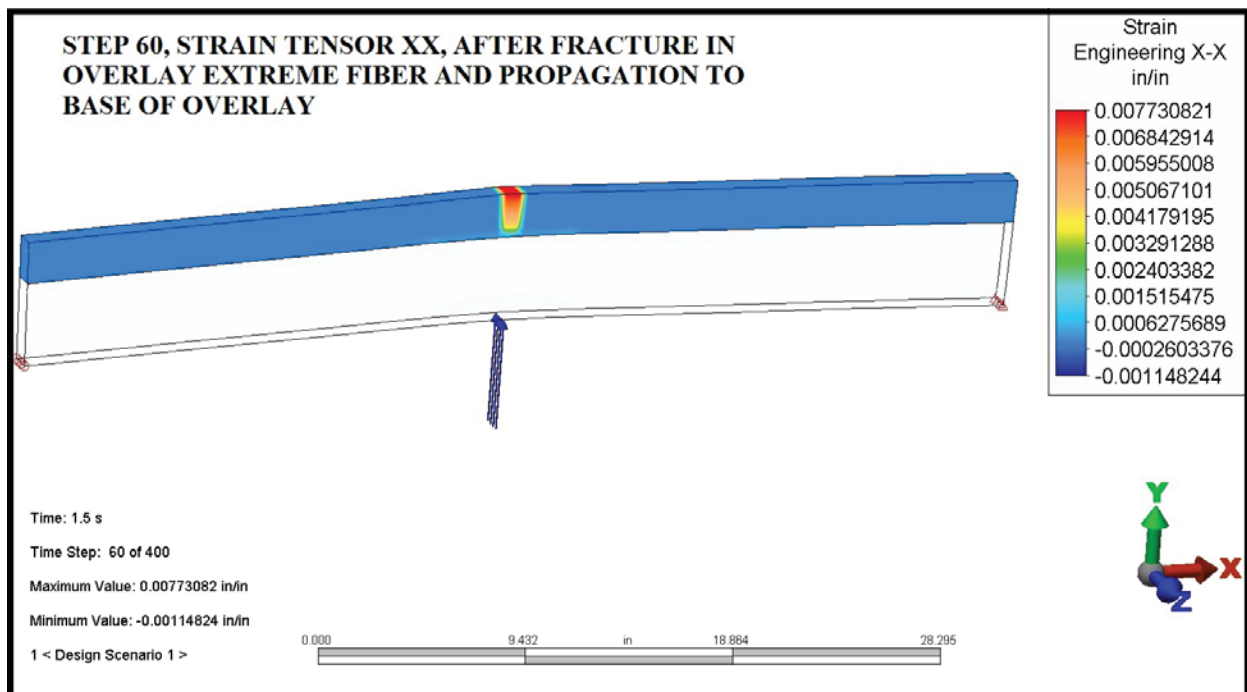
Figure 5.40. Stress tensor X-X at extreme top fiber of overlay after fracture and crack propagation to base of overlay.

73
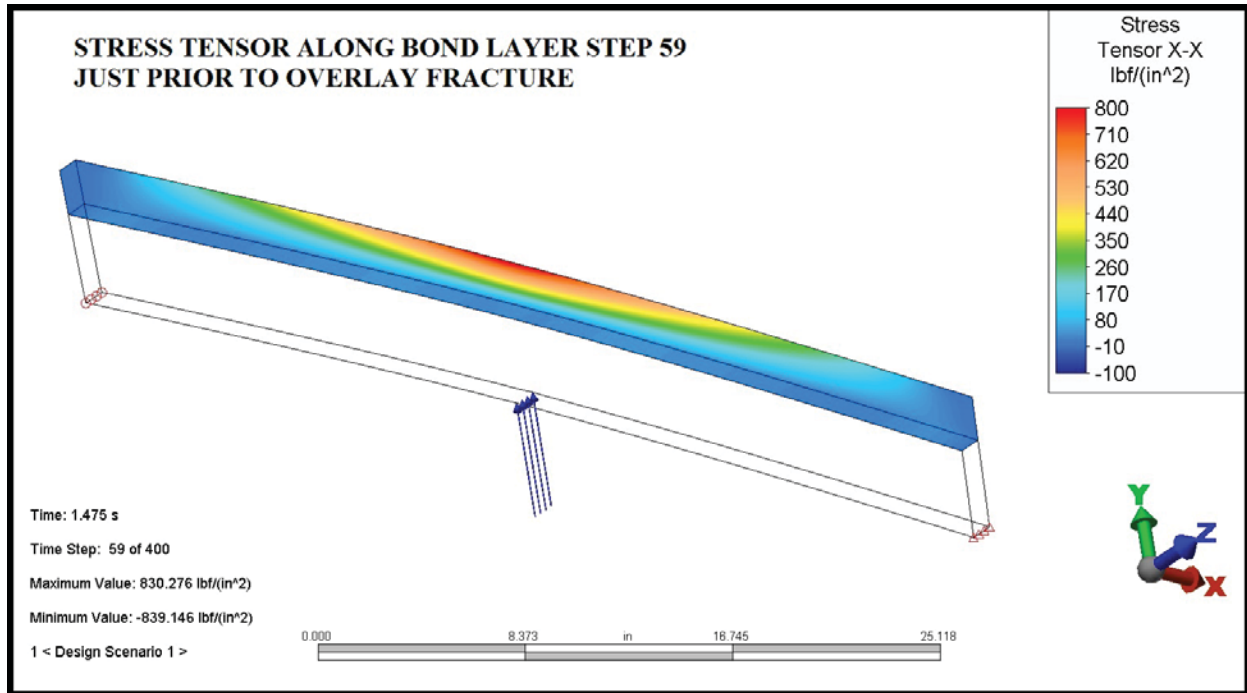
Figure 5.41. Stress tensor X-X along bond layer prior to overlay tensile fracture.
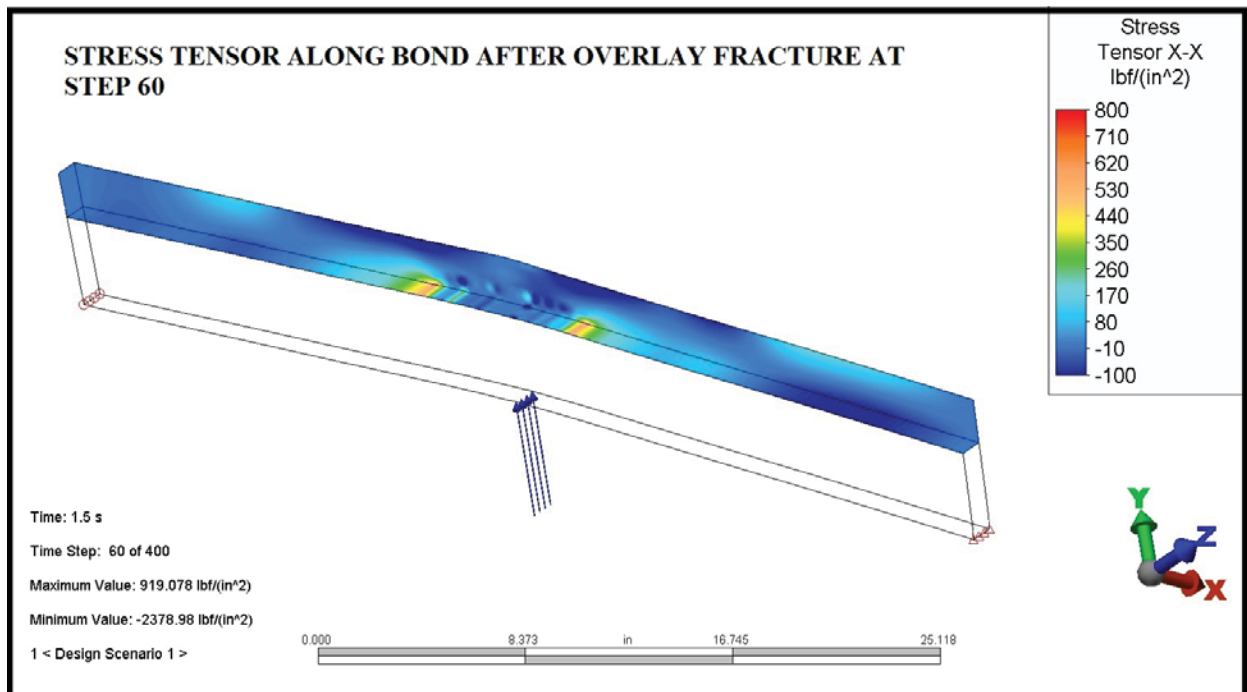
Figure 5.42. Stress tensor X-X along bond layer after overlay tensile fracture.

74

5.6   FINDINGS, DISCUSSION AND CONCLUSIONS

The general criteria for this analysis consisted of a range of compressive strengths for the overlay material and a range of shrinkage factors relative to the bridge deck. Overlay concrete strengths from 4,000 psi (27.6 MPa) to 10,000 psi (69.0 MPa) were investigated with the overall observation that the higher strengths resulted in the earlier formation of closely spaced cracks.

The shrinkage factors were 0.02, 0.03, 0.05, 0.07 and 0.09 percent. It was determined that micro-cracking would appear at approximately the 0.03 percent point in the time line. These initial locations then acted as stress relief mechanisms, generally growing wider as the shrinkage factor was increased. Ultimately, the higher levels of shrinkage, from 0.05 percent through 0.09 percent resulted in wider initial crack separations and the formation of additional micro-cracks, on shorter intercrack dimensions, between large crack locations.

Crack formation mechanics were observed to initiate at the bottom of the overlay with a tensile stress field exceeding the tensile strength of the overlay (approximately 10 percent of compressive strength). Cracks propagated vertically upward until surfacing and proceeding to open with additional shrinkage. Compressive zones were noted on the surface above cracks as the material lower in the overlay fractured.

The non-linear FEA formulations suggest several general findings that may increase our understanding of laboratory testing results and/or field observations of overlay formulations.

1. Shrinkage is restrained by the bond between the overlay and the bridge deck. Our models, therefore, show that a tensile stress area forms below an insipient crack with a corresponding compressive zone above. The shrinkage cracks thus initiate at the bond interface and propagate upward until the stresses in that area are relieved by the formation of a crack.

2. Crack interval at shrinkage magnitudes of 0.02 percent to 0.05 percent appeared to be on the order of 8 inches (203 mm) on center with $E_c = 4.5 \times 10^6$ psi (31,026 MPa) concrete (8,000 psi/800 psi, 55.2 MPa/5.5 MPa and mu = 0.15) and decreased with increasing stiffness up to $E_c = 6.5 \times 10^6$ psi (44,816 MPa). At higher shrinkage magnitudes of 0.07 percent and 0.09 percent, additional intermediate microcracks appeared, reducing the overall crack spacing.   In all cases, models were subjected to previous shrinkage magnitudes, on the way to the higher values. Therefore, as an example, cracks that formed at 0.02 percent and 0.03 percent were present at 0.07 percent and 0.09 percent.

3. We noticed that early forming cracks occasionally would relax slightly if adjacent areas subsequently formed cracks that relieved stresses that had led to the formation of increased opening of the early cracks. This mechanism may not actually be present in the actual overlay since our idealized concrete materials model allows somewhat more elasticity than might be expected in the field.

4. Bond stresses noted between the overlay and deck were complex on a relative small scale and dependent on the pattern of cracks and microcracks in the overlay. We noted that high localized bond shear stresses developed as cracks formed in adjacent areas.

5. The development of very high small-scale local bond stresses due to the stress relief mechanism of shrinkage crack formation suggests that this may be one possible cause of observed delamination and potential bond failure.

6. Deck flexure due to wheel loads depends largely on the location of an overlay section relative to bridge structural members, with areas directly above stiff supports likely to be subject to tensile conditions leading to crack formation. Likewise, areas subject to compressive conditions would be less likely to crack due to this mechanism.

7. The amount of flexure necessary to initiate an overlay failure was quantified in our study by using the arbitrary 48 inch (1219 mm) simply supported length and applying a negative (upward) bending moment to the overlay. The relevant parameter is the deflection vertically at failure of between 0.013 inches (0.330 mm) and 0.017 inches (0.432 mm) that occurred between steps 59 and 60.

6.0   SUMMARY OF CONCLUSIONS AND RECOMMENDATIONS

The laboratory, field, petrographic and analytical work performed for this research project produced many findings and conclusions. Sections 6.1 – 6.4 primarily summarize the findings and conclusions pertaining to the premature bridge deck overlay failures.

Section 6.5 presents the key recommendation produced from this research effort to mitigate the most likely cause of the premature overlay failures. Section 6.5 establishes the maximum recommended ASTM C157 or laboratory concrete bar shrinkages for the overlay concrete to limit the shear stresses along the bond line between the overlay and substrate concrete. Section 6.6 presents future research topics related to this research project.

6.1   IN-SITU BOND STRENGTH (PULL-OFF) TESTING

Below are the conclusions derived from the 178 pull-off tests performed in accordance with ASTM C158 on old or existing silica fume concrete bridge deck overlays and new overlays with different surface preparation procedures.

a. The average pull-off strengths for the old overlays was 95 psi (655 kPa). All pull-off strengths were less than the 200 psi (1379 kPa) bond strength recommended by the American Concrete Pavement Association (ACPA) for 3 inch (76 mm) overlays or thicker. In fact, all bond strengths were less than 175 psi (1207 kPa) indicating a damaged or inadequate bond surface. From this data, the author has concluded the bond strength of the old overlays was inadequate at the time of the pull-off testing.

b. For the new concrete overlays, the average pull-off strengths were 147, 204, 186, 207 and 404 psi (1014, 1407, 1283, 1427 and 2786 kPa) for the various data sets (Figure 2.2). For the 12 individual data sets shown in Figure 2.4 representing all pull-off tests for the new silica fume concrete overlays, only five of the data sets had average bond strengths exceeding the ACPA's recommended minimum 200 psi (1379 kPa) strength. Bond strengths for seven of the data sets fell below the 200 psi (1379) value and six of those fell below 175 psi (1207 kPa) indicating an inadequate bond of the overlay to the concrete substrate.

   Bond strengths for most of the new silica fume concrete overlays were low and for some decks, extremely low. Most likely, this explains why the service life of many of the bridge deck overlays was shorter than expected.

c. In general, the failure zone for the pull-off tests occurred superficially within the concrete substrate or along the top surface of the substrate followed by failure at the bond interface between the overlay and substrate concrete.

d. Overall, pull-off tests indicate the bond strengths of the new silica fume concrete overlays were inadequate to ensure initial and long-term bonding of the overlays. Increasing the bond strength should increase the service life of future silica fume concrete overlays.

e. The rotomilling/hydroblasting surface preparation technique with a mortar primer did not significantly increase the overlay bond strength as compared to using the rotomilling surface preparation technique with a mortar primer.

f. The rotomilling/hydroblasting surface preparation technique without a mortar primer did not significantly increase the bond strength as compared to using the rotomilling surface preparation technique with a mortar primer.

g. For the rotomilling/hydroblasting surface preparation technique, there was no significant difference between the bond strengths with and without a mortar primer.

In summary, most of the bond strengths for the new overlays were inadequate to ensure a long overlay service life. Improving the bond strength should increase the service life of the overlays. The top surface of the concrete substrate was the weakest link within the overlay/substrate cross section. It appears the surface preparation technique with a primed or unprimed surface had little effect on the bond strength indicating the most economical surface preparation technique may be the best choice.

6.2 LABORATORY TESTING

The WYDOT Materials Laboratory measured various fresh and hardened concrete properties for twelve silica fume concrete overlay mixtures. Of the properties measured, the ASTM C157 concrete shrinkage tests (bar length change) provided the most useful information to help characterize and to explain the most likely cause of the premature silica fume concrete overlay failures (i.e., cracking and debonding).

Using 4 in. x 4 in. x 11¼ in. (102 mm x 102 mm x 286 mm) concrete specimens, technicians measured the percent shrinkage in accordance with ASTM C157 after periods of 4, 7, 14, 28, 56 and 112 days of air drying in the laboratory. Table 6.2.1 below summarizes the average concrete shrinkage for the mixtures.

Table 6.2.1. Average ASTM C 157 Shrinkage (Percent) for Silica Fume Concrete Overlay Mixtures

Days of Air Storage					
4	**7**	**14**	**28**	**56**	**112**
0.023	0.046	0.061	0.074	0.08	0.087

From information presented in Chapter 5 and below in Sections 6.4 and 6.5, this author has concluded the shrinkage potential of the silica fume concrete overlay mixtures evaluated was excessive.

As discussed in Chapter 5 and Sections 6.4 and 6.5, the bond line stresses at the interface of the overlay and concrete substrate are dependent on the magnitude of the overlay concrete shrinkage. Bond line stresses increase as the shrinkage potential of the overlay concrete increases. When the bond line stresses exceed the tensile strength of either the substrate or overlay concrete, cracking and debonding of the overlay are likely.

Therefore, it appears limiting the shrinkage potential of the concrete overlay material is the key design consideration to minimize cracking, debonding and premature failure of the silica fume concrete overlays.

6.3   PETROGRAPHIC EXAMINATIONS

David Rothstein, PhD, PG, FACI reported the following:

a. There was no clear evidence that surface preparation affected the bond of the overlay concrete, caused distress, or deteriorated the concrete substrate. Although cracking and microcracking was observed near the bond line of the concrete overlay and substrate and predominately in the top surface of the substrate, there was no evidence to suggest the cracks were caused by the surface preparation (i.e., rotomilling and/or hydroblasting).

b. Cracking and microcracking around the bond line were primarily observed within the concrete substrate and subjacent to the bond line. Typically, cracks are microcracks and located within the top 1/4 inch (6.4 mm) of concrete substrate.

c. Cracks around the overlay and substrate interface are straight, linear and commonly cut though aggregate particles and lack secondary deposits. These observations suggest the cracking occurred after tight bonding was achieved between the overlay and substrate and the cracking mechanism was an externally imposed stress.

d. Evidence of alkali-silica reaction (ASR) was observed in both the overlay and substrate concrete of many of the cores examined. However, no cracking or significant microcracking association with ASR was observed that affected the bond line between the overlay and concrete substrate.

Summarizing, no petrographic evidence of "bruising" or microcracking was found that indicates the surface preparation process damaged the concrete substrate.   Bruising refers to concrete damage consisting of microcracks in the top 1/8-inch (3-mm) layer of the concrete substrate caused by impact loads from the surface preparation process. [16]

Bruising creates a weakened concrete surface layer and typically reduces the bond strength. Depending on the severity, bruising can reduce the service life of the concrete overlay. However, the degree of bruising that may affect the service life of concrete overlays is unknown.

The petrographic findings appear to agree with the conclusions from the pull-off strength testing. Statistically, there was no difference between the pull-off strengths representing the different surface preparation techniques (i.e. rotomilling and/or hydroblasting). In addition, the primary failure location for the pull-off tests was in the top surface of the concrete substrate or in the same location of the observed microcracks.

Evidence of ASR activity was observed in both the overlay and substrate concrete but no evidence was found that suggests ASR caused the microcracking that was observed within the top surface of the concrete substrate. Nevertheless, this finding suggests that perhaps drilled core samples should be examined petrographically as part of the overlay design process to determine the quality of the substrate concrete and to identify any anomalies that may affect the bond or surface life of the overlay.

6.4   FINITE ELEMENT ANALYSIS

Larry Mott, PE investigated the overlay stresses including the bond line stresses at the interface of the silica fume overlay and the concrete substrate using a non-linear, finite element analysis (FEA) computer model. Mott investigated overlay concrete compressive strengths of 4,000 psi (27.6 MPa) to 10,000 psi (69.0 MPa) , modulus of elasticity values (Ec) of 4.5 x 10^6 psi (31,026 MPa) and 6.5 x 10^6 psi (44,816 MPa), and overlay concrete shrinkages values of 0.02, 0.03, 0.05, 0.07 and 0.09 percent.

The results of the FEA are as follows:

    a. Microcracking in the overlay concrete appeared at approximately 0.03 percent shrinkage of the overlay concrete. Cracks in the overlay formed due to the restraint caused by the bonding of the overlay to the substrate concrete. At 0.03 percent shrinkage, cracks started to act as stress relief mechanisms for the overlay concrete and crack widths grew as the overlay concrete shrinkages were increased to 0.05, 0.07 and 0.09 percent.

        As the overlay shrinkage values increased, new cracks formed between the existing cracks, reducing the crack spacing or increasing the crack density in the overlay.

    b. As the compressive strengths and modules of elasticity values of the overlay concrete were increased, crack spacing decreased. As the shrinkage values increased, new cracks formed between existing cracks, reducing the crack spacing.

c. Shrinkage cracks are oriented vertically and initiate at the bond line or at the interface between the overlay and substrate concrete. After initiation, cracks propagate upward to the surface of the overlay.

d. Bond shear stresses between the overlay and substrate were complex on a relative small scale and dependent on the pattern of cracks and microcracks in the overlay. Highly localized bond shear stresses developed as new cracks formed in adjacent areas.

e. Very high small-scale local bond shear stresses due to the stress relief mechanism of shrinkage crack formation suggest this may be one possible cause of the premature overlay bond failures. It appears the localized bond shear stresses related to the overlay shrinkage exceeded the capacity of the concrete substrate just below the bond line.

f. Most likely, wheel loads increase the bond line stresses in the negative moment (tension on top) regions where the deck deflects over supporting structural elements. Therefore, wheel loads may contribute to overlay bonding failures in the negative moment regions of the bridge deck.

6.5   RECOMMENDED MAXIMUM ASTM C157 SHRINKAGE

From the finite element analysis presented in Chapter 5 and summarized above in Section 6.4, overlay microcracking and high bond line shear stresses started to form at the imposed 0.03 percent concrete overlay shrinkage. Results showed the magnitude of the tensile stresses along the bond line at the 0.03 percent shrinkage exceeded the tensile strength of the overlay concrete, creating cracks and large localized shear stresses at the bond line.

Using the Bažant-Baweja B3 Model presented in ACI 209R-92 (2008) and ACI 209.2R-08, the relationships between the ASTM C157 concrete shrinkage (bar length change) and concrete overlay deck shrinkage were computed for different overlay thicknesses and relative humidities as shown below in Table 6.5.1. [17,18]   Specifically, the 28-day (air-dry) ASTM C157 shrinkage to overlay deck shrinkage ratios were computed for determining the 28-day ASTM C157 shrinkage that corresponded with a concrete overlay deck shrinkage of 0.03 percent.

The Bažant-Baweja B3 Model considers the following factors: age of concrete when drying starts and age of concrete at loading, cement and aggregate contents, concrete compressive strength, curing method, relative humidity, shape and volume to surface ratio of specimen or concrete element, and the water content in the concrete. A Microsoft EXCEL spreadsheet was created using the information from Tables 3.1 and 3.3 to compute the recommended maximum 28-day ASTM C157 shrinkages shown below in Table 6.5.1.

Table 6.5.1. Maximum 28-day (Air-dry) ASTM C157 Shrinkage (Percent) to Limit Overlay Concrete Shrinkage to 0.03% for Different Overlay Thicknesses and Relative Humidities*

Overlay Thickness (inch)	Relative Humidity (Percent)						
	20	30	40	50	60	70	80
1.0	0.011	0.011	0.011	0.012	0.014	0.016	0.022
1.5	0.014	0.014	0.015	0.016	0.018	0.021	0.029
2.0	0.018	0.018	0.019	0.020	0.023	0.027	0.036
2.5	0.022	0.022	0.023	0.025	0.028	0.033	0.044
3.0	0.026	0.026	0.027	0.029	0.033	0.039	0.052
3.5	0.030	0.030	0.031	0.034	1.037	0.045	0.060
4.0	0.034	0.034	0.036	0.038	0.043	0.051	0.068
4.5	0.038	0.038	0.040	0.043	0.048	0.057	0.076
5.0	0.041	0.042	0.044	0.047	0.052	0.063	0.084

*Estimated from Bažant-Baweja B3 Model from ACI 209.2R-08 Guide for Modeling and Calculating Shrinkage and Creep in Hardened Concrete

As shown above in Table 6.5.1, the recommended maximum ASTM C157 shrinkages are a function of the overlay thickness and drying environment (relative humidity) of the concrete deck overlay. As the overlay thickness and relative humidity decrease, the recommended maximum ASTM C157 shrinkage also decreases to maintain a 0.03 percent maximum concrete overlay shrinkage.

The recommended maximum 28-day ASTM C157 shrinkages in Table 6.5.1 should limit the concrete overlay shrinkage to approximatively 0.03% or the upper limit suggested by the finite element analysis to limit cracking and to maintain acceptable bond line stresses. This author recommends using Table 6.5.1 to evaluate future concrete overlay mixtures for performance and acceptance.

Example: For a designed 2-inch (51 mm) overlay thickness and a predicted drying environment with an average relative humidity of 40 percent, the average laboratory shrinkage for three 4 in. x 4 in. x 11¼ in. (102 mm x 102 mm x 286 mm) specimens should not exceed 0.019 percent as determined by ASTM C157.

In order to obtain the ASTM C157 shrinkage limits shown in Table 6.5.1 above, overlay mixtures will most likely require the inclusion of a shrinkage-reducing admixture (SRA) in addition to optimizing the aggregate gradation and minimizing the total water content of the concrete. SRAs should meet the requirements of ASTM C494/C494M, Type S. [19]

Findings from this research indicate the most likely cause of the premature cracking and bond failures of the silica fume concrete overlays was excessive shrinkage of the overlay concrete. In addition, findings indicate the ASTM C156 shrinkage test and Table 6.5.1 can be used as part of the overlay design process to qualify future overlay mixtures. By limiting the overlay concrete shrinkage to the recommended values in Table 6.5.1, the bond line stresses should be held to acceptable levels so that excessive overlay cracking and debonding do not occur.

6.6   FUTURE RESEARCH

Recommended future research consists of the following:

a. Continue the laboratory concrete shrinkage research to determine the best means to reduce the overlay concrete shrinkage while maintaining the other required durability properties. Items to investigate include aggregate optimization schemes, means to reduce the net water but still maintain a workable mixture, and the inclusion of different types of SRAs to reduce the shrinkage of the concrete overlay mixtures to values recommended in Table 6.5.1.

b. Perform field trials with the new extra-low shrink concrete overlay mixtures to evaluate placing, consolidation, finishing processes and performance. The evaluation process should include at a minimum pull-off strength tests, crack and debonding surveys versus time.

c. Perform field trials with the new extra-low shrink concrete overlay mixtures with different substrate moisture conditions. As previous discussed by Bissonnette, et al. in Reference 3, there may be an optimum substrate moisture condition that maximizes the bond strength. Currently, WYDOT requires a saturated surface dry (SSD) condition; however, a drier surface condition (less than SSD) may improve the bond strength of the overlay by creating a "thirstier" substrate.

d. Investigate how traffic-induced vibrations affect the bond strength of silica fume concrete overlays. WYDOT's current practice includes placing the overlay while the other lane has slow moving traffic. It is unclear how the traffic speeds and related vibrations affect the bond strengths of the overlay.